DOE/NASA/0331-1
NASA CR-187111

Thick Thermal Barrier Coatings For Diesel Components

T.M. Yonushonis

August 1991

Prepared for
NATIONAL AERONAUTICS AND SPACE ADMINISTRATION
Lewis Research Center
Under Contract DEN3-331

for
U.S. DEPARTMENT OF ENERGY
Conservation and Renewable Energy
Office of Propulsion Systems

DISCLAIMER

Printed in the United States of America

Available from
National Technical Information Service
U.S. Department of Commerce
5285 Port Royal Road
Springfield, VA 22161

DOE/NASA/0331-1
NASA CR-187111

Thick Thermal Barrier Coatings For Diesel Components

T.M. Yonushonis

August 1991

Prepared for
NATIONAL AERONAUTICS AND SPACE ADMINISTRATION
Lewis Research Center
Under Contract DEN3-331

for
U.S. DEPARTMENT OF ENERGY
Conservation and Renewable Energy
Office of Propulsion Systems

TABLE OF CONTENTS

LIST OF FIGURES

LIST OF FIGURES (Cont'd)

LIST OF FIGURES (Cont'd)

LIST OF FIGURES (Cont'd)

LIST OF FIGURES (Cont'd)

LIST OF FIGURES (Cont'd)

LIST OF TABLES

LIST OF TABLES (Cont'd)

1.0 SUMMARY

The objective of this program was to develop zirconia based thick thermal barrier coatings for in-cylinder insulation for heavy duty diesel engines. The specific objectives were to develop thermal barrier coatings with a thermal conductance of 410 W/m^2K (.5 $BTU/hr\text{-}in^2F$) which could survive a minimum of 100 hours of operation in a single cylinder research engine.

The approach selected utilized existing coating property data bases augmented, where necessary, by the collection of additional data, modeling of stresses in the coatings by finite element techniques, and extensive rig and engine tests. The engine tests were conducted over a wide range of operating conditions.

Diesel engine performance modeling indicated that the major fuel economy benefits would be obtained by applying a thermal barrier coating on the piston and the cylinder head. Insulating the cylinder walls and valves was not predicted to result in any significant performance improvement. Therefore, this effort concentrated on the development of piston and cylinder head insulation. With the insulation levels targeted in this program, the model predicted that in-cylinder heat rejection would be reduced by 38%. Estimates of fuel economy improvements ranged from 2% for a turbocharged engine to 3% for a turbocompound engine.

Evaluation of the piston coatings by one dimensional and two dimensional finite element techniques and cylinder head coatings by three dimensional methods indicated that a properly designed multilayer coating could meet the thermal conductance goal and survive the diesel engine conditions. The multilayer coating design selected contained intermediate cermet layers which reduced the critical tensile stresses in the coating and at the coating to metal interface. Also, the cermet layers have increased strength compared to ceramic coatings which results in an additional design margin. The selected coating system employs a metallic bond coat and three insulating layers for a total thickness of 2.5 mm (0.100 inch).

Bench test evaluations conducted at United Technologies Research Center (UTRC) confirmed that the multilayer coatings can survive steady state thermal gradients in excess of those modeled. Engine tests at Cummins confirmed that the coating can survive steady state conditions at 1.38 MPa (200 psi) brake mean effective pressures or less for periods of time up to 100 hours.

In the area of coated component fabrication, considerable emphasis was placed on developing the robotics, coating residual stress control, and plasma spray procedures necessary to obtain the desired coating properties over the entire piston bowl surface. Although the piston bowl geometry appears simple, it is quite complex from a coating processing standpoint. Robotic plasma gun manipulation programs were developed to obtain uniform coating properties and coating thicknesses. Special heating torches and air cooling nozzles were employed when coating the pistons to control the residual stresses in the coatings.

Similar development programs were conducted to obtain uniform multilayer coatings on the cylinder head. On this component, masking techniques were required to selectively coat the combustion face of the cylinder head.

Single cylinder tests with coated components installed failed to confirm the fuel economy gains predicted for the insulated engine. Volumetric efficiency changes versus heat rejection were as predicted with the volumetric efficiency decreasing as heat rejection decreased. However, the effect of insulation and oil cooling on engine heat rejection was not as predicted. A major reduction in engine heat rejection was observed when substituting an oil cooled metal engine cylinder head compared to the water cooled baseline engine. The addition of insulated components to this oiled cooled engine resulted in only a minor further decrease in heat rejection. The original predictions suggested that oil cooling and insulation would both have major effects on heat rejection. The test results indicate that the change to oil cooling had a major effect on heat rejection which minimized the effect of insulation. It should be noted that for this study an oil cooled engine was obtained by flooding the cylinder head water cooling passage with oil. The cylinder head was not specifically designed to incorporate oil cooling and the cylinder block was uncooled.

Apparent heat release data indicated that the insulated engine had a longer combustion duration than the metal engine when operated with an oil cooled cylinder head. In these specific studies, insulated engine fuel economy was approximately 2% worse than an oil cooled metal engine without insulation.

Reliability and durability of thermal barrier coatings remain major issues. Information obtained from this program revealed that the fuel injection and diesel combustion process results in thermal gradients and thermal stresses that are different in nature from those predicted using the boundary conditions input into the models.

In summary, considerable technology and knowledge was developed during this DOE/NASA effort supported by the Heavy Duty Transport Program. Our understanding of the effects of thermal barrier coatings on engine performance and methods of applying thermal barrier coatings was significantly enhanced. During the course of the program, it became apparent that precise understanding and modeling of the operating conditions for the engine are required to properly design durable coatings. Also, careful control of the plasma spray coating process is needed to assure that the coatings meet the design criteria. Our goal is to apply information gained in this program to future diesel engine systems.

2.0 INTRODUCTION

Considerable effort has been expended on the development of thermal barrier coatings for turbine and diesel engine applications [1-5]. In the case of turbine engines, most effort has concentrated on thin thermal barrier coatings, approximately 0.5 mm (0.020) inch thick. The coatings were primarily plasma sprayed zirconia with stabilizers consisting of MgO, CaO, or Y_2O_3. Considerable information is available in the literature on the zirconia coatings and the effect of the bond coat [6-10] . Most of the recent gas turbine efforts have concentrated on the yttria stabilized zirconia because of the higher temperature capability. Gas turbine engines operate at considerably higher average gas temperatures than the diesel engine components. Therefore, most thermal barrier coating efforts have been concerned with bond coat oxidation, modifying percent Y_2O_3 content to improve the thermal shock resistance, and more recently, development of life prediction models [11-14].

In the diesel engine applications at Cummins, most effort has been concentrated on the development of relatively thick thermal barrier coatings, coating thickness greater than 1.5 mm (0.06 inch) in thickness. These coating thicknesses have been derived from a need to reduce in-cylinder heat rejection in the diesel engine. The primary coating process techniques investigated have been to use the turbine technology developed for thin coatings and apply thicker duplex systems. In some cases graded and other layered coating systems have been evaluated.

In the present program the primary coating approach was to utilize the experience of UTRC in the engineering and controlled fabrication of thick coatings, 5 mm (0.20 inch), for turbine tip seal applications. The diesel coatings developed in the current program used the layered coating design approach and controlled the coating residual stresses. The outcome of these efforts was a control of the coating physical properties.

The program consisted of three major tasks which are summarized in Table 2.1.

Table 2.1

THICK THERMAL BARRIER COATINGS PROGRAM TASKS

	TASK I ANALYSIS AND DESIGN		TASK II BENCH TEST EVALUATIONS		TASK III SINGLE CYLINDER ENGINE TESTING
A.	Diesel Cycle Modeling	A.	Plasma Spray Parameters	A.	Test Instrumentation
B.	Component Thermomechanical Analysis	B.	Microstructure & NDE	B.	Water Cooled Baseline
C.	Coated Component Design	C.	Environmental Screening and Property Measurements	C.	Coated Component Fabrication NDE
				D.	Insulated Engine Tests

Section 3.0 reports on the Task I activities and results, while Sections 4.0, and 5.0 report on the bench test evaluations and engine tests, respectively.

3.0 TASK I - ANALYSIS AND DESIGN

Task I, Analysis and Design, was comprised of diesel cycle modeling and the establishment of boundary conditions for the component structural analysis, one dimensional analysis of the multilayer coatings systems, two dimensional finite element modeling of the piston coatings and three dimensional finite element modeling of the cylinder head coatings. In addition to the modeling of steady-state conditions, one dimensional models of the effects of thermal transients were generated to determine the effect of a transient of the coating stresses. Results of these efforts are documented in the following sections.

3.1 DIESEL CYCLE MODELING - OVERVIEW

The reduction of heat rejection from the diesel engine combustion chamber has been the subject of a great deal of focus in recent years [15-16]. The efforts being reported in this section focus on the analysis of the effects of coatings on engine performance and heat rejection. For this analysis the conventional water cooled engine was compared with an engine having limited oil cooling, and utilizing zirconia coated cylinder head firedecks and piston crowns. Initial analysis showed little or no benefits of insulating the valves or cylinder liner; therefore, the valves and cylinder liners were not insulated. The insulated engine configuration was predicted to result in a modest direct performance improvement; a three percent fuel consumption improvement in the turbocompound configuration. For the engine studied, a thirty-eight percent reduction in the in-cylinder heat rejection was predicted. This change in heat rejection would allow further performance improvements through the reduction in cooling system parasitic losses, and potential improvements in vehicle aerodynamics due to the reduced heat exchanger frontal area. There was no attempt to quantify these benefits in this program.

Component thermal analysis was conducted using finite element models of the piston and cylinder head firedeck. These models provided additional insights regarding the nature of the heat rejection reductions, and critical temperature control.

3.1.1 Engine Configuration

In order to maximize the potential payoff of the coating development activities, it was necessary that an engine configuration representative of the state-of-the-art in heavy duty commercial engines be selected. The dual goals of improved fuel consumption and increasingly stringent emission standards have led to a trend toward higher peak cylinder pressure, higher specific power output, and high fuel injection pressure with direct injection combustion chambers. The engine chosen for this program, as representative of these trends, was the Cummins V903, eight cylinder, direct injection diesel engine. This is a four stroke engine of 140 mm bore and 120 mm stroke. A rating of 360 KW (485 HP) at 2100 RPM was chosen for the turbocharged configuration. The geometric compression ratio chosen for this work was 13.5:1, and the peak cylinder pressure was limited to a maximum of 13.8 MPa (2000 psi). A turbocompound configuration, rated at 400 KW (540 HP) at 2100 RPM, was also considered.

The analysis which follows compares various insulating configurations with a water cooled baseline engine. The comparisons were made at a constant rated air-fuel ratio of 30:1, and a fixed peak cylinder pressure of 13.8 MPa (2000 psi). The air-fuel ratio was held constant by adjusting the casing size of the turbocharger turbine, while the peak cylinder pressure was fixed by changing the fuel injection timing. The intake manifold temperature was held constant at 60 C (140 F). The turbocharger compressor and turbine efficiencies were assumed to be 0.78 and 0.76 respectively. A power turbine efficiency of 0.80 and gear train efficiency of 0.90 were used for the turbocompound system, based on previous tests using similar hardware.

3.1.2 Diesel Engine Cycle Simulation

Thermodynamic analysis of the diesel engine cycle was conducted to elucidate the impact of thermal barrier coatings on the diesel cycle efficiency. A Cummins TRANSENG cycle simulation used for this analysis was based on a model developed at Imperial College [17,18]. Although the model has been confirmed for a wide variety of engine families and test conditions, it must be realized that the thermodynamic processes occurring in the diesel engine are complex. Therefore, the cycle simulation remains empirical in nature and subject to deviation when the modeling becomes extrapolative for a radically different engine configuration such as an insulative combustion chamber.

The TRANSENG code at Cummins has undergone a great deal of modification and validation efforts using experimental data from both cooled and insulated Cummins diesel engines. A modified Woschni heat transfer correlation was used to describe the combustion chamber gas-to-wall heat transfer process [19]. A 61 node finite difference thermal network scheme was used to describe the combustion chamber and port walls, thus enabling the assessment of the effects of insulating individual components on performance, heat rejection, and critical temperatures.

The predicted effect of piston and head insulation on in-cylinder heat rejection is summarized in Figure 3.1. The percent reduction of in-cylinder heat rejection is plotted versus insulation thickness for several different cooling strategies. The insulation chosen for this analysis was a multilayer zirconia/CoCrAlY composite having a thermal conductivity of 0.79 W/mK (0.46 BTU/hr-ft-F). The vertical dashed line in Figure 3.1 indicates the insulation thickness required to meet the program goals of 410 W/m^2K when using this coating. The curve showing the lowest reduction in heat rejection is representative of a fully water cooled engine. The next two curves represent cases for which the water coolant has been eliminated from the block, while the cylinder head remains cooled, first with conventional water jackets, and next with limited oil drillings through the valve bridges and injector bore. The final curve represents the case where all coolant has been removed from the engine. For the current program it is proposed to develop the configuration using minimal oil cooling. At the goal, the insulation level the proposed configuration shows a 38 percent reduction of in-cylinder heat rejection compared to the water cooled baseline diesel engine.

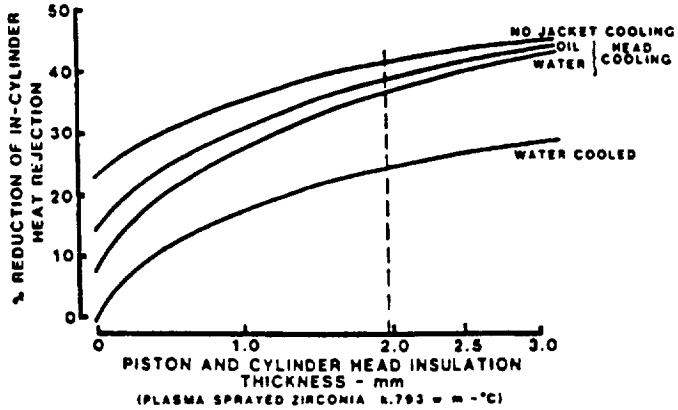

Figure 3.1: Predicted effect of insulation on in-cylinder heat rejection.

The predicted performance improvements directly attributable to the reduced in-cylinder heat rejection are summarized in Figure 3.2. Again the vertical dashed line represents the goal of the current program. A three percent fuel consumption improvement is predicted in the turbocompound configuration and a two percent improvement for a turbocharged engine. This fuel consumption improvement was accompanied by an approximately three percent drop in volumetric efficiency, and a 40 C (105 F) increase in exhaust temperature.

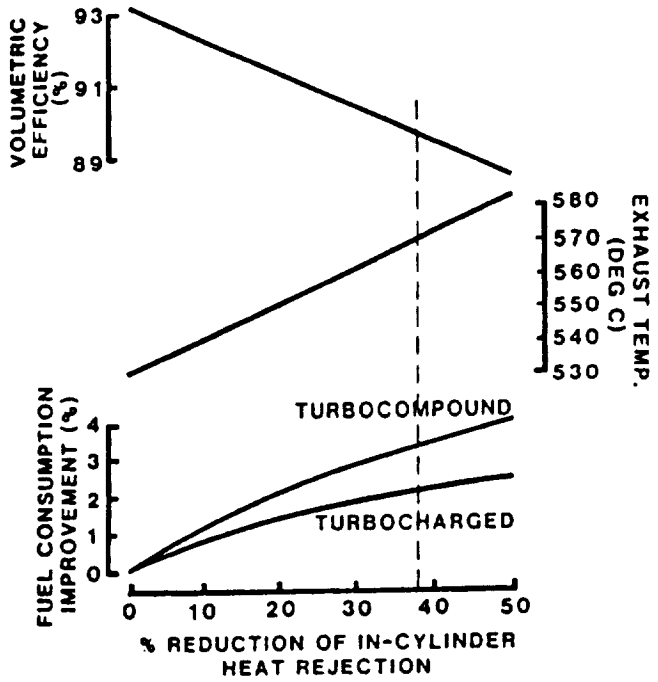

Figure 3.2: Predicted effect of % reduction of in-cylinder heat rejection on volumetric efficiency, exhaust temperature, and fuel consumption.

The impact of the reduced in-cylinder heat rejection on the total specific heat rejection of the engine is given in Figure 3.3. The total specific heat rejection represents the combined impact of in-cylinder heat rejection, friction, and heat rejection to the aftercooler. The 38 percent reduction of in-cylinder heat rejection represents a 22 percent reduction in total specific heat rejection, and therefore cooling system load. This reduction in cooling system load represents an additional significant benefit of insulation. Insulation allows a reduction in parasitic losses due to lower cooling fan requirements. Furthermore, the reduced heat exchanger size may be utilized to improve vehicle aerodynamics, resulting in further efficiency improvements, and increased design latitude.

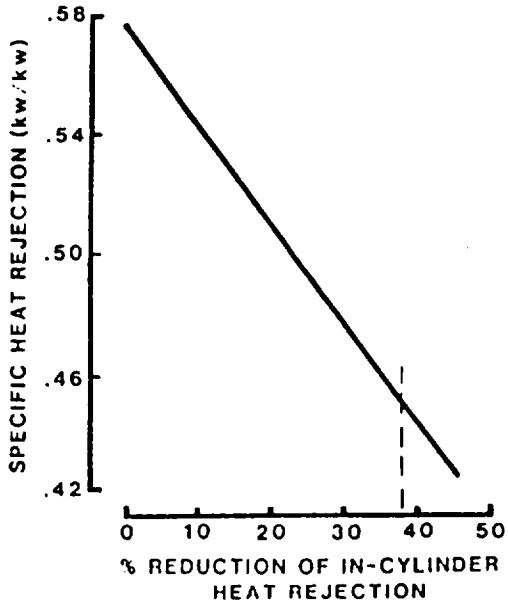

Figure 3.3: Specific heat rejection versus % reduction of in-cylinder heat rejection.

The previous discussion focused on the impact of piston and cylinder head insulation. The impact of liner insulation, as well as insulating the valve faces was also analyzed. The detailed thermal network incorporated in the cycle simulation was utilized for this analysis. The cylinder liner was described using a two dimensional, axi-symmetric thermal network, with five zones in communication with the combustion chamber. The heat transfer could then be calculated into each zone, as shown in Figure 3.4. Only the uppermost zone is exposed to combustion gas throughout the cycle, and therefore receives the greatest portion of the heat transfer to the liner. In this analysis, approximately 50 percent of the heat transfer to the liner was through this upper one fifth of the liner. It was therefore concluded that insulating the upper portion of the liner would provide the greatest benefit, while not increasing the temperature of the liner in regions where the rings traveled, which would adversely impact the ring and liner tribology.

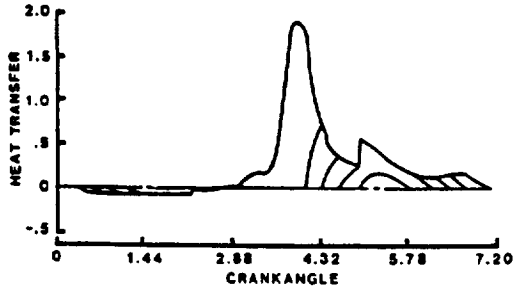

Figure 3.4: Heat transfer versus crank angle.

Applying a 1.2 mm (0.047 in) zirconia coating with a 0.79 W/mK conductivity to the upper liner zone was found to reduce in-cylinder heat rejection by only slightly more than one percent. The resulting impact on liner temperature is summarized in Figure 3.5. The temperature of the coated surface increased sharply, while the metal temperature beneath the coating was reduced by approximately 30 C (86 F). The liner metal surface temperature throughout the ring travel area was found to increase slightly. This was believed to be due to the upper ring traveling into the insulated zone when near top dead center. The ring was caused to run hotter, thus heating the rest of the liner. In practice the insulation, if used, would probably not be extended into the ring travel area, and thus the increase in liner metal surface temperature would not be expected.

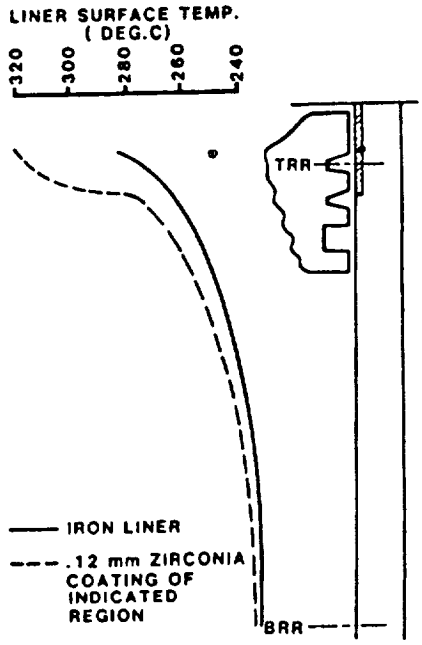

Figure 3.5: Impact of insulating top portion of cylinder liner.

The effect of applying a 1.2 mm (0.047 in) coating to the faces of all of the valves (intake and exhaust) was analyzed next. Coating the valve faces was found to reduce in-cylinder heat rejection by less than one percent. Although the valve faces represent a significant fraction of the cylinder head surface (almost one half on the V903), they already represent a relatively high thermal resistance. Little heat transfer occurs through them in the baseline engine, so adding insulation has little further impact. The effect of valve face insulation on valve temperatures, as predicted using the cycle simulation, is summarized in Table 3.1. The insulated face does provide a reduction in valve metal temperature. This temperature reduction may be a worthwhile benefit in engines with limited cooling, where the reduced metal temperature may improve component durability.

Table 3.1

Effect of Insulation on Valve Face Temperatures

	Predicted Temperature, C (F)	
	Uncoated	Coated
Exhaust Valve		
Surface	697(1285)	750(1380)
Metal Face	697(1285)	607(1125)
Fillet Surface	653(1207)	590(1095)
Intake Valve		
Surface	577(1070)	663(1225)
Metal Face	577(1070)	420(788)
Fillet Surface	489(910)	392(737)

3.1.3 Detailed Thermal Modeling

As a means of further assessing the impact of ceramic coatings on piston and cylinder head temperatures and heat rejection, finite element models of these components were constructed. A two-dimensional, axi-symmetric model of the piston was constructed as shown in Figure 3.6. This model is representative of the upper portion of a two-piece, articulated piston. Thermal boundary conditions were applied which provided close agreement with measured data. The combustion chamber heat transfer coefficient was varied spatially over the piston crown, after the method of Seale and Taylor [20], Figure 3.7. This correlation has been found to provide excellent agreement with measured piston temperatures. The underside of the piston was treated to represent forced oil cooling from a spray nozzle, and the ring lands were assigned temperatures and heat transfer coefficients representative of the contact resistance at the piston/ring/liner interface. The results obtained through exercising this

model are summarized in Table 3.2. Both ductile iron and aluminum base materials were considered. In either case the predicted heat rejection was substantially reduced with the addition of coating. It should be noted that the heat rejection of the coated piston was almost insensitive to the base material. This insensitivity is due to the fact that the thermal conductivity of the coating is much lower than that of either aluminum or iron, and dominates the heat transfer through the piston. The coating results in a large increase in piston surface temperature and a reduction of over 100 C (212 F) in the maximum metal temperature.

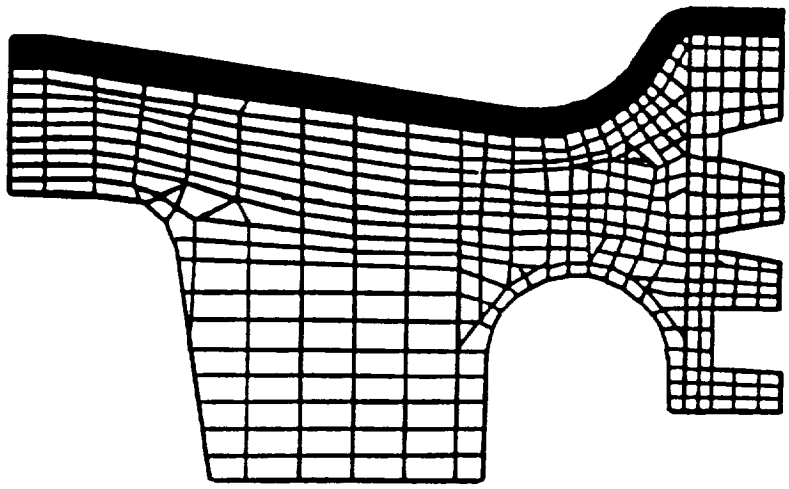

Figure 3.6: Piston model showing 0.100" multilayer coating.

Table 3.2

Predicted Heat Flow and Temperatures For Pistons With and Without Coating

Piston Configuration	Heat Flow Thru Pistons kw	Temperature, Deg. C Maximum	Maximum Metal	Ring Groove
Ductile				
No Coating	48.4	512	512	402
With Coating	19.3	751	379	344
Al_2O_3 SiO_2 Fiber Reinforced Aluminum				
	63.7	429	429	384
No Coating	19.4	696	321	314
With Coating				

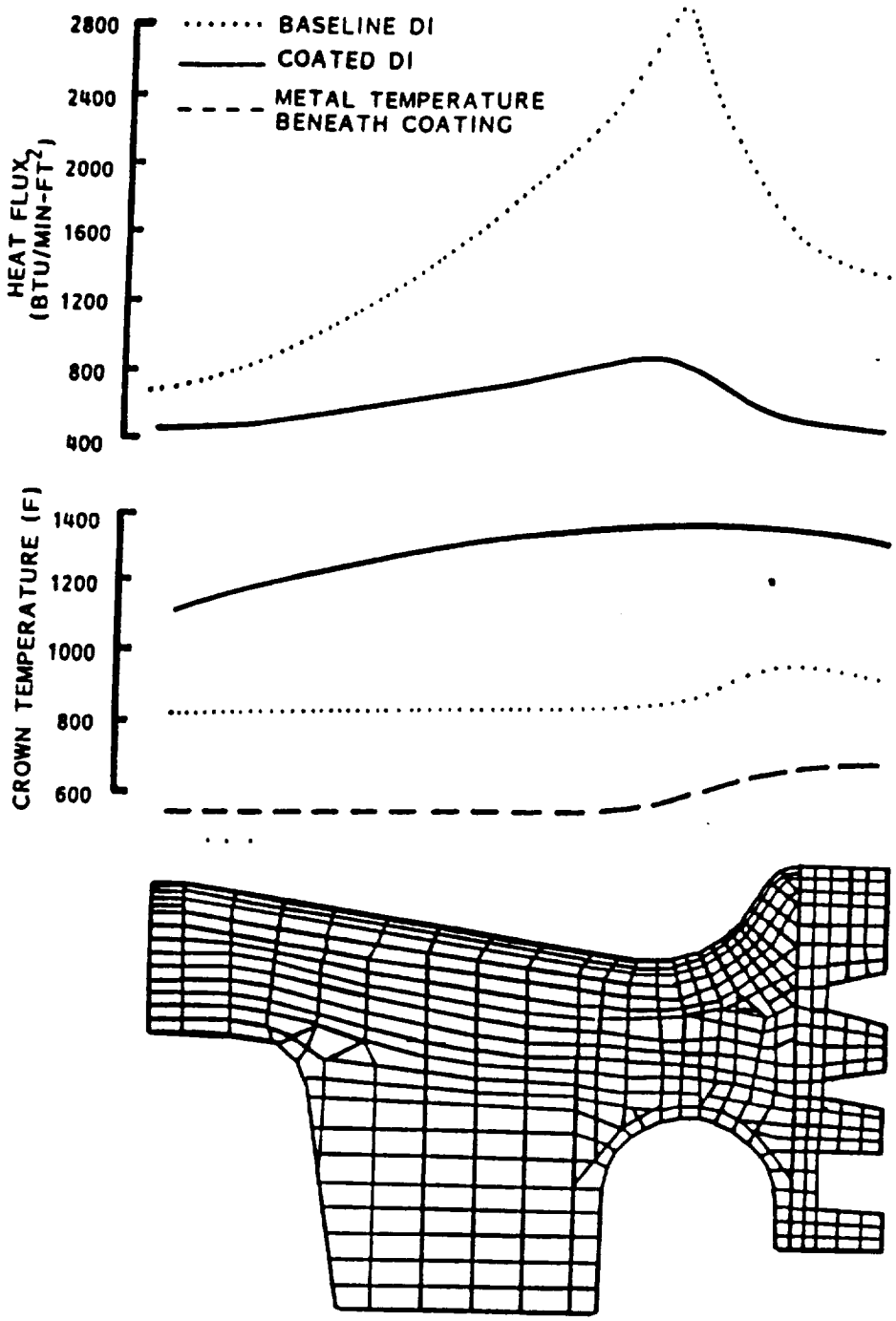

Figure 3.7: Heat flux and temperature variation as a function of radial location on the piston. Piston center is on the left of this figure.

The coating was also effective in reducing the top ring groove temperature, with either aluminum or iron pistons. The predicted temperature profiles for the ductile iron piston, and the coated ductile iron piston are given in Figures 3.8 and 3.9 respectively. The insulating coating contains a steep thermal gradient resulting in a general cooling of the metal piston.

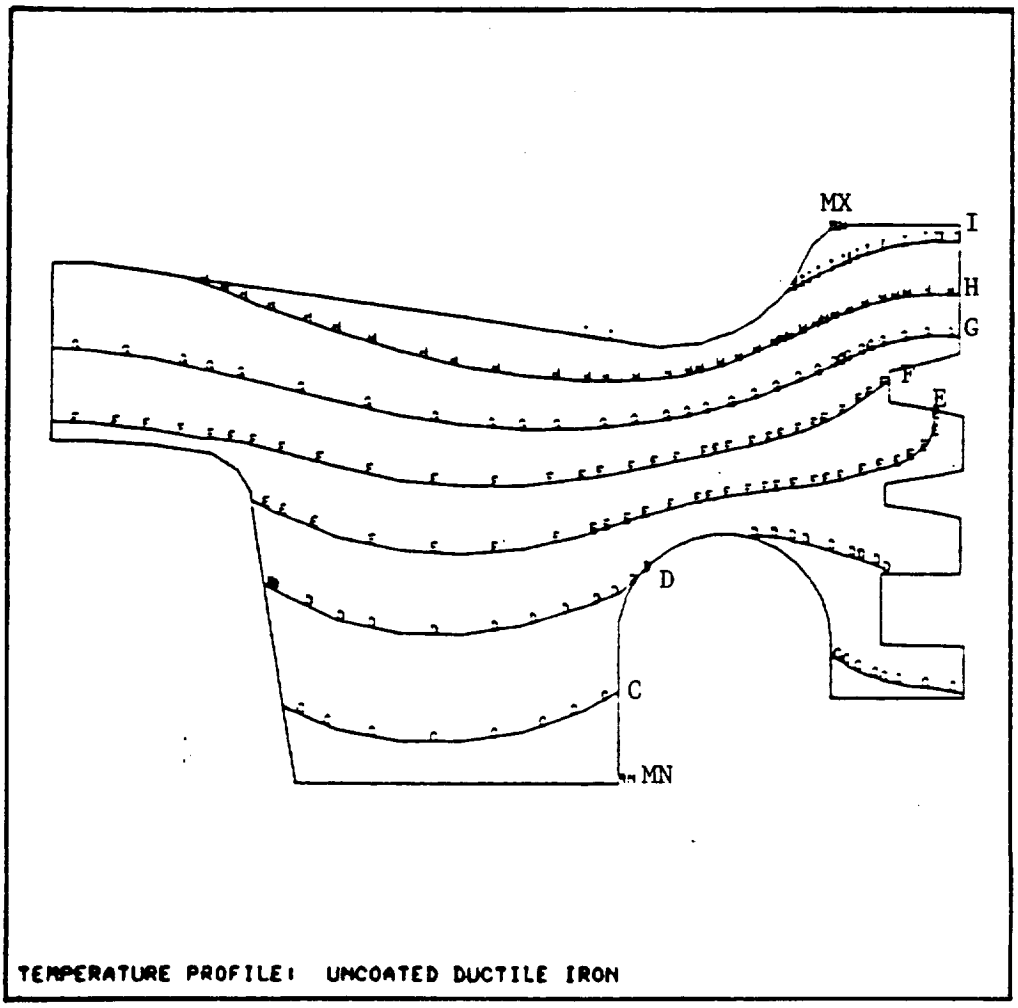

	C	F
MX	575	1065
MN	170	340
C	205	400
D	260	500
E	315	600
F	370	700
G	425	800
H	480	900
I	538	1000

Figure 3.8: Uncoated ductile iron piston temperatures, °F.

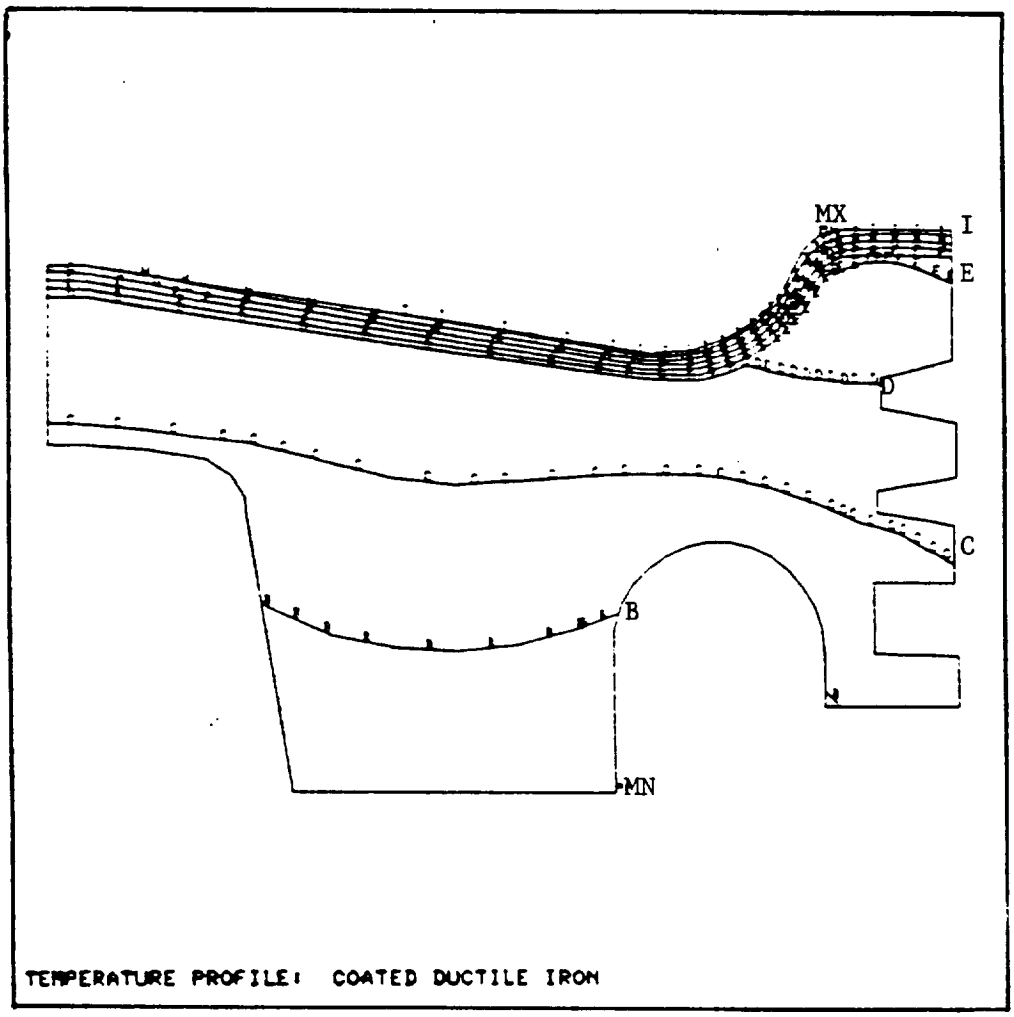

F	C
MX-1372	745
MN-296	147
B-375	190
C-500	260
D-625	330
E-750	400
F-875	470
G-1000	540
H-1125	610
I-1250	675

Figure 3.9: Coated ductile iron piston temperatures, F, 0.100" multilayer coating.

A finite element model of the cylinder head firedeck was constructed, and used to assess the effect of cooling strategy and ceramic coating on critical temperatures and heat rejection. This model is shown in Figure 3.10. A plane of symmetry was assumed through the injector centerline, with one intake and one exhaust valve considered in the analysis. The boundary conditions were carefully matched to measured engine data. The predicted heat rejection and cylinder head temperatures are summarized in Table 3.3. The water cooled baseline condition is reported first, followed by the case where the water coolant has been replaced with limited oil cooling. This case shows a significant reduction in heat rejection through the cylinder head, but an increase of approximately 130 C (266 F) in the maximum metal temperature. Coating the oil cooled cylinder head resulted in a further reduction in heat rejection while reducing the peak metal temperature by about 60 C from the uninsulated oil cooled case. The fatigue life of the cylinder head is determined to a great extent by its operating temperature. Thus, the use of ceramics provides an additional benefit in the control of component temperatures.

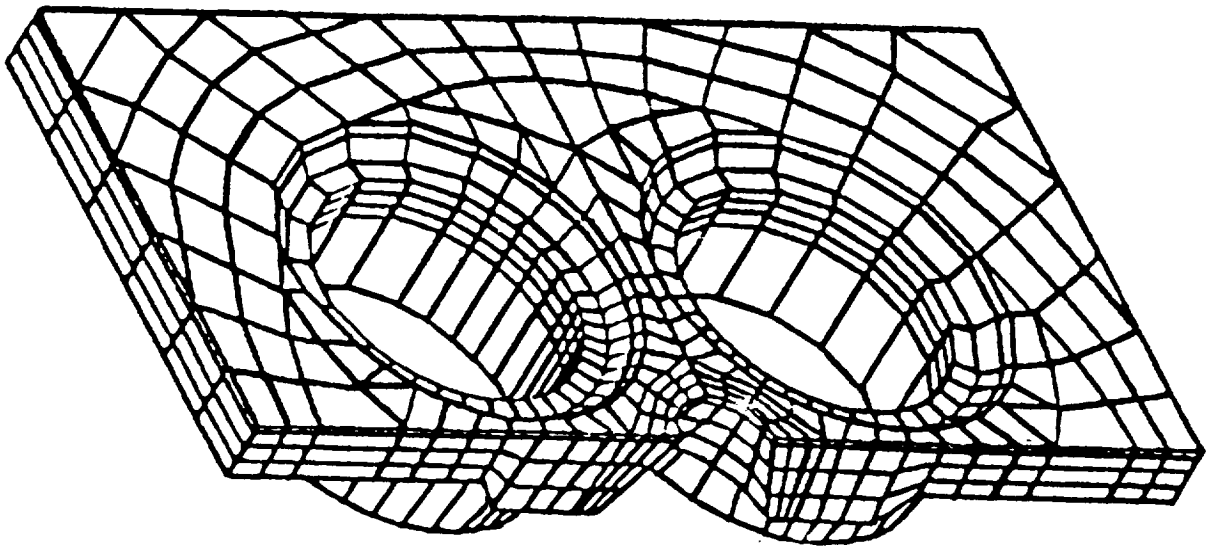

Figure 3.10: Model of cylinder head firedeck.

Table 3.3

Predicted Heat Rejection and Temperatures For Cylinder Head Firedeck

	Heat Rejection Through Firedeck (KW)	Max Surface Temperature (Deg. C)	Max Metal Temperature (Deg. C)
Water Cooled Baseline	33.3	314	314
Oil Cooled	23.4	448	448
Coated Oil Cooled, 0.100" Multilayer Coating	20.5	671	390

3.2 COMPONENT THERMOMECHANICAL ANALYSIS

Extensive thermomechanical modeling of various thermal barrier coating systems was conducted to identify coating systems that meet the thermal conductance goals while achieving the lowest overall state of stress. The initial analysis was comprised of one dimensional models to sort through various coating systems. Later analysis tasks evaluated geometric effects on stresses by two and three dimensional models. Because of the results from the diesel cycle modeling which suggested that only the cylinder head and piston required coating, the thermal barrier coatings were modeled on the piston and cylinder head surfaces. Initial emphasis was placed on the piston coating with a secondary emphasis on the cylinder head. Previous work at Cummins had demonstrated that the piston insulation failure was more common than cylinder head insulation [21].

The piston coating was modeled by United Technologies Research Center using a one dimensional model to obtain preliminary guidelines for the more detailed analysis. Cummins then conducted a one dimensional transient analysis and a two dimensional analysis of the coated piston. The cylinder head coating was modeled using a modified three dimensional model of an L10 cylinder head. Cylinder head geometry was similar for the L10 and V903 engine which allowed guidelines for cylinder head coatings to be inferred from this model.

The following sections described the results of the modeling effort.

3.2.1 One Dimensional Model - Coating

3.2.1.1 Coating Model - Thermal Conductance and Heat Flux

UTRC conducted a one-dimensional thermal stress analysis to provide an initial prediction of the operating temperature, heat rejection and state-of-stress present in a thick thermal barrier coating sprayed on a flat surface piston. The thermal structural analysis used was a one-dimensional linear elastic model which calculates the stress state developed in a multilayered coating. The development of this analysis is based on three assumptions. The first assumption states that the conditions being analyzed are far from any edges, therefore, assuming an infinite plate. No edge effects are taken into account in this analysis. The second assumption states that the through-thickness stress was equal to zero. This assumption is made by noting that, in plate theory, the through-thickness stress is small compared to the other stress components and can be neglected when there is no concentrated transverse load. The final assumption states that the in-plane stresses vary only in the through-thickness direction. This assumption simplifies the solution by making the problem one-dimensional.

The one-dimensional thermal-structural model was used to predict both the temperature gradients across layer interfaces of candidate coating systems and overall coating state-of-stress at maximum operating conditions. Predicted temperatures from the thermal analysis were used to predict stresses within the coating systems at a diesel engine maximum operating condition. This process allowed us to rank the candidate coating systems to select the coating system that best met the thermal conductance criteria and achieved the lowest overall state-of-stress. Boundary conditions representing the V903 engine were provided by

Cummins. For this initial one-dimensional model, existing properties from the previously generated UTC data base were used.

This model was calibrated by testing a series of coating specimens fabricated with different material properties. The model was then modified as needed to evaluate the influence of process variables on coating constituent material properties and, ultimately, on overall coating performance.

Five zirconia-based coating systems were identified for thermal-stress analysis. Since all five coating systems met the thermal conductance requirements, an additional three reduced coating thickness systems were evaluated to determine what improvement in coating stresses could be obtained by changing coating thickness. These systems are shown in Figure 3.11.

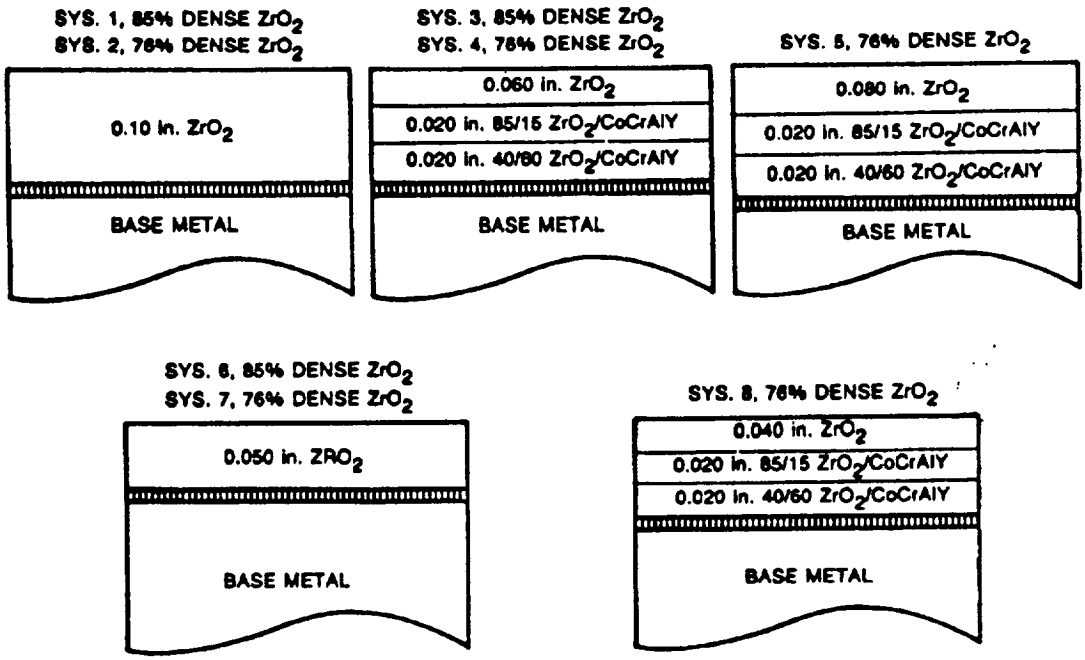

Figure 3.11: Various coating systems investigated representing eight coating systems.

Systems 1 and 2 were basically thick thermal barrier coatings, 2.54 mm (0.1 inch), with the zirconia layer being of different porosity levels in the two systems. Systems 3 and 4 incorporate two discrete ceramic/metallic layers to transition from the base metal to the top ceramic layer. System 5 is similar in composition to System 4 with the exception that the thickness of the 76% dense zirconia material was increased to 2.3 mm (0.080 inch). In Systems 6 and 7, the zirconia thickness is reduced by 50% in comparison to Systems 1 and 2. The calculated thermal conductance for System 7 is within the design criteria. The thermal conductance for the 85% dense zirconia coating of System 6 exceeds the design criteria by approximately 30 percent, but this system could be tailored to meet thermal conductance goals. System 8 is a second modification to System 4; it reduces the thickness of the 76% dense zirconia top coat from 1.5 mm (0.060 inch) to 1 mm (0.040 inch), and the overall coating thickness from 2.54 mm (0.10 inch) to 2.3 mm (0.080 inch). The resulting thermal conductance of this system is 360 W/m^2K (.44 $Btu/hr\text{-}in^2\text{-}F$) which is within the design criteria. The effect of coating thickness versus thermal conductance for each of the proposed systems is shown in Figure 3.12.

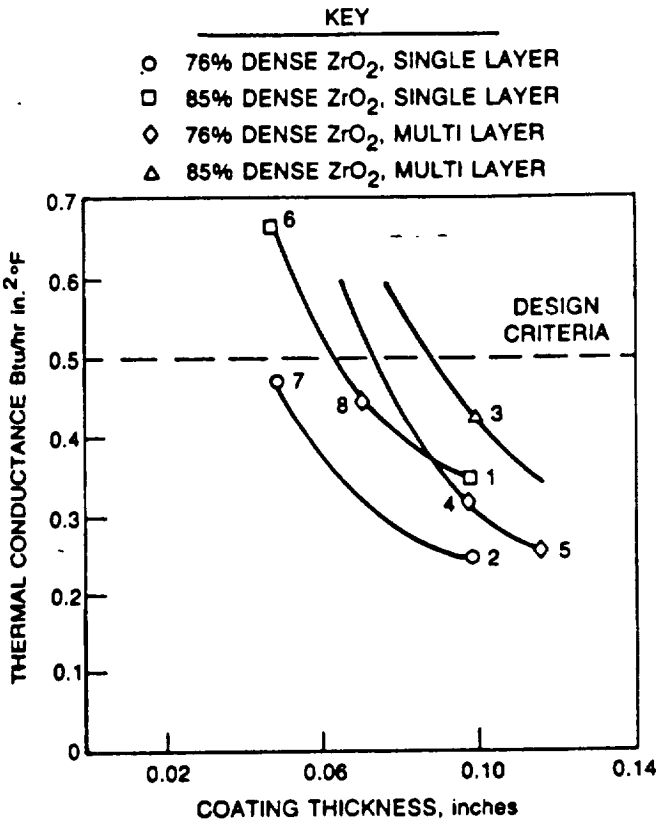

Figure 3.12: Thermal conductance of various coating systems. (Systems 1 through 8 described in Figure 3.11)

As part of the thermal stress analysis, all of the eight systems were placed on each of the three proposed piston substrates (ductile iron, superalloy and fiber-reinforced aluminum). Three stress-free fabrication temperatures were identified (low, medium, and high) for this parametric study. The stress-free fabrication temperature is the temperature at which the coating stresses are set equal to zero for modeling purposes. Each of the coating configurations were run at each of the three stress-free fabrication temperatures to calculate room temperature residual stress. From the calculated heat flow values, surface and interface temperatures were calculated for a maximum engine operating condition. These temperatures, as given in Table 3.4, were then used in the thermal structural analysis to determine the predicted operating stresses.

Table 3.4

PREDICTED MAXIMUM TEMPERATURE CONDITIONS

			Interface Temperatures, F				Heat Flow
System	Base Metal	T_c	T_1	T_2	T_m	T_{sink}	Btu/Min.
Baseline	Ductile Iron	1354	-	-	762	400	117
	B1900	1381	-	-	927	400	93
	Fiber/Aluminum	1259	-	-	563	400	134
1	Ductile Iron	1356	-	-	739	400	107
	B1900	1386	-	-	898	400	87
	Fiber/Aluminum	1275	-	-	556	400	120
2	Ductile Iron	1392	-	-	687	400	84
	B1900	1404	-	-	825	400	71
	Fiber/Aluminum	1309	-	-	542	400	89
3	Ductile Iron	1346	838	729	678	400	124
	B1900	1373	974	887	851	400	98
	Fiber/Aluminum	1248	657	531	467	400	144
4	Ductile Iron	1369	768	674	632	400	104
	B1900	1388	899	823	791	400	85
	Fiber/Aluminum	1280	607	506	454	400	116
5	Ductile Iron	1387	710	631	596	400	88
	B1900	1400	833	767	740	400	74
	Fiber/Aluminum	1304	570	484	444	400	75
6	Ductile Iron	1305	-	-	859	400	160
	B1900	1350	-	-	1047	400	119
	Fiber/Aluminum	1180	-	-	597	400	201
7	Ductile Iron	1336	-	-	797	400	133
	B1900	1368	-	-	974	400	103
	Fiber/Aluminum	1234	-	-	573	400	157
8	Ductile Iron	1342	852	738	687	400	128
	B1900	1370	989	901	862	400	101
	Fiber/Aluminum	1243	666	531	469	400	149

Calculated heat flow and temperature data for each of the systems, shown in Table 3.4 indicate the following trends:

1. As expected, based on thermal conductivity data, the superalloy substrate provided the best thermal resistance for all coating configurations, followed by ductile iron and fiber/aluminum piston materials.

2. Single-layer 76% dense zirconia systems provide a reduced heat flow in comparison to single-layer 85% dense zirconia systems.

3. Multilayered 76% dense zirconia systems provide a reduced heat flow over multilayered 85% dense zirconia systems. However, multilayered coatings slightly increase heat flow compared to single-layered systems, but multilayer systems have been found to reduce operating stresses.

It is possible to reduce the single-layer 76% dense zirconia thickness to 0.050 inch and still meet the design criteria of 410 W/m^2K (0.5 $Btu/hr\text{-}in^2\text{-}F$) which may provide added flexibility in controlling peak stresses anticipated on more complex surface geometry components.

Calculated thermal conductance values for several of the thick thermal barrier systems were well below the thermal conductance goal. In Figure 3.12, the minimum coating thickness is established to meet the thermal conductance goal for each system configuration. These data can be used to provide needed information to tailor a system for both low stresses and minimum heat losses.

3.2.1.2 Coating Model - Stress Analysis

The thermal boundary conditions were used to determine the thermal gradients through the coating systems and predict the thermally induced stress for ductile iron, an alumina-silica fiber reinforced aluminum, and a B1900 superalloy piston.

Tables 3.5 and 3.6 are a summary of the predicted residual or room temperature stresses for each coating layer on ductile iron and fiber/aluminum. The measured basic compressive strength is included in the tables for reference purposes. Stresses developed in-plane within the coating during fabrication exceeding the basic compressive strength of the material would be expected to fail the coating upon cooling from the stress free fabrication temperature to room temperature. Additionally, experience indicates that increased in-plane compression can generate out-of-plane tensile stresses that could result in failure when a two-dimensional or three-dimensional state-of-stress is considered. Therefore, an approximate 70% design margin should be applied to compressive strength data when assessing the results of the one-dimensional stress analysis. By definition, this structural analysis would not accurately predict local stresses in areas of maximum curvature change across the piston head surface. Consideration should be given to geometry redesign to minimize these effects within both the piston bowl and at the outer edge of the crown.

Table 3.5

Predicted Room Temperature Stresses For Coating on Ductile Iron

		Coating Stress, ksi			
		85% Dense ZrO_2	76% Dense ZrO_2	85/15 ZrO_2/CoCrAlY	40/60 ZrO_2/CoCrAlY
Measured Basic Compressive Strength		-42	-15	-48	-71
System	Stress-Free Fabrication Temperature				
1	low	-0.54	-	-	-
	intermediate	-1.01	-	-	-
	high	-1.48	-	-	-
2	low	-	-1.98	-	-
	intermediate	-	-3.70	-	-
	high	-	-5.43	-	-
3	low	-0.42	-	-4.67	-0.94
	intermediate	-0.87	-	-8.74	-1.76
	high	-1.28	-	-12.4	-2.58
4	low	-	-1.96	-4.57	-0.81
	intermediate	-	-3.66	-8.57	-1.50
	high	-	-5.36	-12.5	-2.20
5	low	-	-1.93	-4.52	-0.75
	intermediate	-	-3.61	-8.52	-1.39
	high	-	-5.29	-12.4	-2.04

Table 3.6

Predicted Room Temperature Stresses For Coating on Fiber/Aluminum

		Coating Stress, ksi			
		85% Dense ZrO_2	76% Dense ZrO_2	85/15 ZrO_2/CoCrAlY	40/60 ZrO_2/CoCrAlY
Measured Basic Compressive Strength		-42	-15	-48	-71
System	Stress-Free Fabrication Temperature				
1	low	-4.55	-	-	-
	intermediate	-8.51	-	-	-
	high	-12.4	-	-	-
2	low	-	-5.09	-	-
	intermediate	-	-9.51	-	-
	high	-	-14.0	-	-
3	low	-4.24	-	-10.1	-8.22
	intermediate	-7.92	-	-18.9	-15.4
	high	-11.6	-	-27.7	-22.5
4	low	-	-4.87	-10.0	-8.11
	intermediate	-	-9.10	-18.8	-15.2
	high	-	-13.3	-27.5	-22.2
5	low	-	-4.74	-9.83	-7.84
	intermediate	-	-8.85	-18.4	-14.6
	high	-	-13.0	-27.0	-21.5

For Systems 1 through 5, fabrication on ductile iron would produce a successful coating, as predicted stresses are well below the basic strength. This is also true for superalloy where room temperature stresses were predicted to be approximately 60% greater than those for the coating on ductile iron. Since the stresses for ductile iron are low, this is still well within the acceptable range. When using fiber/aluminum as the base metal, the stresses are 2 1/2 to 10 times greater than the ductile iron stresses, in some cases approaching the compressive strength of the coating. As expected, increasing the fabrication temperature increases the room temperature residual stresses. From the stresses reported in Table 3.6, it can be seen that the high stress-free fabrication temperature, in combination with the 76% dense zirconia top coat may fail upon cooling to room temperature. Incorporation of metal bearing layers helps to reduce the level of compressive stress developed in the zirconia layer, but not significantly enough to warrant additional design efforts.

Figure 3.13 is a comparison of residual coating stresses at room temperature for each substrate material at the intermediate stress-free fabrication temperature.

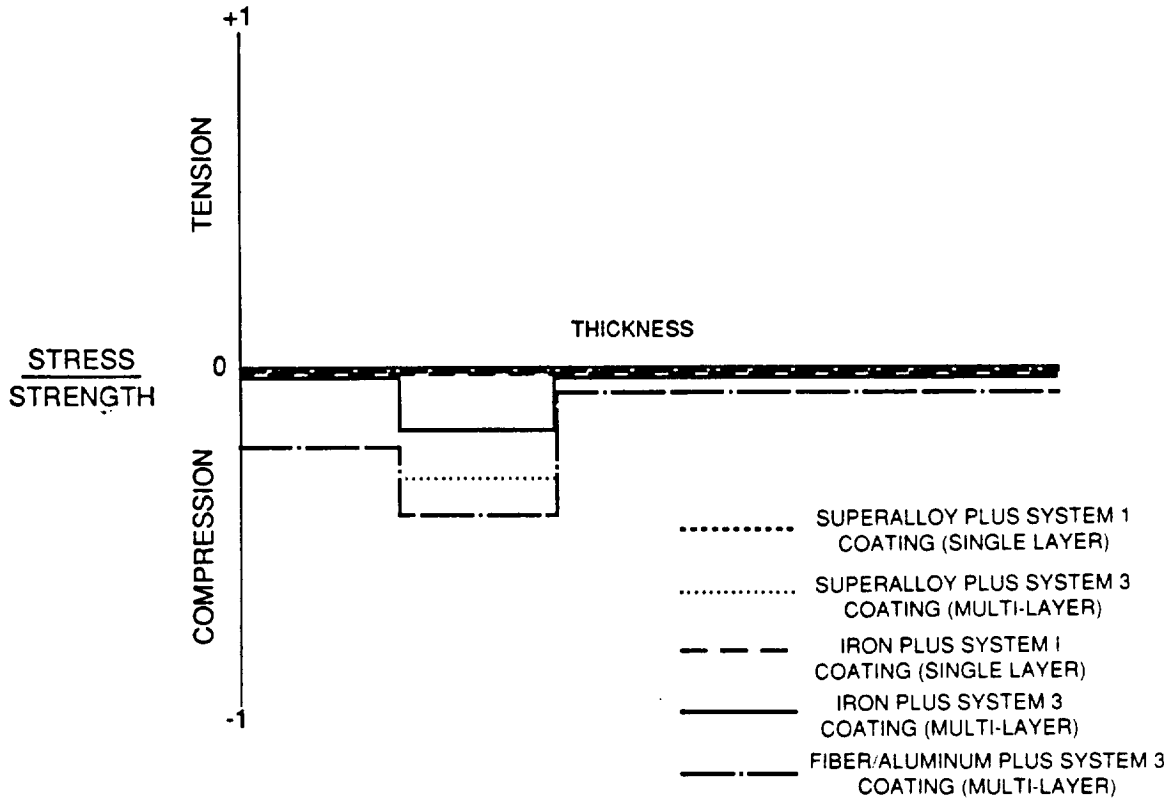

Figure 3.13: Predicted residual coating stresses at room temperature for the intermediate stress-free fabrication temperature.

The most important trends are summarized based on the analysis of the effect of stress free fabrication temperature:

- Single-layer coating systems produce lower residual stresses at all fabrication temperatures. Multilayer coating systems produce slightly lower stresses in the top zirconia layer at the expense of increased tensile stresses at the top of the base metal.

- Single-layer coatings for both ductile iron and superalloy base metals are most uniform and lowest stressed.

- Multilayered coating systems produced peak stresses in the 85/15 ZrO_2,/CoCrAlY layer. These peak stresses can be reduced by either tailoring the stress-free fabrication temperature in the area of peak stress or by adjusting the composition of the 85/15 layer to more closely match the material properties of its neighboring layer's.

- Independent of the operating state-of-stress differences for these coating systems, the ease of fabrication of the single-layer systems should not be overlooked.

Typical through coating thickness stress distribution profiles on a superalloy substrate are shown in Figure 3.14. The state-of-stress in each coating configuration at a high stress-free fabrication is noted for both the residual and a maximum test condition. Single-layer coating systems are in compression at the top of the coating and in tension at the bond/substrate interface. A reduction in ceramic layer thickness favorably decreases in-plane compressive stress with a corresponding slight increase in in-plane tensile stress within the coating. In-plane tensile stress in the ceramic top layer can be reduced through the use of multilayer coating systems.

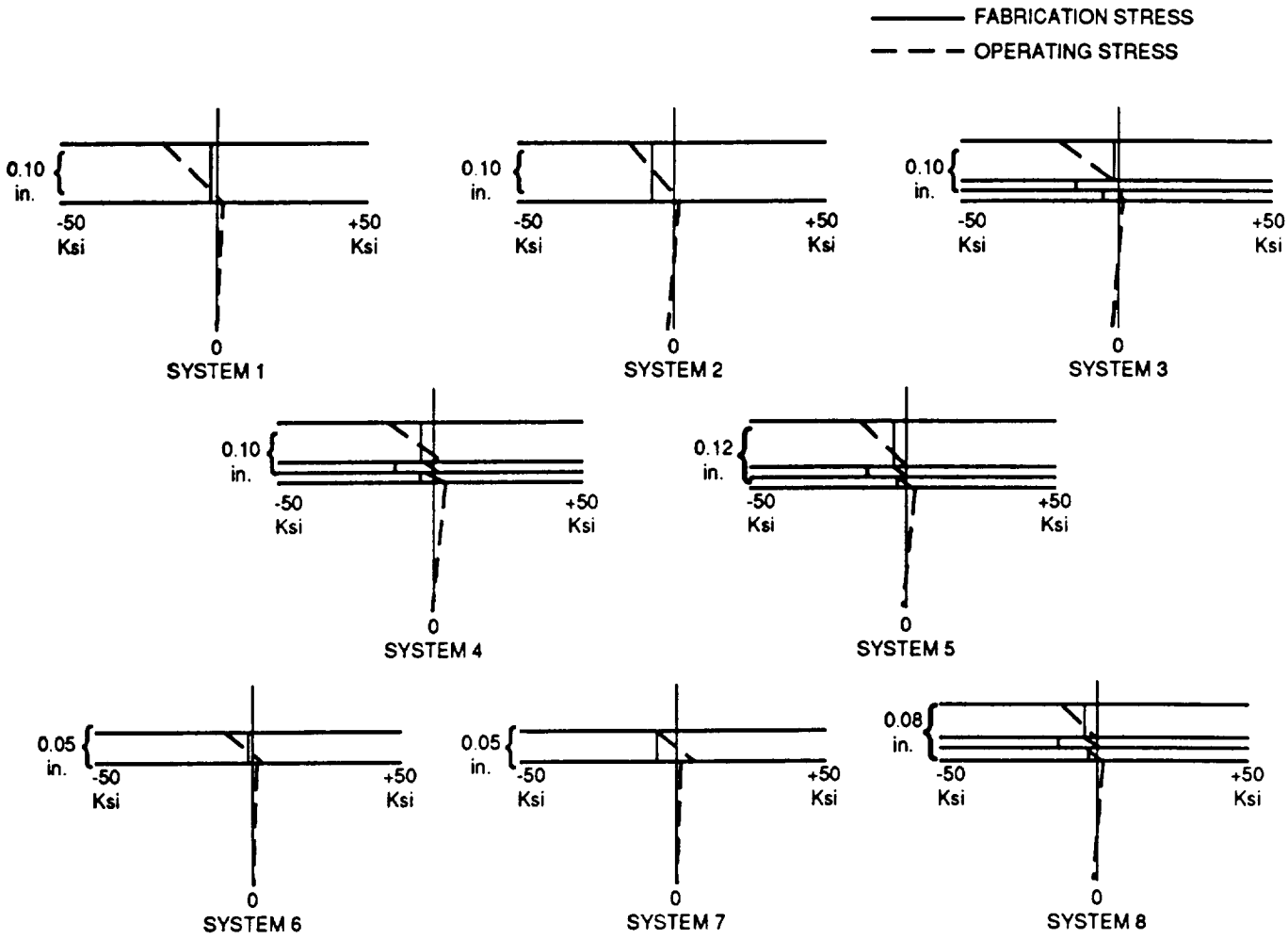

Figure 3.14: Typical stress distribution profiles on a superalloy substrate when fabricated at the high stress free temperature.

Furthermore, as shown in Figure 3.15, multilayer coating systems sprayed on a superalloy substrate produce a lower predicted state-of-stress during a maximum engine operating condition. Again, local prestress and material compositional changes will further reduce peak stresses and result in the most neutral state-of-stress through the coating thickness. Additionally, multilayer coating systems reduce local tensile stresses at the coating to substrate interface which have been predicted to be greater in single-layer coating systems. In reference to Figure 3.15, coating systems applied to the fiber reinforced aluminum base metal have the highest in-plane compressive stresses at maximum engine operating point. Increased tensile stresses in the base metal are predicted and, therefore, necessitates an in-depth evaluation of bond coat systems for the fiber reinforced aluminum which are compatible to the coating system.

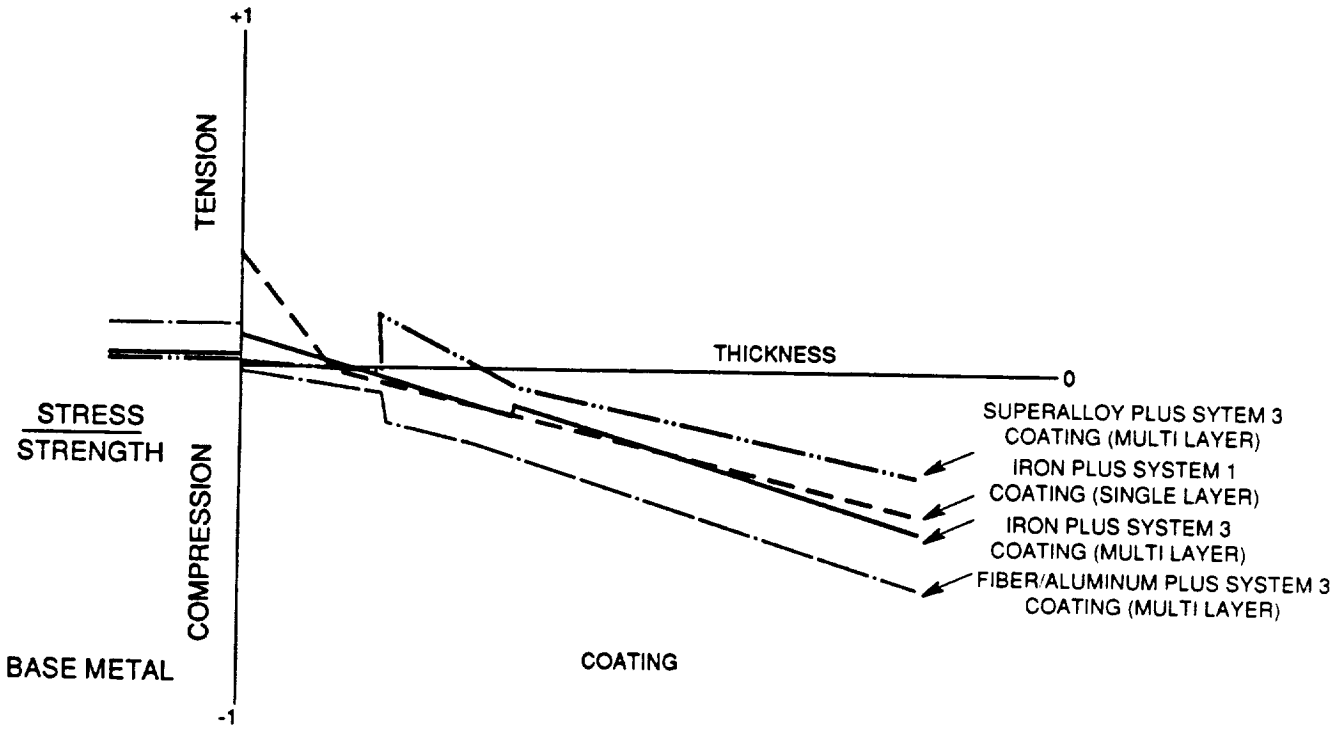

Figure 3.15: Predicted coating stress developed at the maximum engine operating conditions.

The fiber/aluminum base metal generates higher compressive stresses at all temperatures. Coating systems comprised of the 85% dense zirconia top layer may be successfully fabricated with lower probability of failure as the coating residual stresses are well below the measured basic compressive strength of the constituent layers. Coating systems comprised of an 76% dense zirconia top layer may be successfully fabricated at lower fabrication temperatures. However, as the fabrication temperature is increased, more compressive stress is built into the system such that, at the high fabrication temperature, the coating would be expected to separate from the substrate upon cooling to room temperature.

Typical coating stress data predicted at a maximum engine operating condition shown in Figure 3.15 indicates the following trends:

- Single-layer coating systems are in compression at the top of the coating and tension at the bond/substrate interface.

- Multilayer coating systems reduce in-plane tensile stress in the ceramic top layers.

- Reduced total thickness coating systems exhibit slightly increased in-plane tensile stress at the ceramic to metal bearing layer interface with a corresponding decrease in compressive stress at the top of the all-ceramic layer. This change is viewed as significant since thermal barrier coatings can fail under excessive compressive loading.

Base metal residual and operating stresses were also calculated. No substrate yielding problems are anticipated with either ductile iron or superalloy.

In summary, for all base metals, coating system 3 shown in Figure 3.11, produced the lowest predicted stresses at both room temperature and engine operating conditions. These analyses confirm that thermal barrier coatings sprayed an a superalloy base metal would produce both the most durable, longest life; and lowest heat rejection system. However, the superalloy is the most expensive substrate. Therefore, for economic considerations ductile iron and a fiber reinforced aluminum alloy were selected for further evaluation.

3.2.1.3 L10 Piston Crown Model

In addition to the V903 research engine modeling, some limited modeling of a L10 engine was conducted. This work effort was initiated because of plans to conduct a limited amount of L10 evaluation. When conducting the one-dimensional thermal-structural analysis for the L10 piston crown, the properties input into the model reflect actual material properties measured for the single-layer constituents of the coating system generated during the V903 development effort. A standard gas temperature and a peak gas temperature were defined by Cummins Engine. The standard gas temperature was 14 C (26 F) lower than that used for the baseline multilayer coating/ductile iron V903 configuration (1460 F vs 1486 F). Other significant differences in the L10 model were in the reduced surface area of the piston crown (0.85 f^2) for the V903 vs 0.151 f^2 for the L10) and the increase in the thermal conductivity of the steel base metal over the ductile iron by a factor of two.

Analytical predictions from the L10 thermal-structural model of a 2.54 mm (0.100 inch) baseline multilayer coating at two prestress temperature levels reflected these differences relative to the V903.

- Calculated heat flows for the multilayer coating were found to be 9% lower than those for the V903 configuration due to the reduced surface area of the piston crown.

- Predicted top surface temperature was less for the L10 configuration at the standard gas temperature of 793 C (1460 F).

- Top surface temperatures were found to increase from 1304 F to 1508 F under the peak gas temperature condition of 927 C (1700 F).

- Predicted interface temperatures decreased by as much as 18% at the standard gas temperature. The most significant decrease occurred at the bond to base metal interface.

- The interface temperature increased from 292 C (558 F) to 312 C (594 F) for the bond/base metal at the peak temperature condition.

- The compressive stress within the coating was reduced by as much as 40% for the peak operating condition primarily as a result of the lower elastic modulus for the V903 material relative to the UTRC data base.

- The overall state-of-stress decreases with reduction in coating thickness consistent with V903 predictions.

In addition, a modified top layer zirconia material was considered in order to increase the strength of the layer and durability of the overall coating system. Two gun power levels identified as Power Mod. 1 and Power Mod. 2 and representing a 6% and a 12% increase in gun power level, respectively, over the baseline were used for spray fabrication trials. Properties were measured for the resulting materials and incorporated into the thermal-structural model. Substitution of the top coat material had minimal effect on the calculated heat flow and predicted top surface and interface temperatures. Likewise, substitution of an increased strength top layer material into the thermal-structural model slightly decreased the overall coating state-of-stress. This result was attributable to the increase in both strength and modulus relative to that achieved with the baseline V903 sprayed coating material.

Thermal conductance, heat flow and predicted interface temperatures are summarized in Tables 3.7 and 3.8. Thermal stresses for selected test cases are shown in Figures 3.16 through 3.17.

Table 3.7

Thermal Conductance and Heat Flow L10 Configuration

System Configuration				
Composition	Thickness mils	Tgas	Thermal Conductance (Coating) Btu/hr-in^2 F	Heat Flow (System) Btu/min
Standard Engine Condition				
ZrO_2/15,40/60 (V903 Baseline)	60,20,20	1460	0.42	113
	40,20,20	1460	0.56	138
	20,20,20	1460	0.86	176
ZrO_2,85/15,40/60 (Power Mod. 1)	40,20,20	1460	0.52	131
	20,20,20	1460	0.81	171
ZrO_2,85/15,40/60 (Power Mod. 2)	40,20,20	1460	0.53	133
	20,20,20	1460	0.82	172
Peak Engine Condition				
ZrO_2,85/15,40/60 (Baseline)	60,20,20	1700	0.42	139
	40,20,20	1700	0.56	170
	20,20,20	1700	0.86	217
ZrO_2,85/15,40/60 (Power Mod. 1)	40,20,20	1700	0.52	161
	20,20,20	1700	0.81	210
ZrO_2,85/15,40/60	40,20,20	1700	0.53	163
	20,20,20	1700	0.82	212

Table 3.8

Temperature Conditions For Engine Operation Test Cases L10 Piston Crown Configuration

System Configuration				Interface Temperature, F			
Composition	Thickness mils	Tgas	Tsink	Tc	T1	T2	Tm
The following predicted temperatures are for a standard engine condition.							
ZrO_2,85/15,40/60 (V903 Baseline)	60,20,20	1460	400	1304	741	616	558
	40,20,20	1460	400	1270	813	662	592
	20,20,20	1460	400	1217	925	734	646
ZrO_2,85/15,40/60 (Power Mod. 1)	40,20,20	1460	400	1279	794	650	583
	20,20,20	1460	400	1225	910	724	638
ZrO_2,85/15,40/60 (Power Mod. 2)	40,20,20	1460	400	1277	798	653	585
	20,20,20	1460	400	1223	913	726	640
The following predicted temperature are for a peak engine condition.							
ZrO_2,85/15,40/60 (V903 Baseline)	60,20,20	1700	400	1508	818	665	594
	40,20,20	1700	400	1466	907	722	637
	20,20,20	1700	400	1401	1044	810	703
ZrO_2,85/15,40/60 (Power Mod. 1)	40,20,20	1700	400	1478	882	706	625
	20,20,20	1700	400	1411	1023	797	692
ZrO_2,85/15,40/60 (Power Mod. 2)	40,20,20	1700	400	1475	889	710	628
	20,20,20	1700	400	1408	1028	800	695

where Tc = maximum coating temperature
T_1 = zirconia 85/15 interface temperature
T_2 = 85/15 - 40/60 interface temperature
Tm = metal temperature

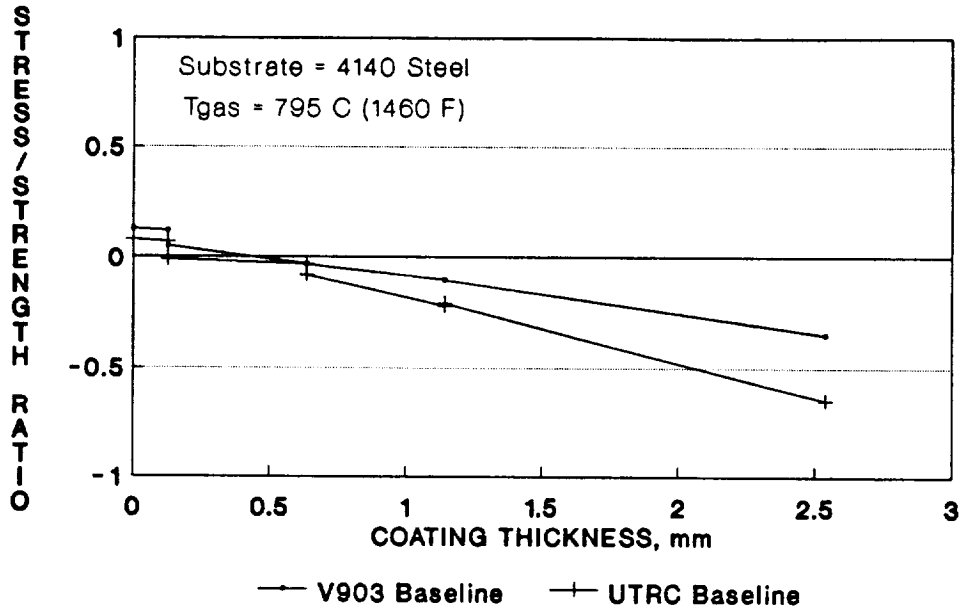

L10 Standard Conditions
High Prestress

Figure 3.16: Stress/strength ratio for multilayer coating on piston.

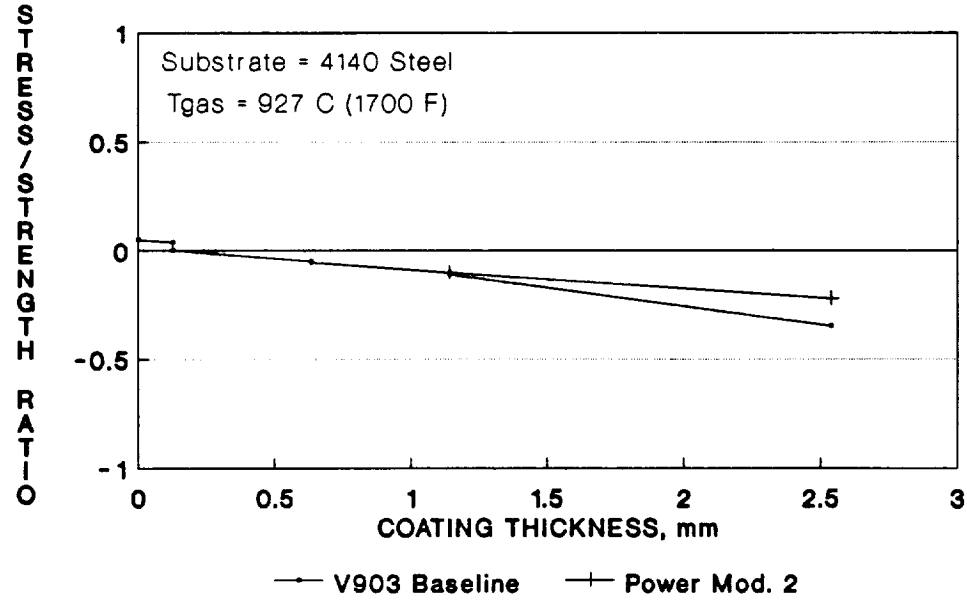

L10 Peak Conditions
High Prestress

Figure 3.17: Stress/strength ratio for multilayer coating on piston.

In summary, the one-dimensional thermal-structural model provided a fundamental understanding of thickness and prestress effects for ranking candidate coating systems. This model provided a simplified means to evaluate variable operating conditions and loads associated with different diesel piston crowns such as V903 and L10. Multilayer coatings were predicted to meet thermal conductance criteria and provide the lowest overall state-of-stress.

3.2.1.4 Analysis of Thermal Transients

It has previously been demonstrated in several studies that it is important to consider thermal transients when designing with ceramic materials. The low thermal diffusivity of the ceramics causes their temperatures to quickly respond to changes in operating environment, while the temperatures of the base materials respond much more slowly. This causes significantly different temperature and thermal stress profiles to be encountered under transient operation than those observed at steady-state.

Transients need to be considered at two levels. First, even at steady-state operation the combustion chamber surfaces are continually exposed to rapidly changing gas conditions. The temperature, pressure, velocity, and composition of the in-cylinder gases continually change as the engine goes through the various strokes of its operating cycle. In a four stroke engine operating at 2000 RPM this transient cycle will be experienced 1000 times per minute. In this section these transients will be referred to as cyclical transients. The second type of transient which must be considered is that associated with changes in engine operating conditions. Changes in engine speed, and more importantly load, bring about changes in the in-cylinder gas conditions to which the combustion chamber surfaces are exposed.

Although important to consider, transient analysis is often rejected because of the excessive computational time required. Single step changes in load generally require 10 to 15 computational runs, and the cyclical transients described above require 60 or more. This becomes prohibitive even with a simple two-dimensional model such as the piston considered in the steady-state analysis. For this reason a simple finite element model, representative of an infinite flat plate to which a ceramic coating was applied, was constructed for the coating. The model was constructed to provide a detailed representation of the coating, while being simple enough to assess transient operation with reasonable calculation time. The model was constrained against horizontal movement on two planes. The remaining vertical planes were constrained to move in a fixed plane - the horizontal displacement of all elements in the plane must be the same. In this way the model was made representative of an infinite plate. Thermal boundary conditions were applied on the two horizontal faces, that exposed to the combustion gas at the top, and that exposed to coolant at the bottom. This is representative of the United Technologies "System 3" coating applied to ductile iron. A reference temperature of 370 C was used in this analysis. This was assumed to be the temperature at which the coating was applied, and would therefore be the zero-stress condition.

The first transient considered was a sudden cooling of the combustion face. Calculations were made at steady-state for conditions representative of full load operation at rated speed. At time equals zero, the in-cylinder conditions were suddenly changed to those representative of no-load conditions. The changes in temperature through the coating with time are

summarized in Figure 3.18. As can be seen, the surface temperature drops rapidly, while the interior temperature of the coating reacts more slowly. With increasing time, the dropping temperature penetrates further into the coating. The thermal stresses in the coating are summarized in Figure 3.19. The trend shows a relaxation of the compressive stress at the surface with time. This results in a slight reduction in the tensile stress experienced in the bond coat adjacent to the substrate.

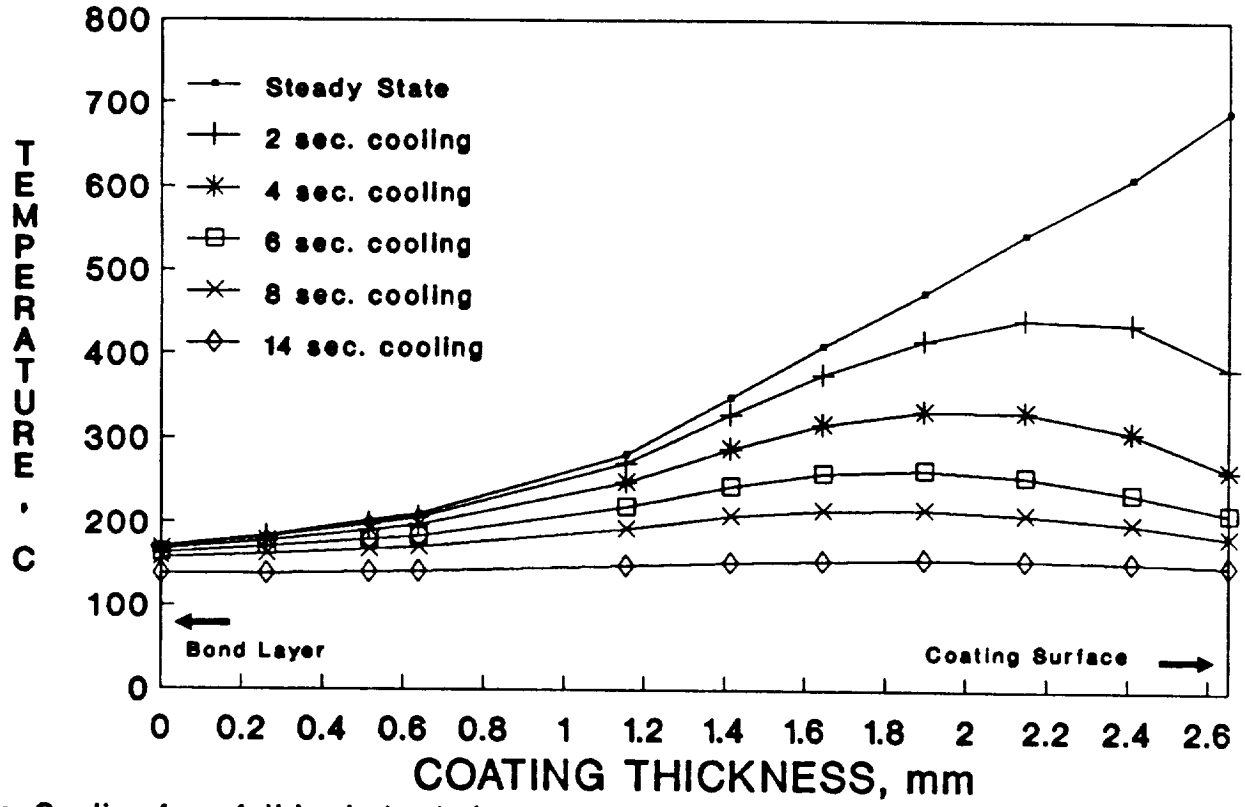

Note: Cooling from full load at rated speed.

Figure 3.18: Effect of deceleration on coating temperatures.

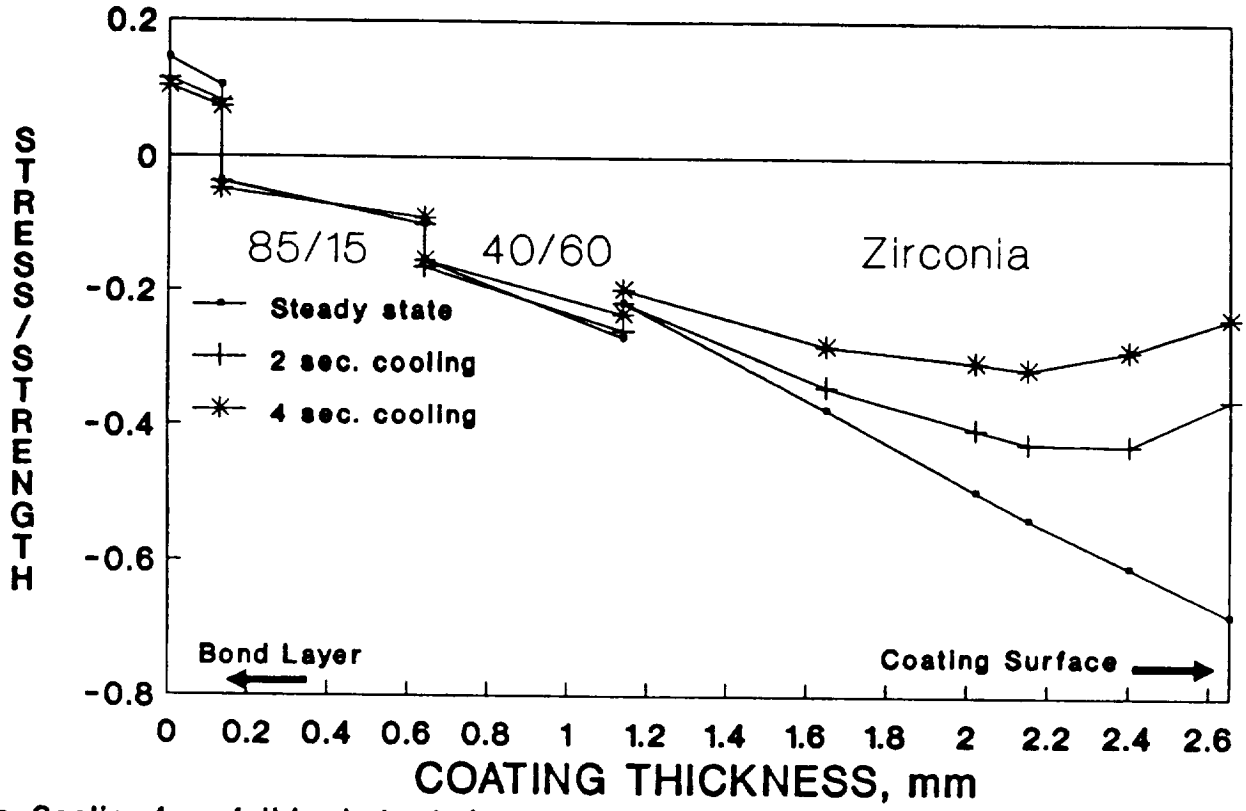

Figure 3.19: Effect of deceleration on coating stresses.

The second transient considered was that of a sudden load increase. In this case, the rapid increase in load from zero to full load is considered - a reversal of the step change in boundary conditions considered previously. Although a step change is an accurate portrayal of the in-cylinder changes seen in load reduction, it is more severe than would actually be seen during increasing load. The actual change would occur over a three to five second ramp governed by turbocharger response capability. The transient modeling is thus slightly more severe than would actually occur in an operating engine. The change in coating temperature is shown in Figure 3.20. Again it can be seen that the surface temperature reacts rapidly while the interior temperature changes more slowly. The changes in thermal stress throughout the coating are portrayed in Figure 3.21. As expected, the compressive stress increases most rapidly at the surface, showing a slight overshoot of the steady-state value due to the slower temperature increase of the coating interior. More significant, though still not predicted to be prohibitive, was an increase in the tensile stress within the bond coat, reaching a maximum almost twice that seen at steady-state, early in the transient.

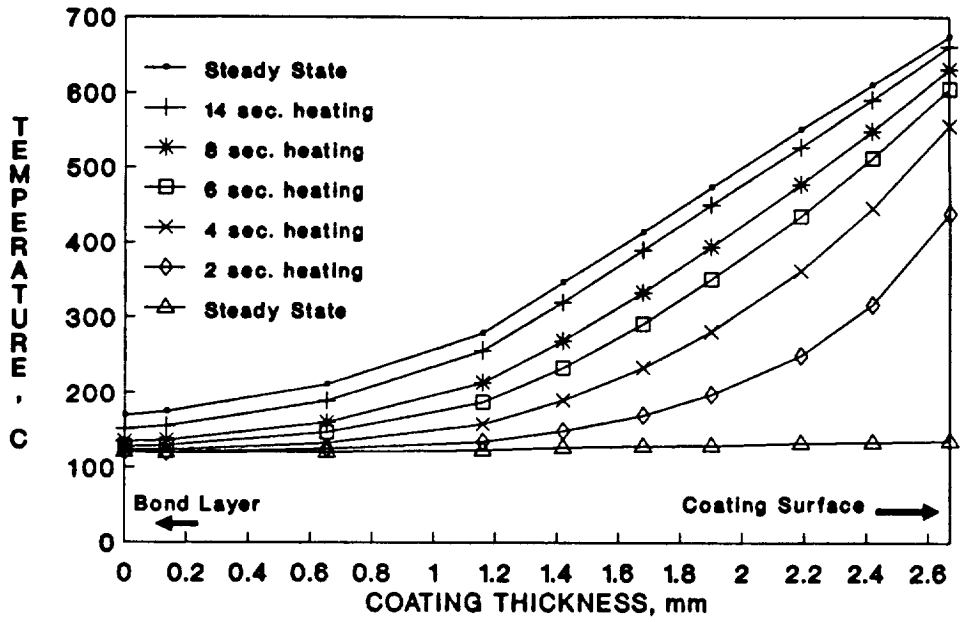

Note: Load increased from zero to full load.

Figure 3.20: Effect of acceleration on coating temperature.

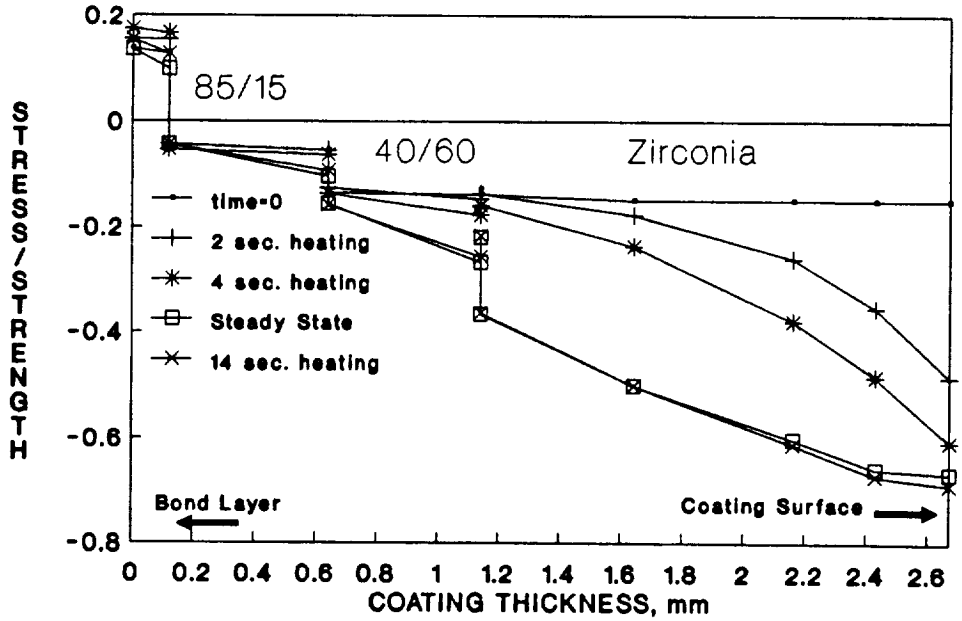

Note: Load increased from zero to full load.

Figure 3.21: Effect of acceleration on coating stresses.

In order to address firing cycle transients, a diesel cycle simulation program was utilized to generate predicted changes in the gas temperature and heat transfer coefficient with crank angle.

The surface temperature swing predicted by this model is shown in Figure 3.22, where temperature through the coating is plotted. A predicted surface temperature swing of 225 C (437 F) resulted, which was primarily additive to the 675 C (1250 F) cyclical average temperature. The penetration depth of the transient, as shown in Figure 3.22, was predicted to be approximately 0.13 mm, with temperatures beneath this depth matching the previously calculated steady-state values. This zone was slightly more than two element thicknesses into the finite element model (element spacing near the surface was 0.05 mm). The resulting surface stress envelope is shown in Figure 3.23. As can be seen from the figure, stresses at the surface were predicted to approach the compressive strength of the coating. This localized compressive stress would be expected to result in shallow surface cracking.

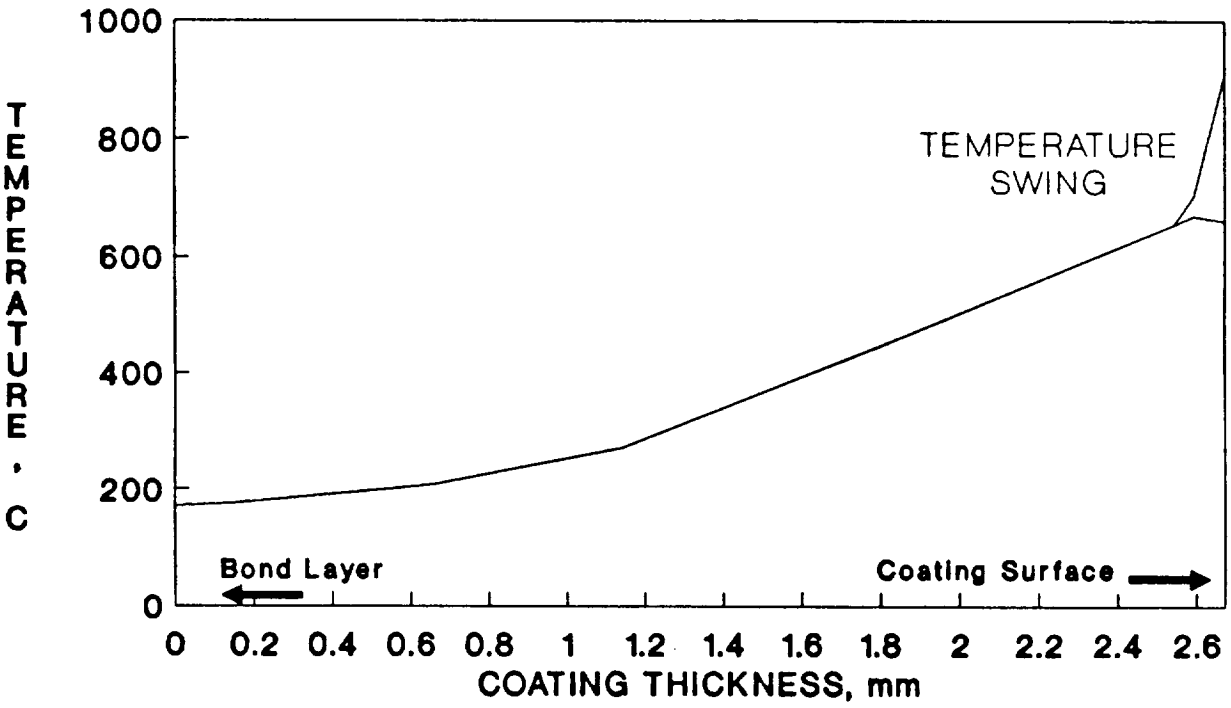

Figure 3.22: Effect of firing cyclic transient on coating temperature swing.

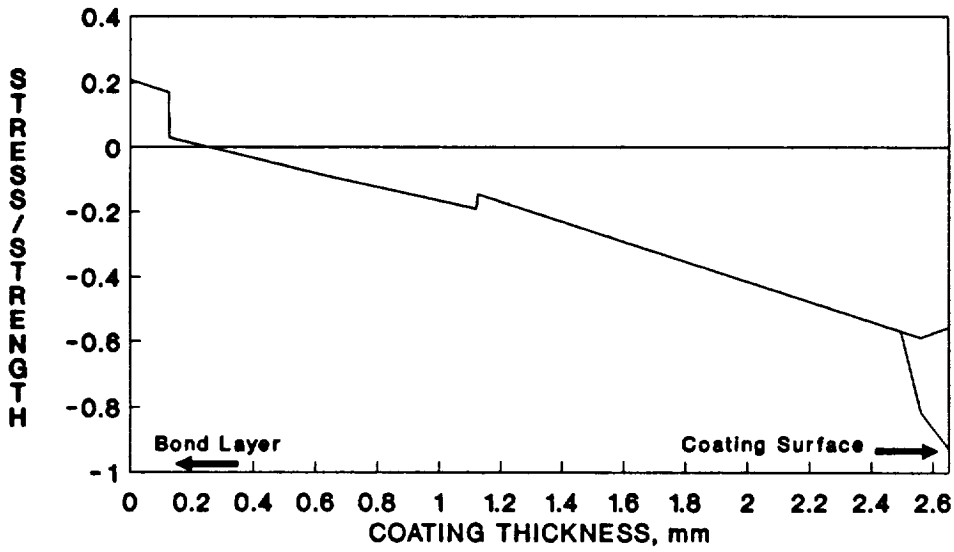

Figure 3.23: Effect of firing cyclic transient on stress/strength ratio showing deviation at coating surface.

Through this simple finite element model, it has been shown that:

1. Temperature and stress profiles under transient conditions were found to be significantly different than those at steady-state.

2. Engine load changes, though resulting in a change in stress profiles, were not predicted to result in coating failure for the cases considered.

3. Firing cycle transients resulted in a predicted surface temperature swing of 225 C, and resulted in increased compressive stresses in the surface layers of the coating. These were predicted not to penetrate further than 0.13 mm into the coating.

3.2.2 Two Dimensional Model - Piston

A two dimensional axisymmetric finite element model was used for the stress analysis of various thermal barrier coating designs. The primary reason for choosing this type of model was to gain insight into the effects that piston geometry might have on the stresses within a thick thermal barrier coating. The ANSYS finite element program was used for all phases of the modeling effort: preprocessing, solving, and postprocessing. The mesh is shown in Figure 3.24. The dense mesh on the top of the piston corresponds to the ceramic coating. A piston model with a significant metal thickness was used for comparison of the various piston substrate materials. The effects of the thick crown geometry were expected to be minimal, since in all piston design cases the piston crown can be considered thick compared to the

coating thickness. Also, due to the difficulty of modeling the bond coat it was decided to consider the bond coat to be part of the substrate. This assumption was reasonable based on the examination of failed piston coatings. The ceramic coating tends to separate from the bond coat, while the bond coat remains attached to the substrate. The piston model and boundary conditions represent an articulated oil cooled piston operating in a low heat rejection V903 diesel engine at 2600 RPM.

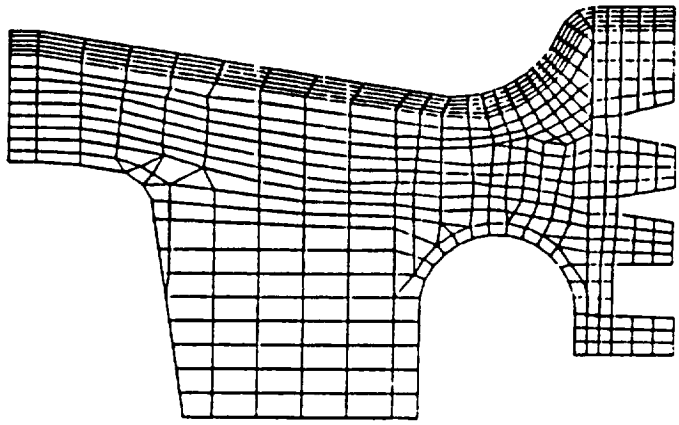

Figure 3.24: Finite element axisymmetric model.

Several coating systems were considered: a layered system with a 2.5 mm thickness; a layered system with a 1.5 mm thickness; a variable thickness layered coating; and, various thicknesses of a single layer coating. These ceramic coatings were modeled in conjunction with three piston materials, or substrates: fiber reinforced aluminum, ductile iron, and a superalloy (nickel-based B1900).

Two types of loading were considered: thermal and pressure. A uniform gas temperature was applied as a boundary condition above the piston. Although the actual gas temperature varies as a function of many factors (turbomachinery configuration, engine load, position, and etc.), 850 C was felt to be representative of the combustion gas temperature. The cylinder pressure was assumed to be 13.8 MPa (2000 psi) based on the engine operating conditions (600 HP V903 operating at 2600 RPM).

To evaluate the effect of coating thickness on the magnitude of stress, a single substrate, a ductile iron piston substrate was chosen. Single layer coating thicknesses of 0.5, 1.0, 1.5, 2.0 and 2.5 mm were applied to the ductile iron. The coating material consisted of zirconia. Figure 3.25 illustrates the dependence of coating stress on coating thickness. Maximum principal stresses in the ceramic coatings were found to be linearly related to coating thickness.

It was of interest to investigate the contribution that each type of loading (pressure and thermal) contributed to the total coating stress contour. It was necessary to present the contours in a distorted shape to clarify the stress distribution. (Refer to Figure 3.24 for geometric perspective.) Figure 3.26 shows the stress distribution resulting from the application of the 13.8 MPa (2000 psi) pressure loading for a 2.5 mm thick layered coating. The resulting stresses were relatively low and considered to be insignificant compared to the thermal stresses. The effects of thermal loading are presented in Figure 3.27. Very high tensile stresses were produced. Figure 3.28 illustrates the stress field resulting from the composite loading condition. Note that the maximum stress appears on the top land of the piston crown. This result is dependent upon boundary conditions and may be manipulated by changing the top ring location. Further, note that the effect of the pressure loading was to reduce the high tensile stresses resulting from thermal loading. Figures 3.29 and 3.30 illustrate the stress fields resulting from the use of ductile iron and fiber aluminum substrates, respectively. Of particular interest was the large increase in the maximum stress observed with the use of the fiber aluminum substrate. It must be acknowledged that the material properties data set for this material was not as complete as the data sets for ductile iron and superalloy. Although this short-coming certainly affected the analysis results, the excessively high stresses predicted serves as a cautionary note.

The layered coating was also analyzed for a thickness of 1.5 mm on all three substrates. Coating thickness affected maximum stresses, but had only a small effect on the stress distribution; therefore, the stress contours for the 1.5 mm thick layered coating are not shown. Table 3.9 offers a comparison of the stresses associated with the two different coating thicknesses for each of the substrates.

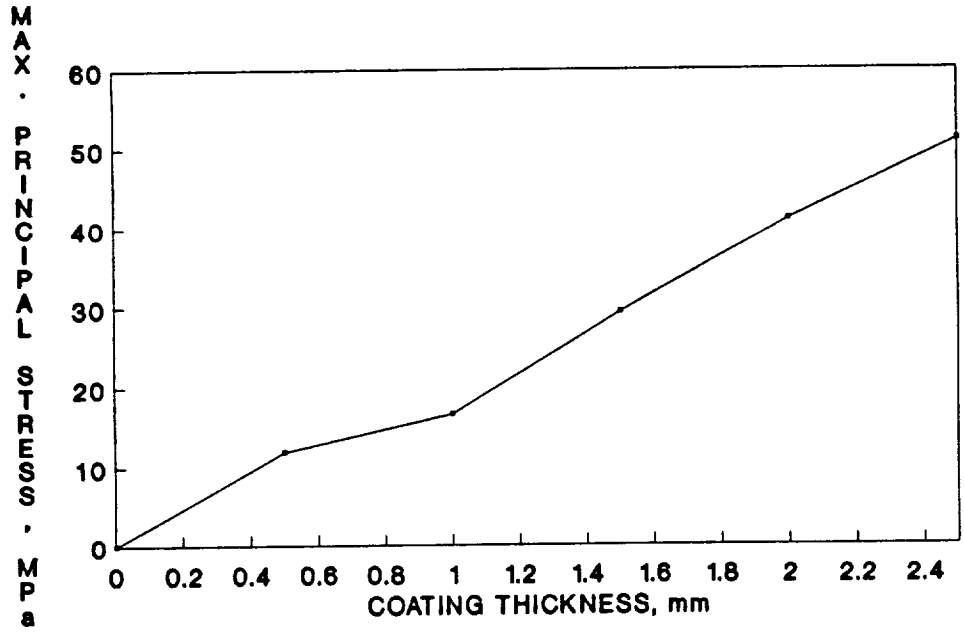

Figure 3.25: Predicted stress variation with coating thickness for a ductile iron piston and single layer zirconia coating.

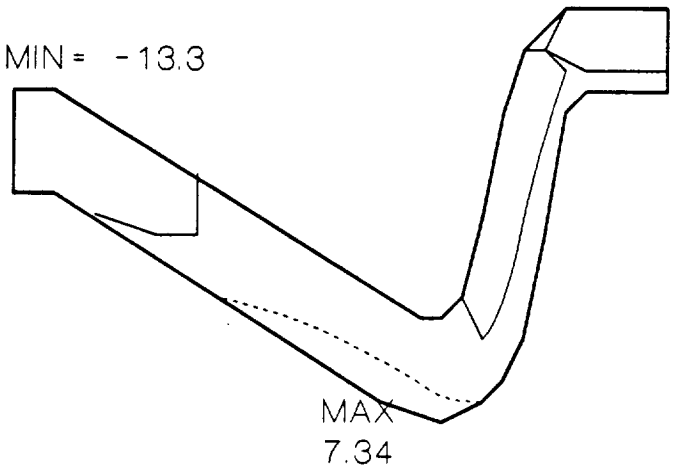

Figure 3.26: Effect of 13.8 MPa pressure load on a 2.5 mm coating. Stress contours: 7 MPa.

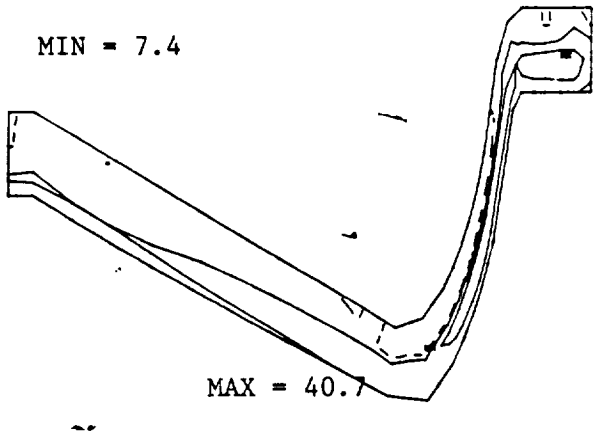

Figure 3.27: Stresses induced by thermal loading on a piston coating. Stress contours: 17 MPa.

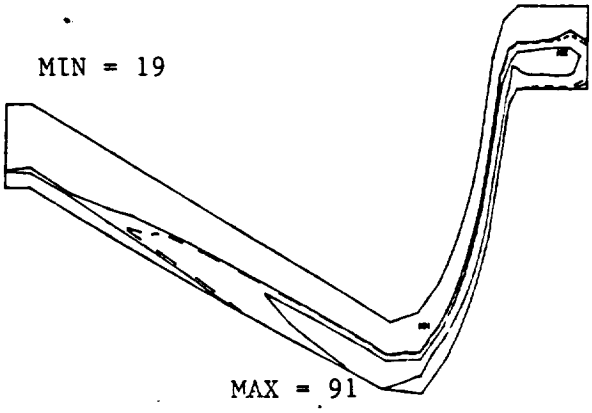

Figure 3.28: Stresses induced by combined pressure and thermal loads on a superalloy. Stress contours: 17 MPa.

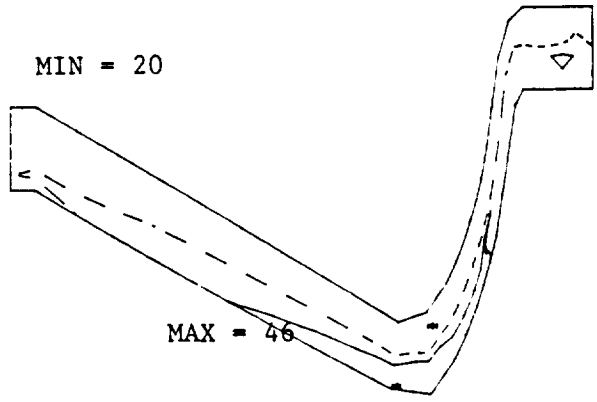

Figure 3.29: Stress induced by combined pressure and thermal loads on ductile iron. Stress contours: 23 MPa.

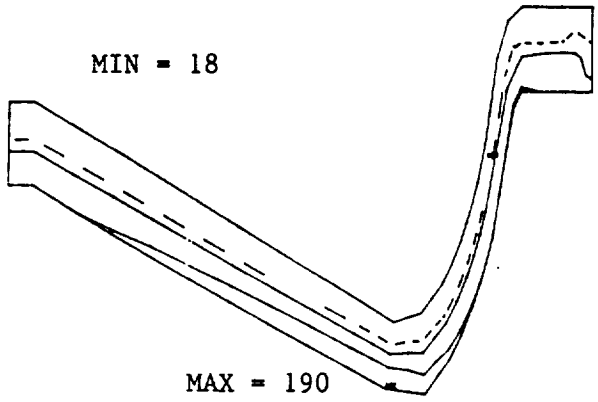

Figure 3.30: Stress induced by combined pressure and thermal loads on a fiber reinforced aluminum piston. Stress contours: 50 MPa.

Table 3.9

Variation of Maximum Stress With Coating Thickness For The Layered Coating

Substrate	Coating Thickness (mm)	Max. Stress MPa (psi)
Superalloy (B1900)	2.5	30.6(4,440)
	1.5	21.4(3,110)
Ductile Iron	2.5	46.1(5,700)
	1.5	31.5(4,570)
Fiber Reinforced Aluminum	2.5	130.0(18,900)
	1.5	124.0(18,000)

The knowledge that the stresses within the coating are a function of the coating thickness led to the investigation of a coating of variable thickness. It was postulated that a coating with varying thickness could be tailored to take full advantage of the thermal properties of the ceramic coating, while minimizing the stresses experienced by the coating. The stress contour presented in Figure 3.31 resulted from a combination of two coating thicknesses, 1.5 and 2.5 mm. The layered coating design was used. Although the transition zone between the different thickness layers was rather crudely modeled, the concept of variable coating thickness was demonstrated. The stress distribution can be positively affected by varying the thickness of the coating. The magnitude of the stresses appearing in Figure 3.32 is deceptive; the model used to predict the stresses introduced severe edge effects. Qualitatively, one can recognize the potential of a variable thickness coating.

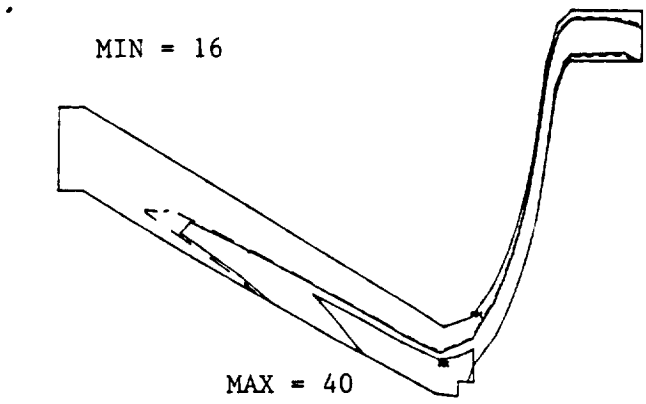

Figure 3.31: Stresses for a variable coating thickness on a B1900 superalloy. Stress contours: 18 MPa.

Conclusions obtained from the two dimensional modeling of ceramic coatings on a piston top were as follows:

1. Coating stresses were very dependent upon the thickness of the coating.

2. Layered coatings did not reduce the stress level significantly under the conditions modeled, but the higher strengths of the ceramic metal mixtures should increase the probability of success.

3. The use of a superalloy substrate resulted in the lowest stress level; use of fiber reinforced aluminum resulted in the highest.

4. Coating thickness can be used as a design variable to produce a more favorable stress distribution.

3.2.3 Three Dimensional Model of Cylinder Head

The purpose of this analysis was to determine, from a thermal stress standpoint, the optimum combination of the available plasma sprayed zirconia coatings for thick thermal barrier coating applications on cylinder heads.

An existing L10 cylinder head finite element model of the firedeck was used for this analysis. It should be noted that the L10 cylinder head is similar in configuration to the V903 cylinder head and, therefore, the results of this analysis are considered applicable to the V903 engine. For the actual spraying process, material equivalent to the desired coating thickness would be removed from the cylinder head. The coatings would then be sprayed on, and the excess machined to be flush with the combustion face of the cylinder head. For modeling purposes, the head was modeled with the coating protruding from the surface of the head. This modification was not considered to be a significant factor in the results, and resulted in fewer model changes. An illustration of the finite element mesh is shown in Figure 3.32.

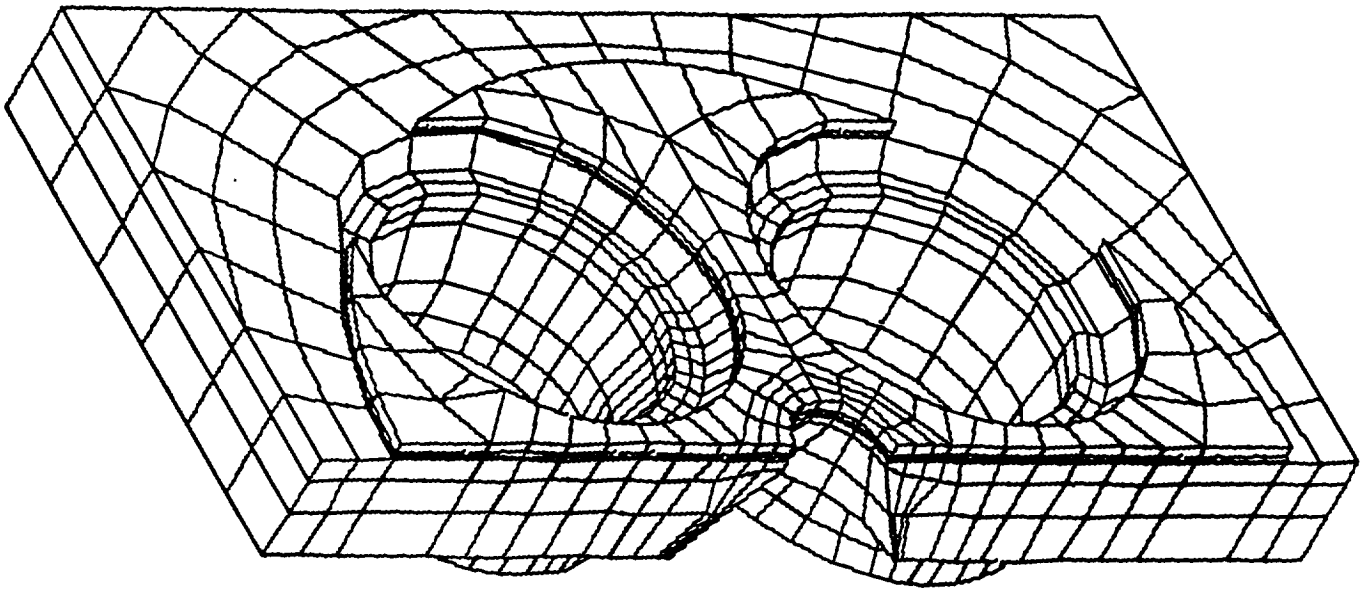

Figure 3.32: Cylinder head finite element model.

Since the ceramic coatings provide a potential for uprate capabilities on future engines, the rating chosen for this analysis was 350 HP at 1800 RPM for the L10 engine. The cooling is representative of a traditional water cooled cylinder head. A function referred to as a "radial combustion gas convection coefficient" was developed based on previous experience for the distribution of heat transfer into the combustion face. This function is displayed graphically in Figure 3.33. A complete listing of the thermal boundary conditions is given in Table 3.10.

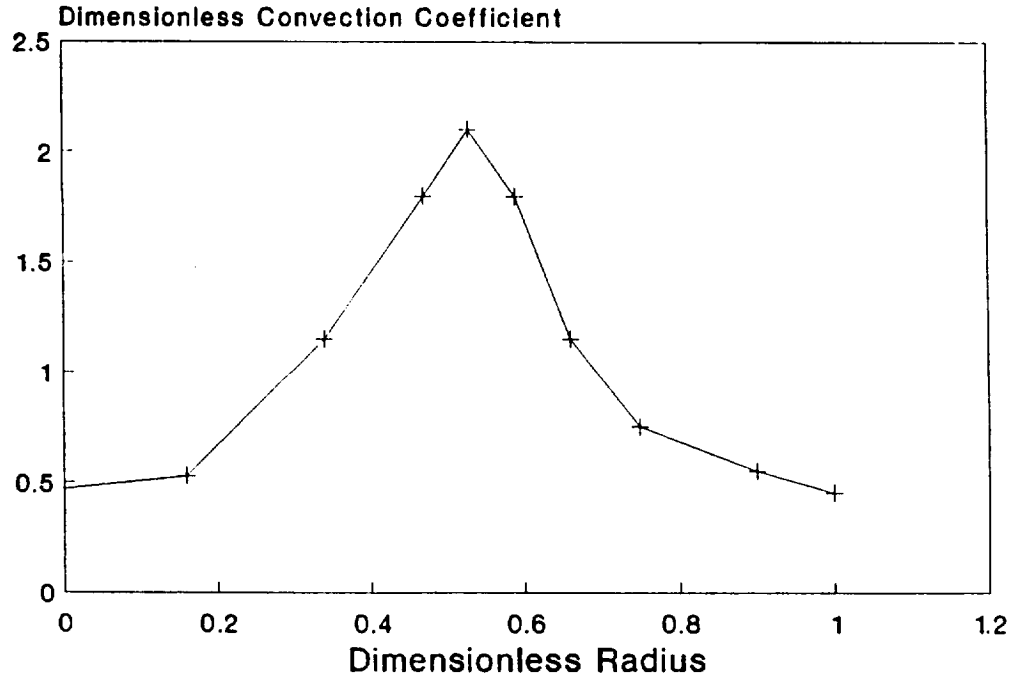

Figure 3.33: Radial convection dependence used in the boundary conditions for the cylinder head model.

Table 3.10

L10 Rated Thermal Boundary Conditions
350 HP @ 1800 RPM

Location	h (Btu/hr-in^{2}F)	C	Temp (F)
Combustion Gas	1.15	838	(1540)
Contact Between Head &Block Top Deck	7.00	150	(300)
Exterior Surface of Head To Ambient	0.0001	121	(250)
Inside Exhaust Port	0.85	596	(1150)
Inside Intake Port	0.40	65	(150)
Exhaust Valve Contact With Seat	4.43	585	(1085)
Intake Valve Contact With Seat	4.84	413	(775)
Inside Injector Bore-Cup Contact Zone	2.00	177	(350)
Water Jacket - Coolant	3.20	110	(230)
(Valve Bridge and Injector Bore Region)	10.0	110	(230)
Ports - Top Cut Surface	0.0001	249	(480)
Exhaust	0.0001	121	(250)
Intake			

For the structural analysis, the head was assumed to be vertically constrained at the head to block interface. Symmetry was assumed at the cylinder bore centerline.

The impact of a thick thermal barrier coating on the cylinder head gray iron material did not vary significantly with coating composition; therefore, the impact of a coating on the gray iron will only be reported for the recommended coating combination.

The heat rejection into the combustion face for the baseline model without a thermal barrier coating was 200 Btu/min/cylinder. This decreased to approximately 144 Btu/min/cylinder when the coating was added. The temperature and stress profiles for the baseline analysis are pictured in Figure 3.34. The corresponding contours for a coated cylinder head are shown in Figure 3.35. As seen in the Figures, the maximum gray iron temperature decreased from 447 C (837 F) to 372 C (702 F).

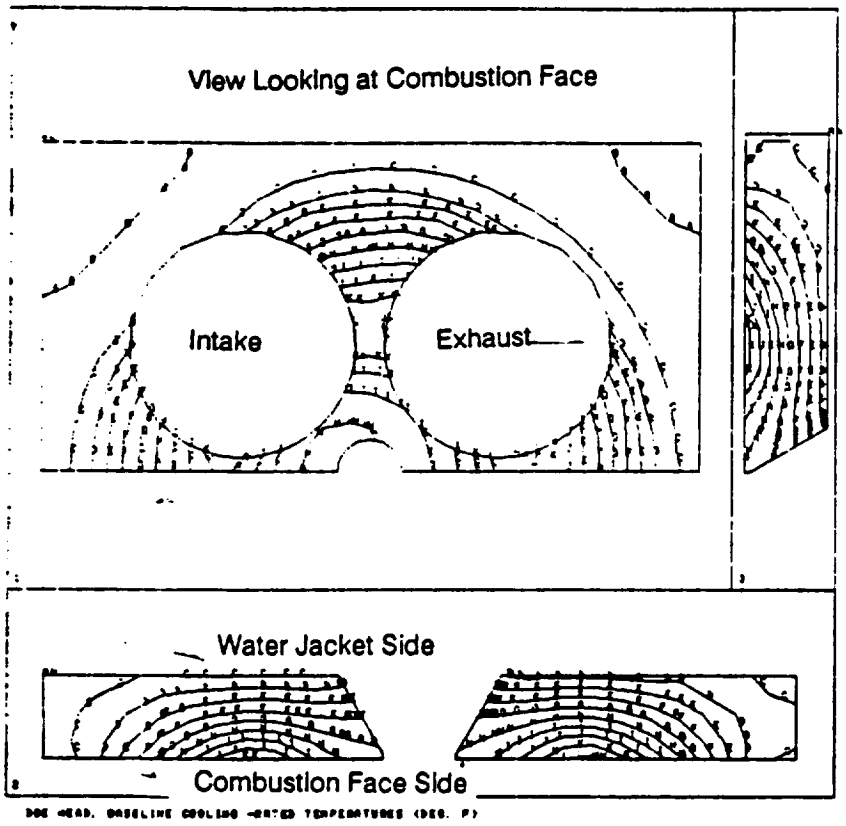

F	C
MX-837	450
MN-290	145
B-150	300
C-175	350
D-205	400
E-230	450
F-260	500
G-290	550
H-315	600
I-345	650
J-370	700
K-400	750
L-425	800

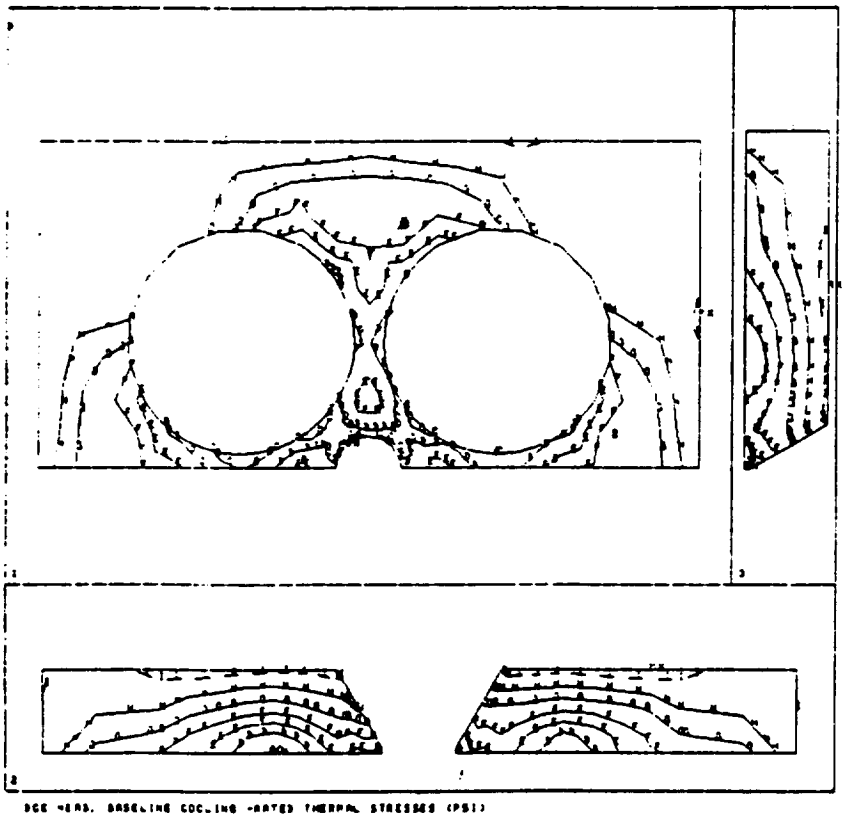

MPa	Ksi
MX +5.5	+.8
MN -245	-35.6
B -240	-35
C -207	-30
D -172	-25
E -138	-20
F -103	-15
G -69	-10
H -34	-5
I 0	0

Figure 3.34: Baseline cylinder head metal temperatures and stresses (no coating).

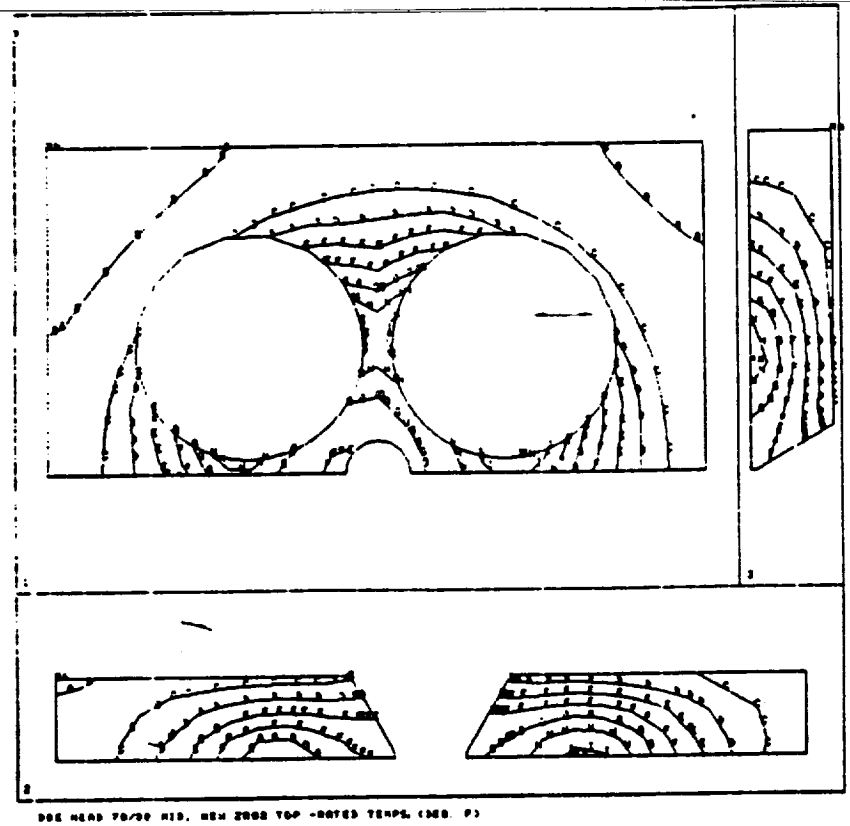

F	C
MX-327	702
MN-143	289
B-150	300
C-175	350
D-205	400
E-230	450
F-260	500
G-290	550
H-315	600
I-345	650
J-370	700

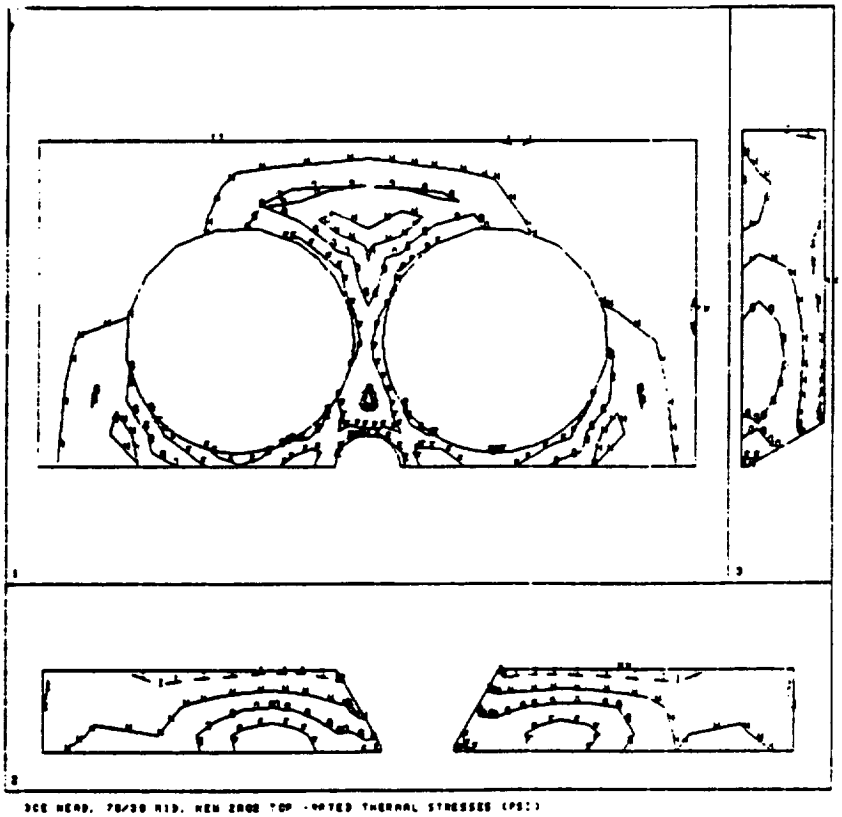

MPa	Ksi
MX 3.8	.550
MN -165	-24.
E -138	-20.
F -103	-15.
G -69	-10.
H -34	-5.
I 0	0

Figure 3.35: Coated cylinder head metal temperatures and stresses.

Next, cylinder head metal fatigue life predictions were calculated. This calculation was based on a cycle between idle and rated. The alternating stress was calculated as one-half the difference between the stress at rated and the stress at idle. Life predictions were then obtained from an S-N Diagram for gray iron which was shifted according to the metal temperature by a factor taken from a fatigue strength degradation curve. The baseline fatigue life for a head without the coating was 226,000 cycles. With a thermal barrier coating, the gray iron fatigue life became essentially infinite.

To determine the effect of coating properties on the coating survivability, four different coating cases were modeled. The four coatings were as follows:

	Bottom Layer	Intermediate Layer	Top Layer
Case 1	40/60 ZrO2/CoCrAlY	85/15 ZrO2/CoCrAlY	76% Dense ZrO2
Case 2	40/60 ZrO2/CoCrAlY	85/15 ZrO2/CoCrAlY	85% Dense ZrO2
Case 3	40/60 ZrO2/CoCrAlY	85/15 ZrO2/CoCrAlY	Higher Strength ZrO2*
Case 4	40/60 ZrO2/CoCrAlY	70/30 ZrO2/CoCrAlY	Higher Strength ZrO2

* Higher strength zirconia was obtained by increasing the plasma gun power while spraying the powder that yielded an 85% dense zirconia layer.

The calculated compressive stress versus strength in each of the layers at their interfaces is shown in Figure 3.36. As seen in the Figure, each of the four cases met the criteria; therefore, compressive stresses should not be the primary mode of failure.

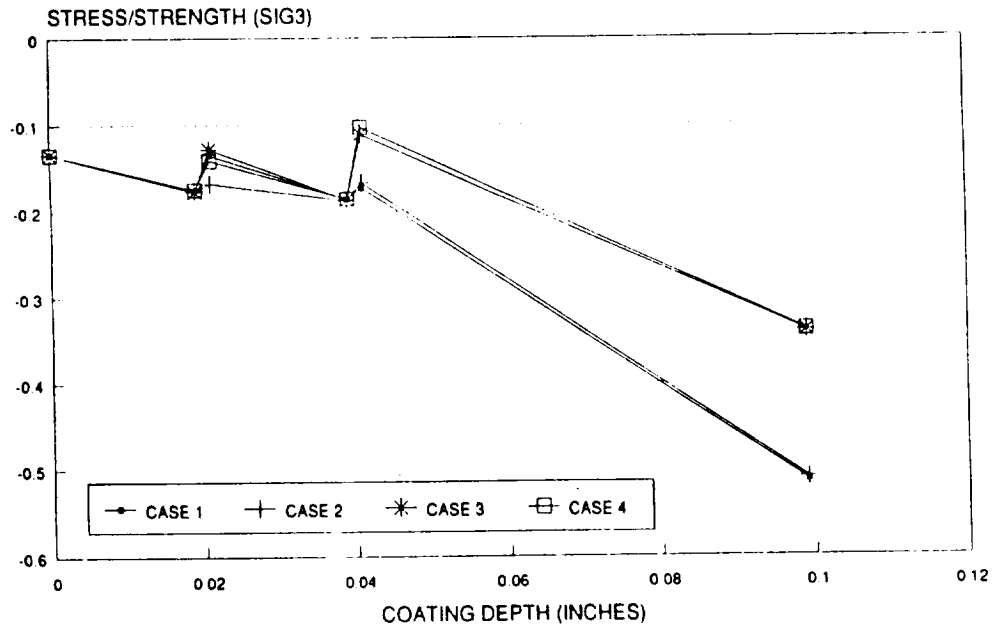

Figure 3.36: Maximum compressive stress/strength ratio (L10 cylinder head/coatings).

The maximum tensile stress versus the corresponding four-point bend strength in each of the layers at the interfaces have been plotted in Figure 3.37. A tensile stress contour plot (typical of tensile stress distributions in other layers) of the 70/30 layer at the interface with the 40/60 coating is shown in Figure 3.38. A ratio less than one indicates that the stresses are within the maximum acceptable stress limit. The only coating combination to meet that criteria in every layer was Case 4. Each of the first three cases failed in the intermediate layer at the interface with the 40/60 coating. In Case 1, the most probable failure location moved to the surface layer, at the interface with the intermediate layer.

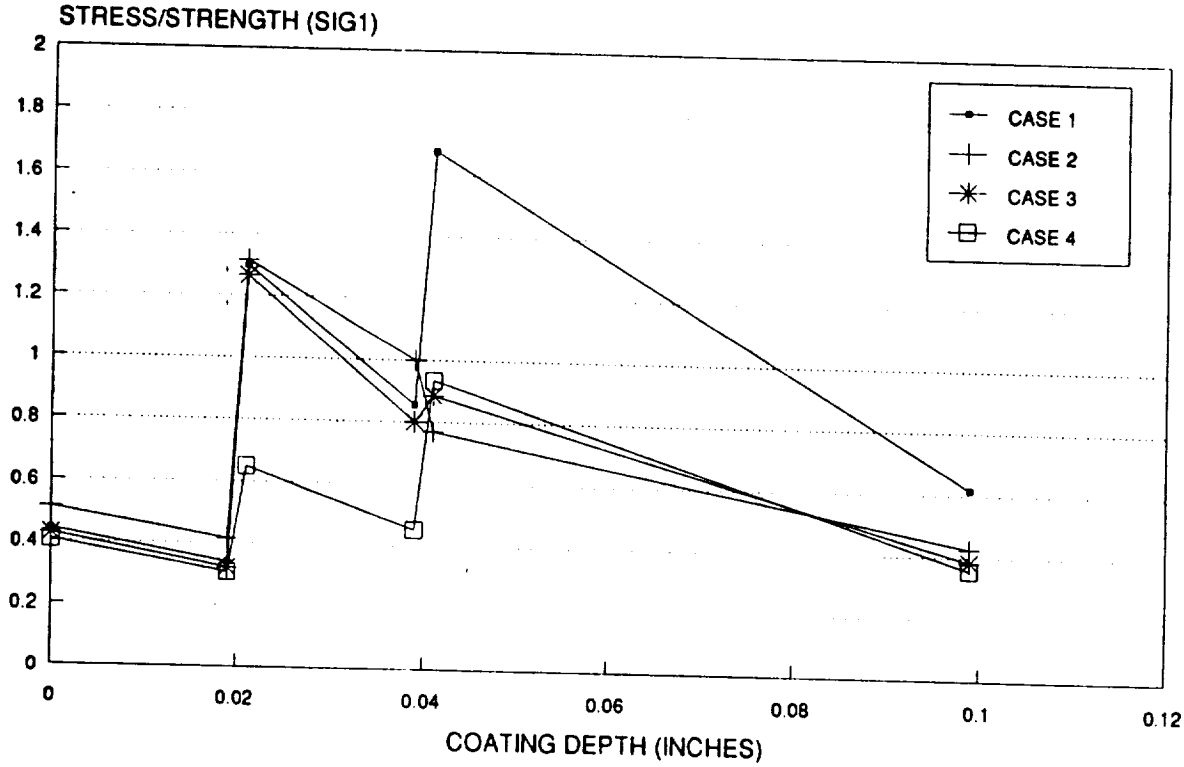

Figure 3.37: Maximum tensile stress/strength ratio (L10 cylinder head coatings).

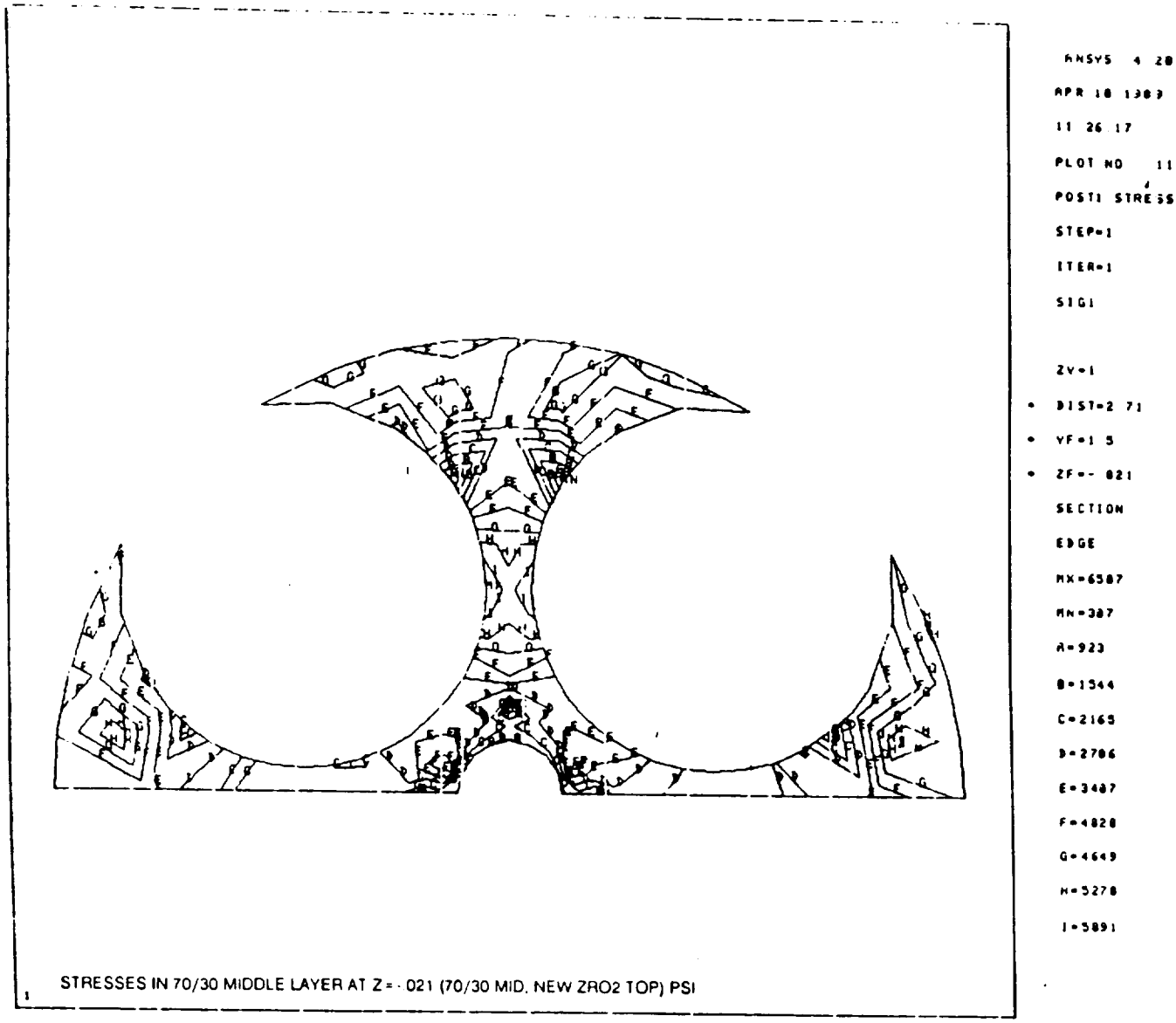

Figure 3.38: Tensile stresses in 70/30 layer for the Case 4 coating, psi.

Shear stresses in the three layers have been plotted in Figure 3.39. The shear strengths of the ceramic coatings are not presently known; however, because the shear stresses are on the same order of magnitude as the tensile stresses, shear stresses present a potential failure mechanism and have been reported for future reference.

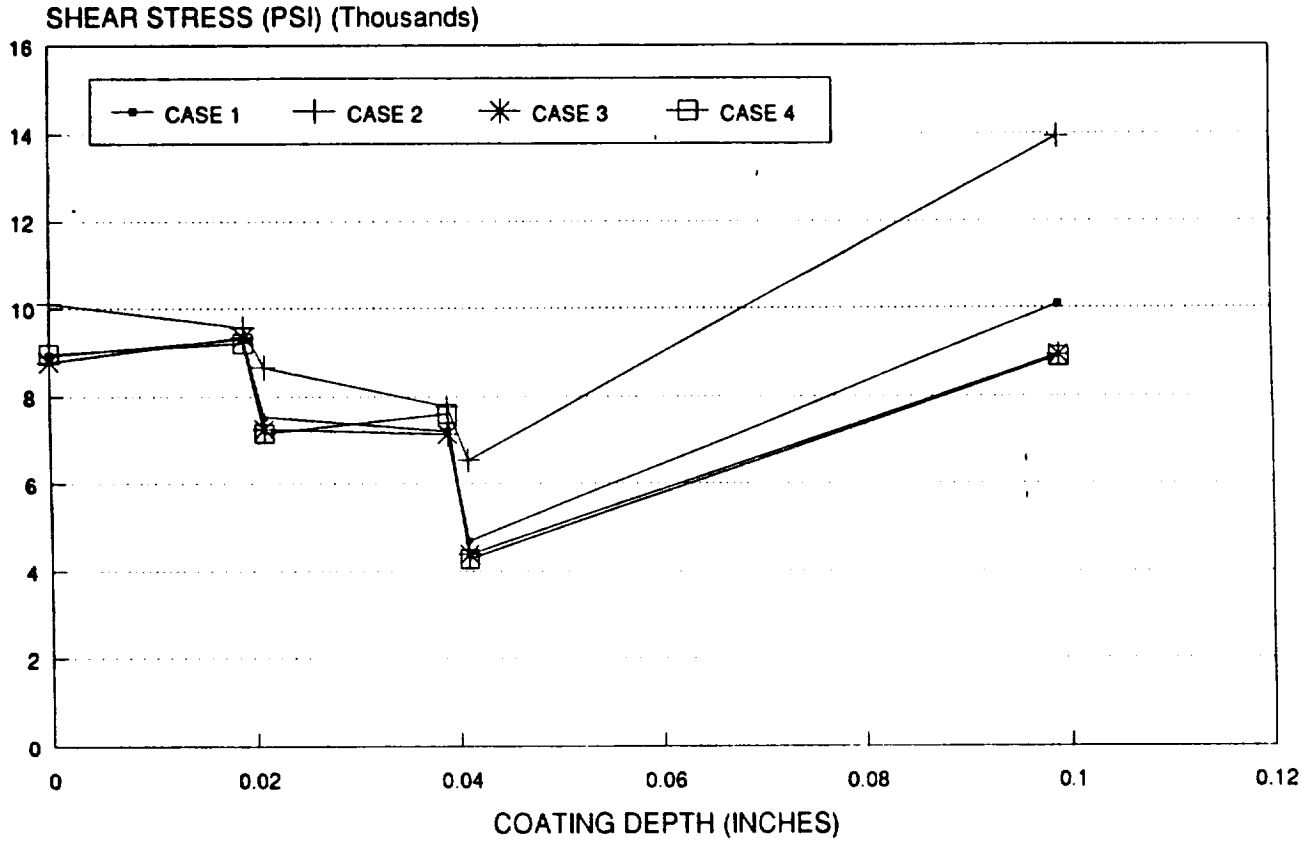

Figure 3.39: Maximum shear stress in cylinder head coating.
(L10 Cylinder Head (350 HP @ 1800 RPM)

The tensile strength of the bond coat is approximately 69 MPa (10,000 psi). The Z-Direction (perpendicular to the combustion face) tensile stresses are shown in Figure 3.40. As seen in the Figure, all stresses were less than the bond strength. Therefore, debond is not predicted to be the primary mode of failure, although debond may result as a consequence of other stresses.

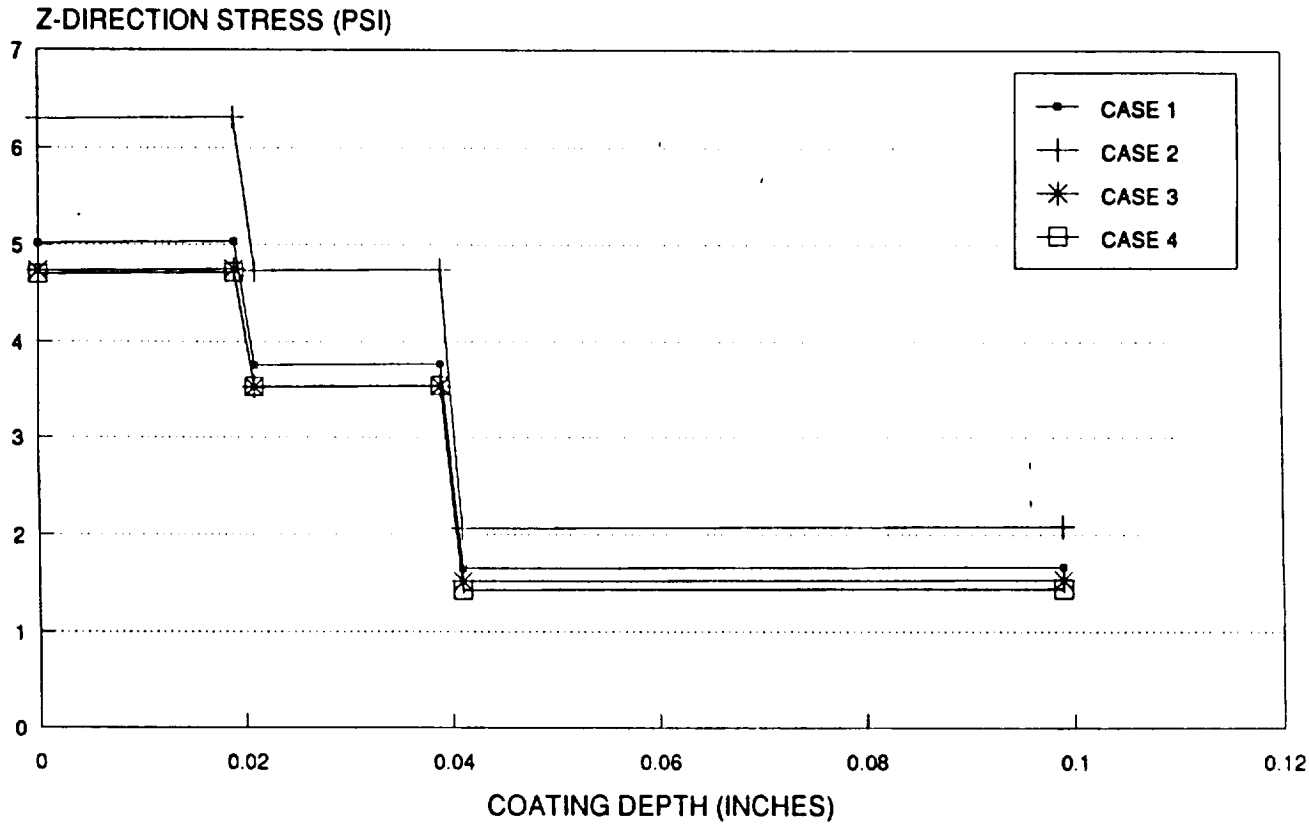

Figure 3.40: Z-direction tensile stress in cylinder head.

The temperature gradient through the coatings was approximately 380 C (718 F). The maximum surface temperature occurred between the exhaust valves, as seen in Figure 3.41.

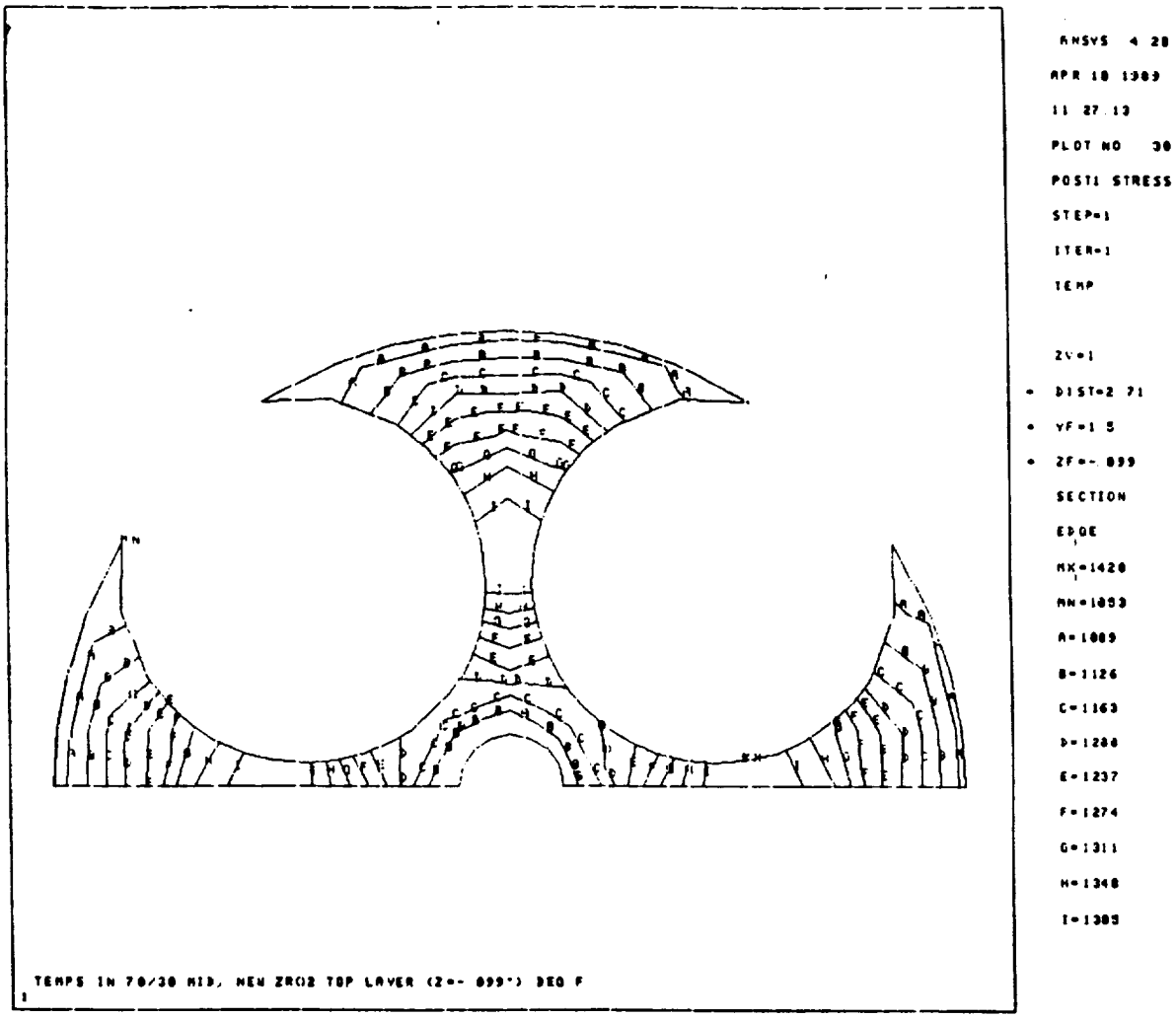

Figure 3.41: Surface temperatures predicted for cylinder head coating, F.

Prior to this analysis, two cylinder heads sprayed with Case 2 were tested. The failure initiation site in the model corresponded to the failure initiation location in the coatings during the engine testing.

The first three cases analyzed with an intermediate layer of 85/15 ZrO2/CoCrAlY, were unacceptable due to high tensile stresses within the intermediate layer, and the surface layer in Case 1. Case 4, which consisted of 40/60 ZrO2/CoCrAlY, 70/30 ZrO2/CoCrAlY, and New ZrO2, met the stress to strength criteria and is the recommended coating composition.

1. The combination of cylinder head coating materials least susceptible to thermally induced cracks consists of a 40/60 ZrO2/CoCrAlY layer closest to the cylinder head, an intermediate layer of 70/30 ZrO2/CoCrAlY, and a surface layer of the New ZrO2 coating, Case 4.

2. The results indicate that each of the three material combinations analyzed with an intermediate layer of 85/15 ZrO2/CoCrAlY, Case 1, 2, and 3, will fail due to tensile stresses within the ceramic coating.

3. The compressive stresses within the coatings are generally higher than the tensile stresses, but are still acceptable due to the high compressive strength of the ceramic coatings.

4. The bond strength was adequate to resist the stresses which could cause debond as a primary mode of failure.

5. Although no shear strength values are available for the ceramic coatings, caution should be taken because the magnitude of the maximum shear stresses developed within the ceramic approached the maximum tensile stresses. The case which predicted the lowest shear stresses was also the combination most desirable for resisting tensile cracks.

4.0 TASK II - BENCH TEST EVALUATIONS

4.1 PLASMA SPRAY PROCESSING

A prototype plasma spray facility was set up to continuously apply multilayered thermal barrier coatings to both V903 piston crowns and single cylinder heads and L10 piston crowns, Figure 4.1. The facility was equipped with a six-axis articulating robot to provide gun motion control. Part holding fixtures for all diesel engine components were developed for both simulations and actual hardware. The fixturing for the piston crown incorporated a flame shroud to provide the capability to heat the piston crown substrate to control fabrication temperature during the spray processing. A powder feed delivery system was used to provide continuous feed rate control during coating deposition. The powder feed system had the capability to deliver four coating materials sequentially.

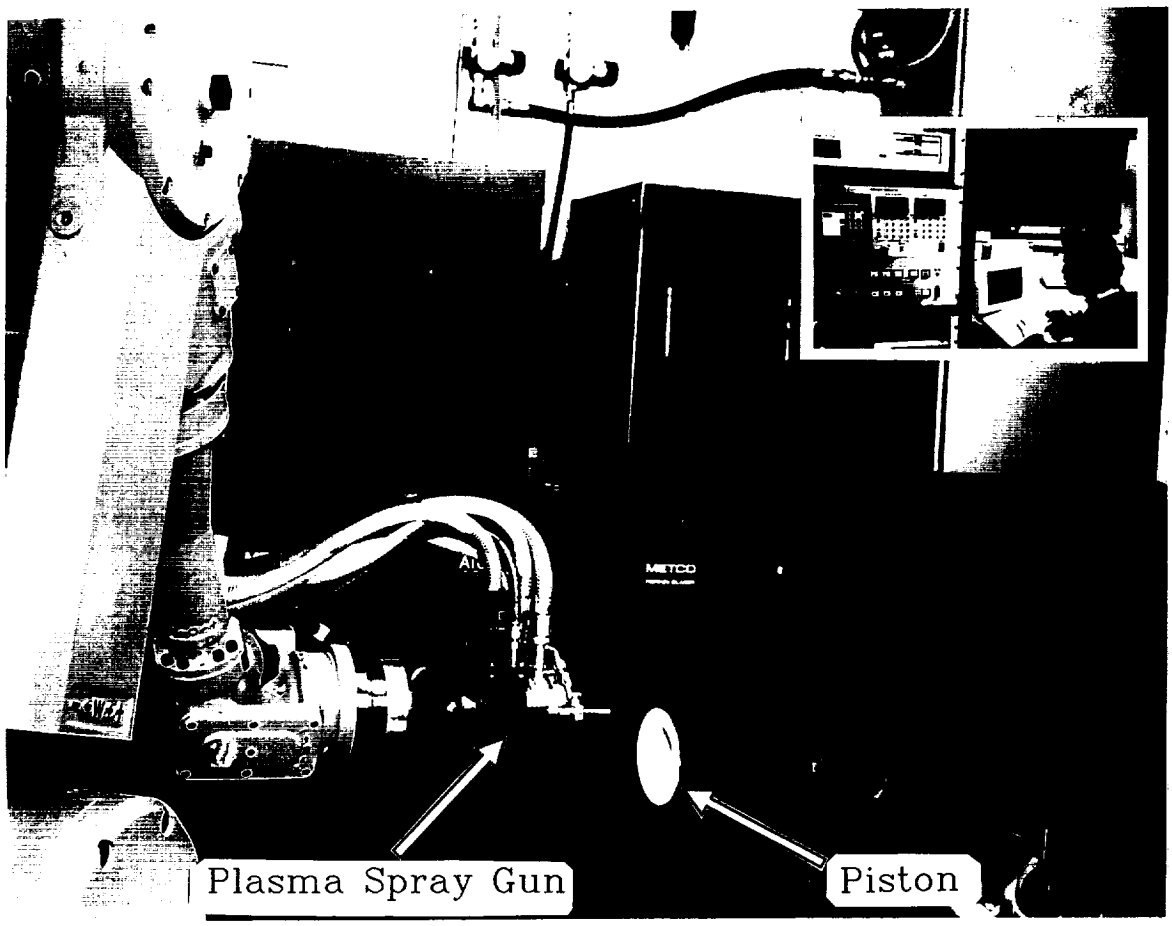

Figure 4.1: Prototype plasma spray facility showing robotics, piston, and operator at the control console (inset).

Spray process parameters to produce zirconia-based thermal barrier coatings on V903 piston crowns and cylinder heads were developed by translating UTRC's experience in producing turbine seal coatings on curved duct segments. Fundamental issues addressed included prestressing technology and special processing techniques needed to coat each of the specific diesel engine components. Concurrently, a basic strength test was developed as a means to calibrate analytical modeling and help correlate material properties with actual spray process parameters.

4.1.1 V903 Piston Crown

Initial processing efforts focused on developing robotic control software for the plasma gun motion for coating the V903 piston crown. Applying the coating system across the piston crown diameter proved to be difficult and variable due to the complex bowl geometry. Simulated piston crowns were machined and used to assess the magnitude of the coating thickness variation across the actual piston crown contour. A combination of single-layer and multilayer coating systems were sprayed on the simulated crown. The simulation was then cut in half and the resulting diameter polished for metallographic examination of the thickness variation of the individual layers, particularly in the bowl area of the crown. From sectioning, it could be clearly seen that the deposition in portions of the bowl was not as efficient as in those areas where a 90 degree angle of the plasma gun to the sprayed surface was maintained. A "circular" type gun motion control including a gun rotation into the wall area was developed to achieve the highest degree of thickness, microstructure and properties uniformity across the crown diameter. Baseline robotic control parameters such as speeds and program increments were determined empirically by conducting a series of coating trials on piston crown simulations.

Baseline spray parameter setpoints for the fabrication of the multilayer thermal barrier coating were established by conducting additional spray trials to produce both properties and coated rig test specimens. A list of process parameters used to produce the baseline coating on actual V903 parts is shown in Table 4.1.

Table 4.1

Plasma Spray Process Parameters

Turntable Speed - 700 rpm
Gun Type - Metco 7MB
#2 Powder Port
Parallel Cooling Jets - 750 SCFH, 50 psi

Process Parameter	Bond	40/60 ZrO_2/CoCrAlY	85/15 ZrO_2/CoCrAlY	Baseline Top Layer Zirconia
Deposition Rate Mils/Pass	0.6	0.6	0.6	0.6
Powder Feed Rate Gm/Min	49	47	47	72
Gun Power KW	35	35	35	35
Gun Volts (Constant)	75-76	75-76	75-76	75-76
Gun Amps (Adjusted)	470-480	470-480	470-480	470-480
Gun Standoff Inches	5.0	5.0	5.0	5.0
Primary Gas (N2) SCFH	145	75	75	75
Secondary Gas (H2) SCFH	14.0	14.0	14.0	14.0
Carrier Gas (N2) SCFH	11.5	9.0	9.0	9.0

During the spray trials for the actual crowns, the fabrication temperature was monitored and recorded. Thermocouples were placed on the underside of the crown with one thermocouple located in the center and two thermocouples located on opposite outer edges. One of the edge thermocouples was selected as the "control" for use in adjusting the heat applied to the crown. A typical fabrication profile is shown in Figure 4.2.

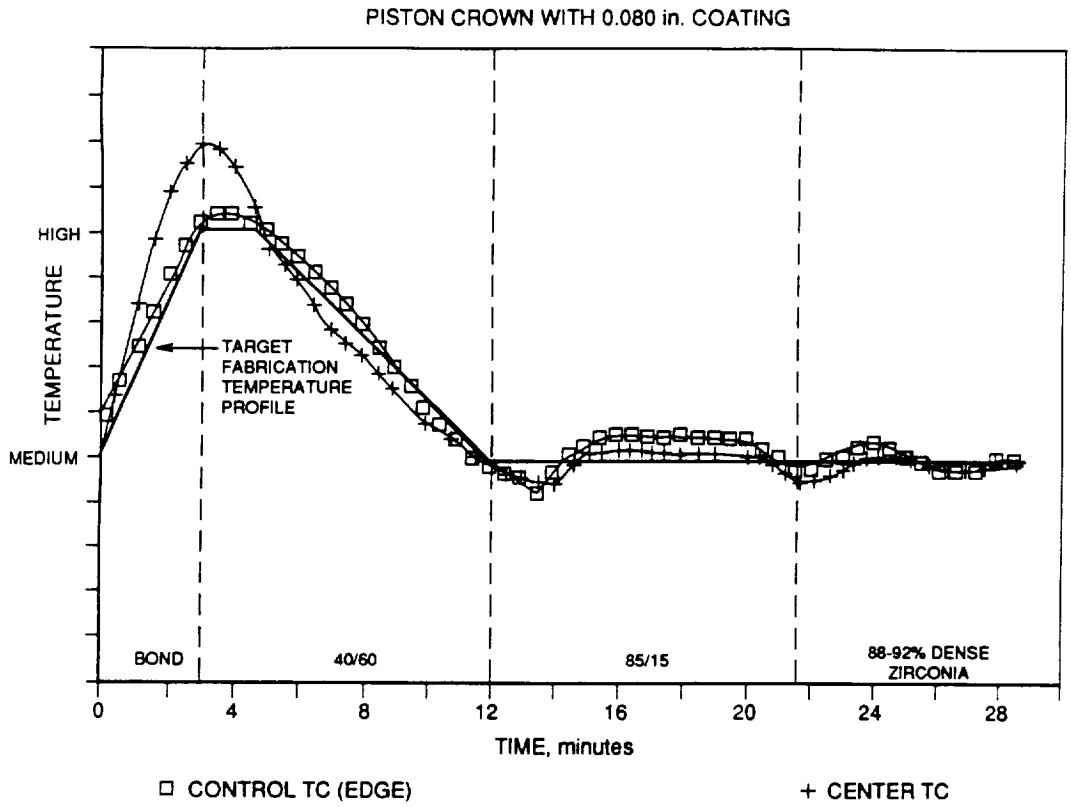

Figure 4.2: Typical fabrication temperature profile curves, showing hybrid processing condition.

In order to assess the coating thickness applied to the actual crown, a measurement technique was developed using a Cordax 1000 measurement/computer system to define the top surface contour of the piston crown prior to coating. Post-spray contour measurements were taken and compared to the initial readings. Cordax values were used in conjunction with the results of the metallographic evaluation of the simulated crowns to yield an assessment of the final coating thickness.

A total of nine ductile iron and one fiber reinforced aluminum piston crowns were coated with the baseline multilayer thermal barrier coating for component and performance engine testing. The baseline multilayer coating consisted of the following layers: NiCrAlY bond coat - 0.005", 40/60 ZrO_2/CoCrAlY - 0.020", 85/15 ZrO_2/CoCrAlY - 0.020", 85% dense ZrO_2 - 0.060". A microstructure of this multilayer coating is shown in Figure 4.3. Note that to obtain modified coating thicknesses the top layer coating thickness was varied. For example, an 0.080" coating consisted of the bond coat, 0.020" of 40/60 ZrO_2/CoCrAlY, 0.020" of 85/15 ZrO_2/CoCrAlY, and 0.040" of 85% dense ZrO_2. The target coating thicknesses on these piston crowns ranged from 1.5 mm (0.060 inch) to 2.54 mm (0.100 inch). The medium (hybrid) fabrication temperature, uniform temperature maintained during deposition of all the layers, was used for all ductile iron piston crowns. A medium fabrication temperature was used for the fiber reinforced aluminum piston crown given its lower metal temperature capability. In order to address concerns of coating durability, a ductile iron piston was prepared with a second intermediate layer of increased metal content and strength and an increased strength top layer zirconia. The summary of the coated pistons is shown in Table 4.2.

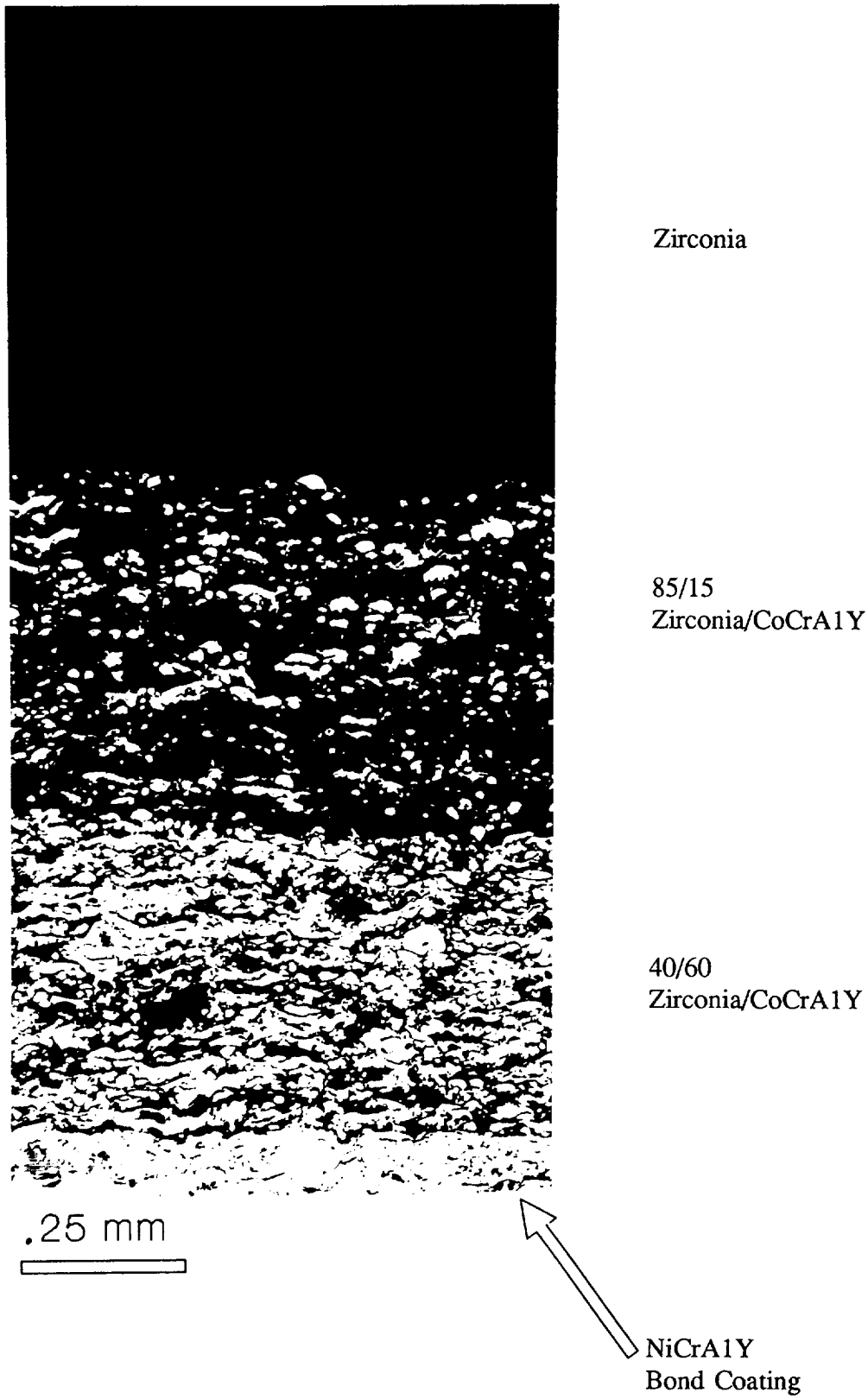

Figure 4.3: Microstructure of the baseline, systems 3, multilayer thermal barrier coating showing the zirconia, 40/60, 85/15, and bond coat layers.

Table 4.2

Coated V903 Piston Crowns

Base Metal	Nominal Coating Thickness		Coating System
Ductile Iron	2.0mm	(0.080 in.)	Baseline V903
"	2.0mm	(0.080 in.)	Baseline V903
"	1.5mm	(0.060 in.)	Baseline V903
"	1.5mm	(0.060 in.)	Baseline V903
"	2.5mm	(0.100 in.)	Baseline V903
"	2.5mm	(0.100 in.)	Baseline V903
"	2.5mm	(0.100 in.)	Baseline V903
"	2.5mm	(0.100 in.)	Baseline V903
"	2.5mm	(0.100 in.)	Incr. Strength Top Coat. Modified (20% gun power increase) Intermediate layer (substituting 70/30 for 85/15 layer)
Fiber/Aluminum	2.5mm	(0.100 in.)	Baseline V903

After removal of the overspray from the edge, the pistons were shipped to Cummins Engine for performance testing. A coated V-903 piston after final contour grinding is shown in Figure 4.4.

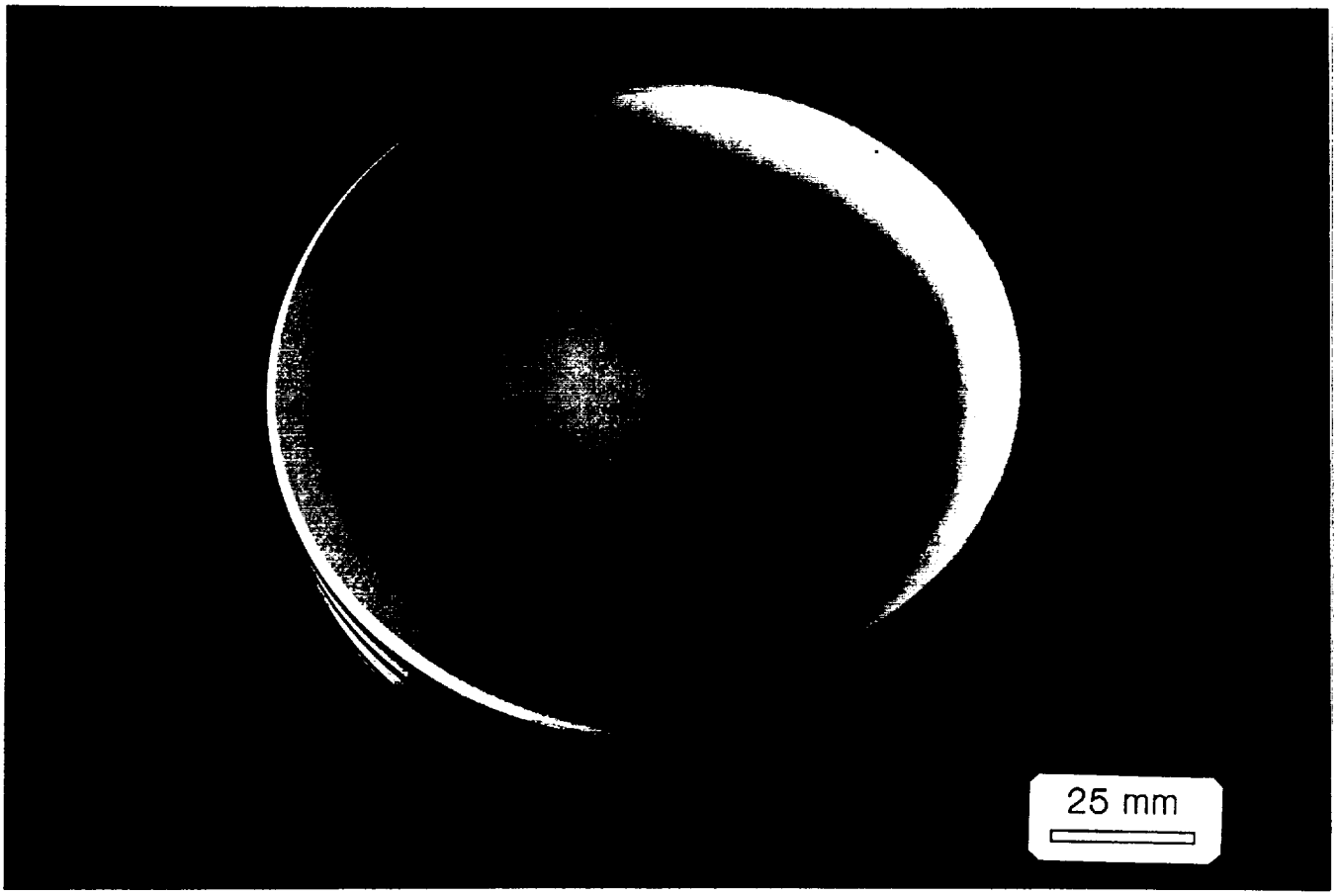

Figure 4.4: Contour ground thermal barrier coating on a V903 piston for engine fuel economy tests.

4.1.2 V903 Single Cylinder Head

A basic "ladder" type X-Y robotic control software for the plasma gun motion was developed to coat the V903 heads. This type of gun motion, in conjunction with masking techniques to provide protection against depositing material in the valve ports, fuel injector port and on non-inlay head surfaces, proved to be effective for the head inlay area.

Fundamentally, all other gun and powder delivery spray parameters were maintained constant with those used to coat the V903 piston crowns. The large mass of the head components precluded the use of standard thermal prestress control techniques used on pistons during fabrication of the cylinder head coatings.

Two V903 cylinder heads were initially coated with the baseline multilayer thermal barrier coating for engine testing. A cylinder head with the combustion face machined to accept an inlayed thermal barrier coating is shown in Figure 4.5. The coating applied to the heads was machined to Cummins/UTRC specifications by grinding the coating flush to the top of the cylinder head. The coating in the valve holes was machined back to maintain the radius of the original valve openings. The coating edges in the fuel injector and pressure tap holes were machined flushed to the inner diameter surfaces.

Figure 4.5: V903 cylinder head machined to accept a thermal barrier coating.

After short test periods (approximately 5 hours) the baseline coating showed cracking and spalling particularly at the valve bridge locations as reported in Section 5.2. The two single cylinder heads were returned to UTRC for refurbishment with a modified thermal barrier coating system. The parts were recoated based on results obtained from material properties and laboratory and rig testing. A substantial effort was conducted to provide coated cylinder head simulations with standard and slotted valve bridges for rig testing at Cummins. Coating systems evaluated included an increased strength zirconia top layer, a partially stabilized zirconia substitute top layer and a low coefficient of thermal expansion ceramic top layer. Alternate intermediate layer compositions were evaluated to produce material properties with increased strength. Additional spray trials were conducted using flat-plate cylinder head simulations to select process parameters to achieve desired material properties. The improved structure selected was a higher strength zirconia top layer on a modified intermediate layer (70/30 ZrO_2/CoCrAlY) to a total thickness of 0.100 inch.

THIS PAGE LEFT INTENTIONALLY BLANK

The higher strength zirconia material was produced by increasing the plasma gun power by 20%. The intermediate layer structure was modified to accept a higher percent metal containing layer to a 70/30 ZrO_2/CoCrAlY ratio. This cylinder head prepared for performance tests is shown in Figure 4.6. The coatings were machined as previously, and the parts were delivered to Cummins for engine testing.

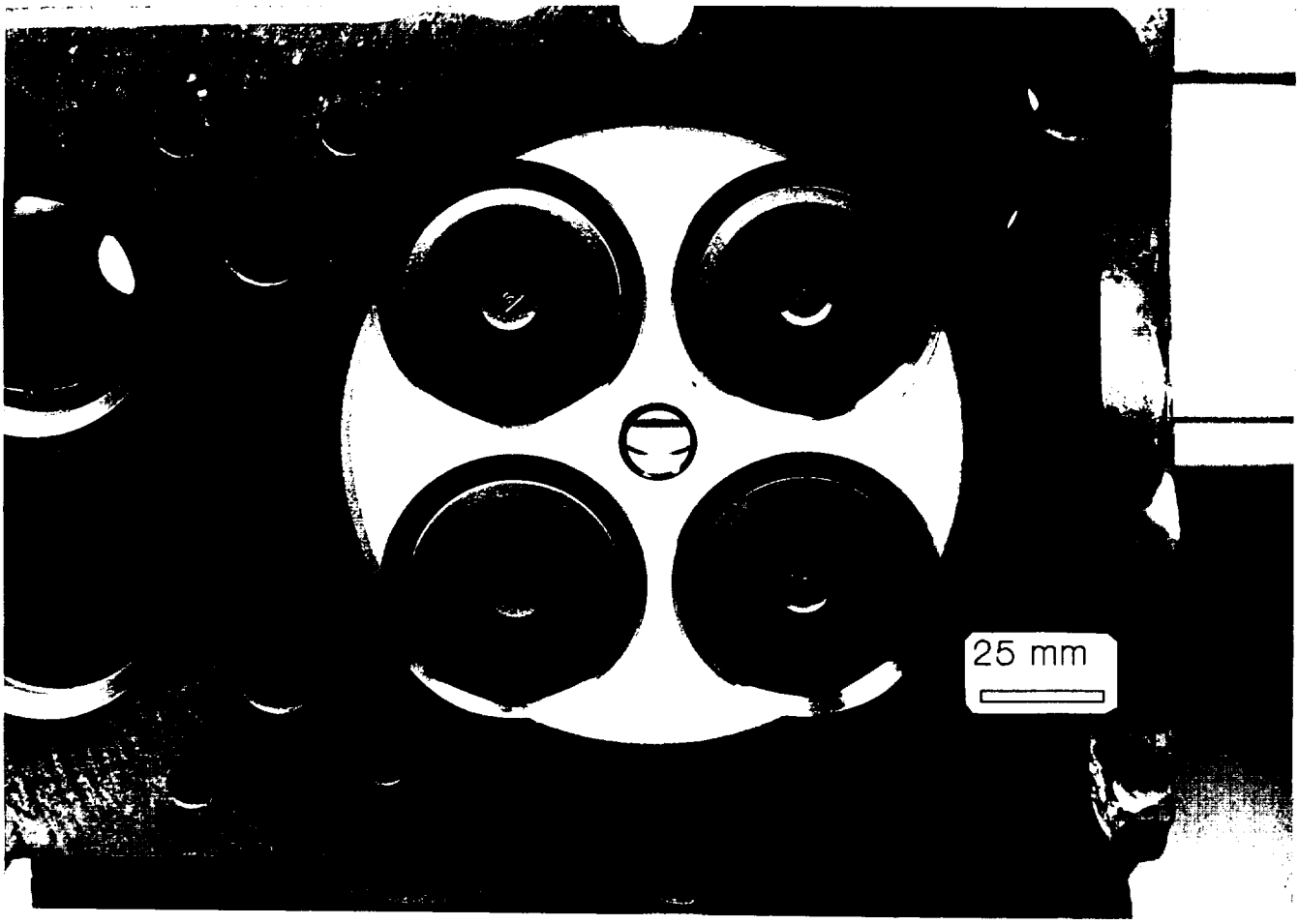

Figure 4.6: Inlayed thermal barrier coating on a V903 cylinder head.

4.1.3 L10 Piston Crown

The part holding fixture design was modified to accommodate the L10 piston crown geometry. The processing parameters used to coat the V903 piston crowns were used as a basis for developing parameters to coat the L10 bowl geometry. Modifications to the basic V903 processing parameters were necessary to achieve equivalent thickness, microstructure and properties due to the deeper bowl geometry of the L10 crown. Even after final robotic setpoints were determined, coating thickness variability across the crown diameter was typically higher for the L10 versus the V903 piston crowns coated for engine performance and component testing.

THIS PAGE LEFT INTENTIONALLY BLANK

All other baseline spray parameter values (e.g. gun power, gas flows, powder feed rate, etc.) were maintained constant for the L10 piston crowns as for coating the V903 piston crowns. Prestress fabrication temperature used to coat the L10 piston crowns was 38 C (100F) lower than for the V903 as dictated by the maximum allowable use temperature of the steel alloy. Examples of the steel articulated L10 pistons are shown in Figure 4.7. These plasma spray parameters, being consistent with V903 with the exception of the top zirconia layer which was sprayed at a 20% increase in gun power, are given in Table 4.1.

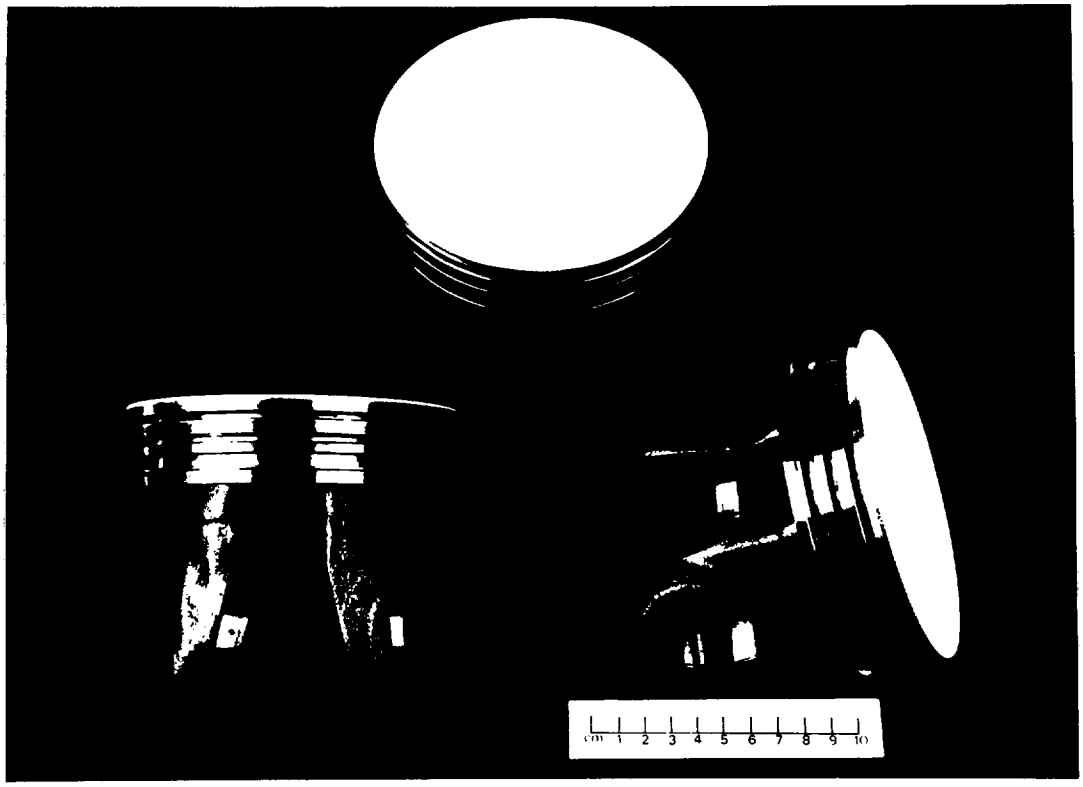

Figure 4.7: Articulated L10 pistons with thermal barrier coating.

4.1.4 Summary - Plasma Spray Processing

The spray process capability to produce multilayer, thick thermal barrier coating systems for V903 piston crowns and single cylinder heads was developed. The spray process parameters used for coating the V903 piston crowns were successfully modified through use of simulation hardware to apply this coating system to the L10 piston crowns. Component simulations were instrumental in the development of processing parameters. In addition, these simulations provided test specimens for directing coating design studies. For example, simulated cylinder heads with coating variations were produced for thermal cycle rig testing of material durability at valve bridge locations.

THIS PAGE LEFT INTENTIONALLY BLANK

A prototype capability was demonstrated to produce both V903 piston crown and single cylinder heads and L10 piston crowns for component engine testing. Machining techniques were developed to finish grind coating surfaces on cylinder head inlays and piston crown rims.

4.2 Materials/Properties

The thermal barrier coating engineering requirements, i.e. thermal conductance goal, dictated that zirconia-based material systems be selected as the prime candidate for diesel engine applications. A material properties library was developed for diesel component coating materials by employing techniques similar to those used to develop the existing UTRC properties data base, Figures 4.8 through 4.11 developed for turbine tip seal applications. The measured material property values obtained provided a means of targeting spray process parameter setpoints as well as providing a basis for determining the uniformity of the sprayed material across the surface of the diesel component.

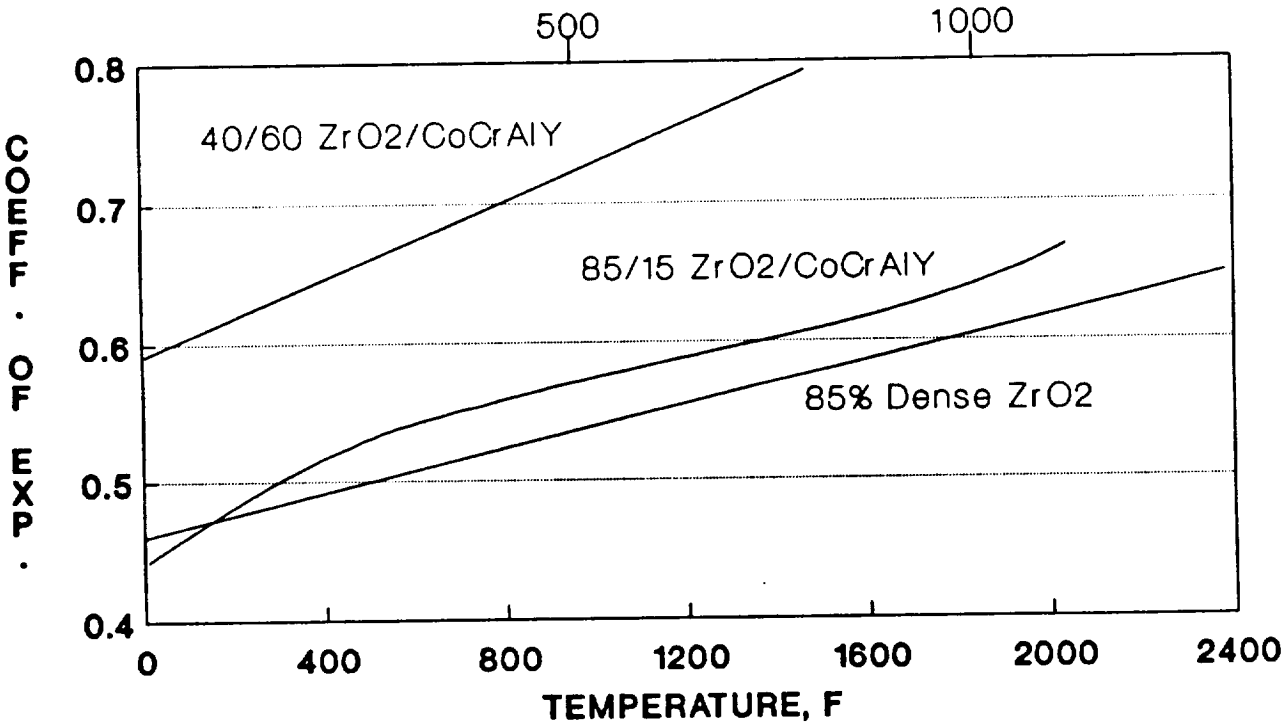

Figure 4.8: Thermal expansion of ceramic and cermet coatings.

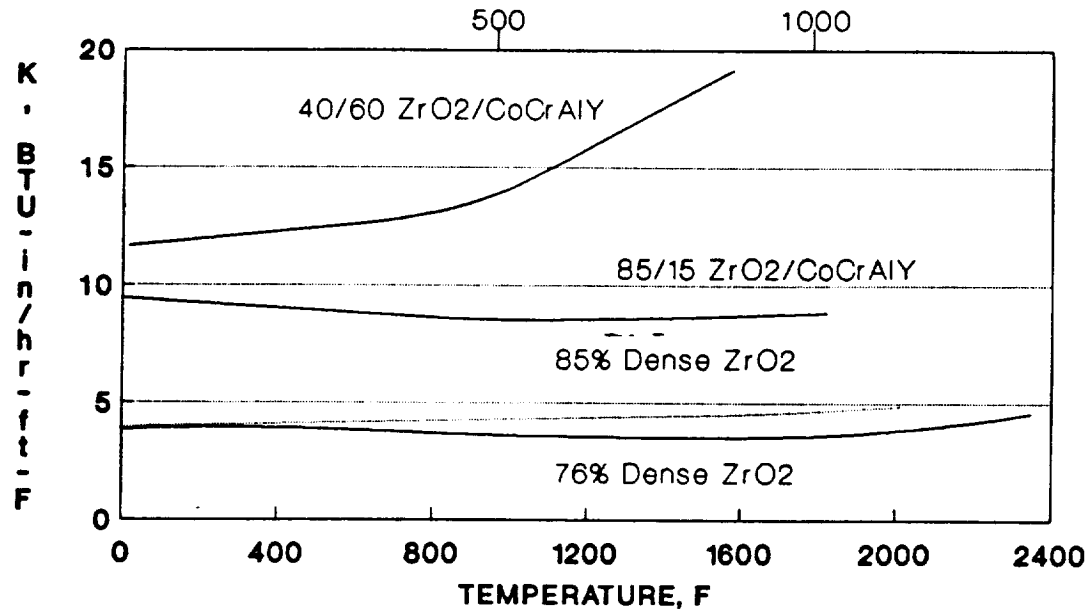

Figure 4.9: Thermal conductivity of ceramic and cermet coatings.

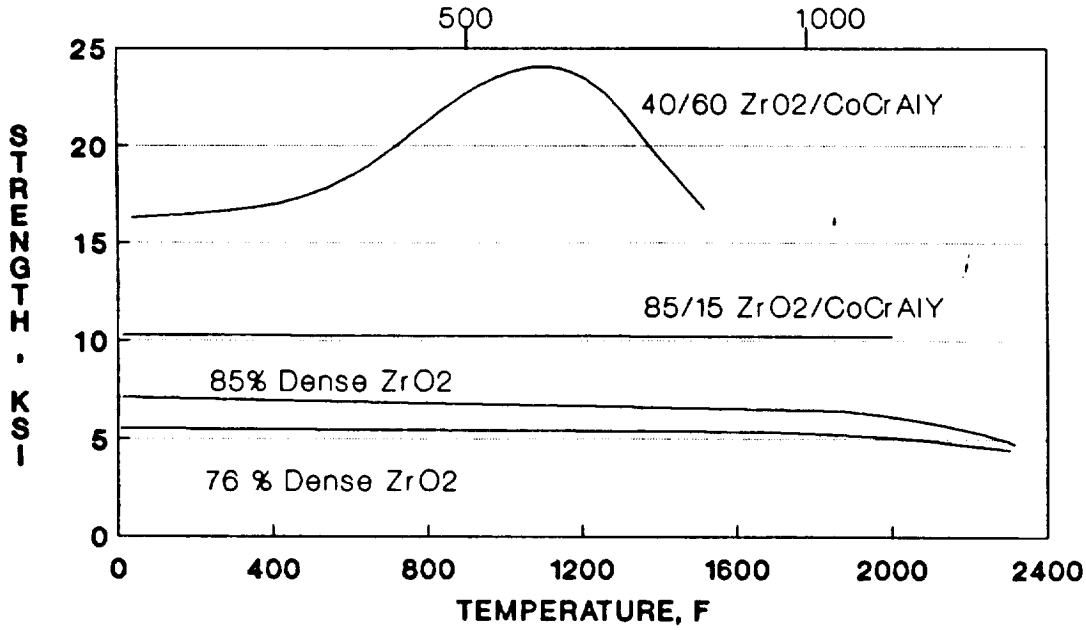

Figure 4.10: Flexure strength of ceramic and cermet coatings.

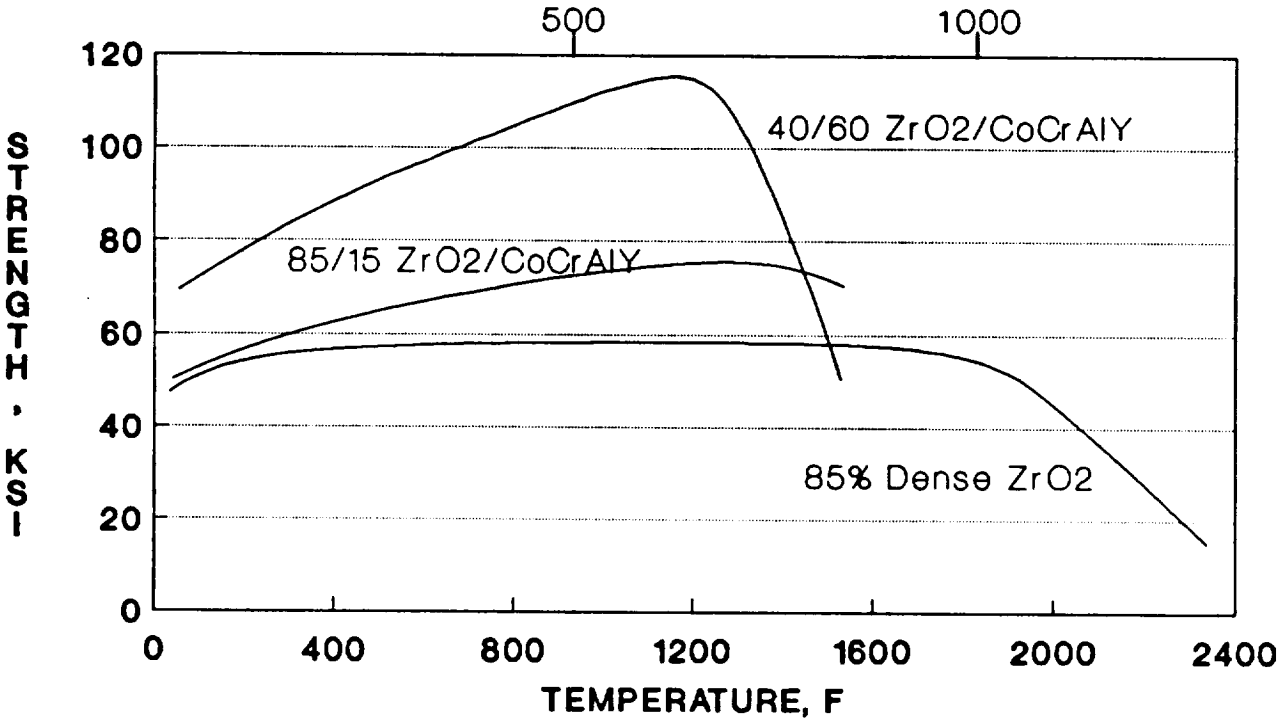

Figure 4.11: Compressive strength of ceramic and cermet coatings.

A spray fabrication technique was developed to define material properties most representative of actual coating material. Flat plate substrates were attached to the rotating holding fixture in areas representing the piston crown diameter. Heat was applied to the panels through the use of small propane torches mounted on a ring that surrounded the base plate. A thermocouple placed on the backside of the substrates of the propane to the torches to maintain the desired prestress temperature through the spray run. The actual robot motion control and spray processing parameters used to coat the piston crowns were used to coat the substrates. Test specimens were fabricated from the substrates in locations indicative of the crown rim and center dome areas as shown in Figure 4.12. This approach was needed to verify uniformity of properties across the crown diameter.

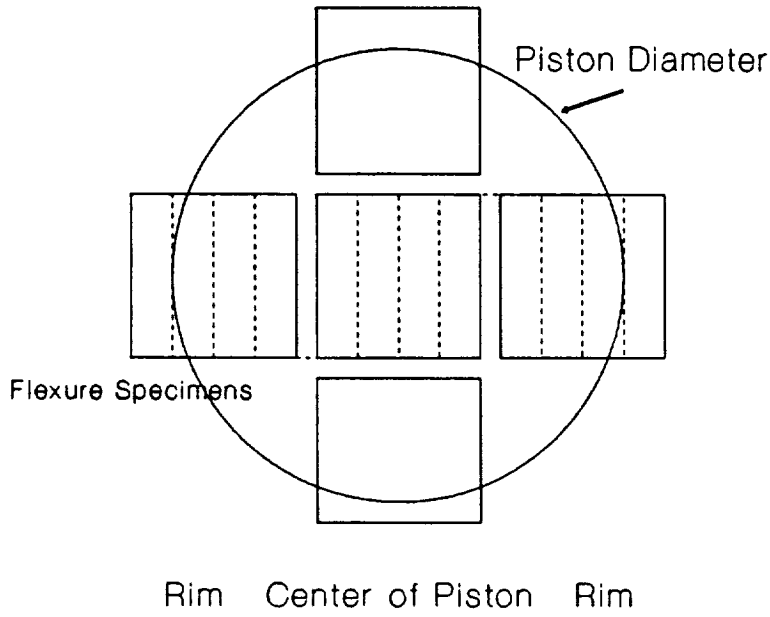

Figure 4.12: Materials properties specimens. Location relative to piston diameter.

V903 Piston Crown

Material properties of the constituent layers of the first generation V903 multi-layer coating including density, porosity, and four point bend strength and modulus properties were measured. The results verified that the final spray parameter setpoints used for processing the actual hardware produced a uniform coating across the crown diameter.

Measured four point bend strength and modulus were also used to determine the effect of gun power variations on the top layer material. Two gun power levels representing 6% and 12% increases over baseline were used to fabricate single layer zirconia material. Resulting four point bend strength and modulus data in comparison with the current top coat material are summarized below.

- The 12% increase in gun power produced a minimum of 72% increase in strength.
- Modulus for the 12% increase in gun power increased 100% at room temperature over the baseline material.

These results confirm that gun power has a significant effect on strength and can be used to change constituent layer material properties.

A compilation of material properties for the constituent layers of the V903 baseline multi-layer coating are given in Table 4.3.

Table 4.3

MATERIAL PROPERTIES OF CONSTITUENT LAYERS AT 25C

V903 Piston Crown and Single Cylinder Head

Property	85% Dense Zirconia	85/15 ZrO_2/CoCrAlY	40/60 ZrO_2/CoCrAlY
Density, g/cm^3	4.88	5.31	6.02
% Porosity	17.4	---	---
Four Point Bend Strength MPa (ksi)	21.7 (3.15)	42.5 (6.16)	182 (26.4)
Modulus of Elasticity GPa (x 10^6 psi)	14.3 (2.08)	22.4 (3.25)	44.7 (6.48)

Additionally, two alternate top coat materials were also identified for the purpose of increasing the strength and durability of the top layer of the coating system. These materials were Metco 204, a yttria partially stablizied zirconia and Metco 205, a ceria stabilized zirconia. The ceria stabilized zirconia was selected as it was expected to be less prone to attack from fuel additives than the yttria stabilized materials. Single-layer test panels were spray fabricated under the same process parameters as the current top coat material, and specimens were machined for measurement of four point bend strength and modulus. The measured material properties data are shown in Figure 4.13. The important points are summarized below.

- Both alternate materials were found to be stronger by a factor of two at room temperature.

- Both alternate top layer materials show a 1.5 increase in modulus at room temperature.

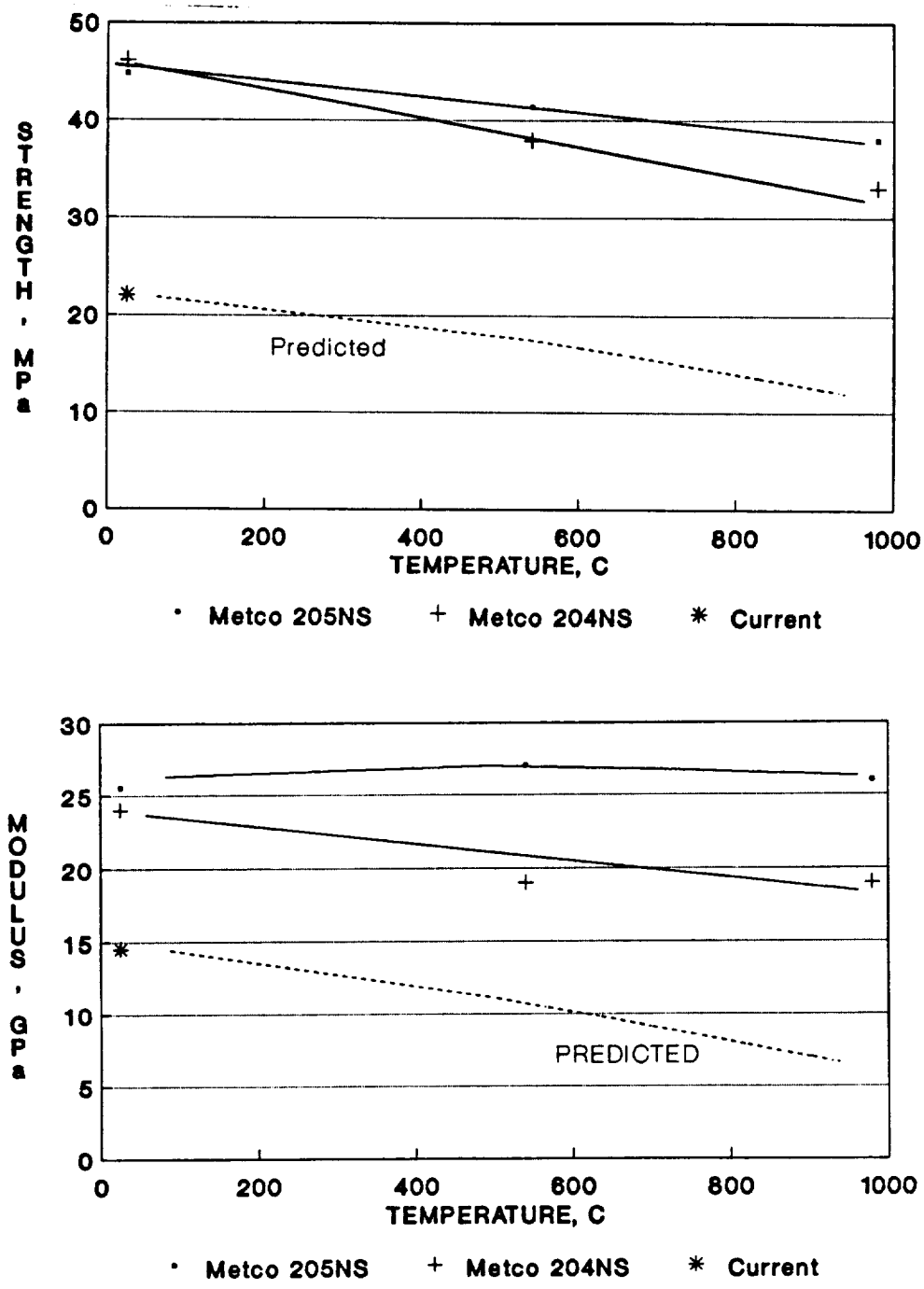

Figure 4.13: Alternate top coat material properties. Four point bend strength and modulus of elasticity.

Neither of these two alternate top layer materials were chosen for follow-on processing trials as they both represented lower strength to modulus ratios than the increased strength zirconia material obtained through gun power modifications and, therefore, analytically would be predicted to have higher thermal stresses.

Three alternate bond coat materials were identified as potential replacements for the current bond coat for use on the fiber reinforced aluminum piston crown. These materials were selected to provide a closer property match particularly for the coefficient of thermal expansion to the fiber/aluminum. Benefit was also expected to be derived for the steel base metal of the L10 piston cylinder crowns which exhibit an increased coefficient of thermal expansion over that of ductile iron. A comparison of the composition of the bond coat materials is given in Table 4.4.

Table 4.4

Comparison of Composition
Alternate Bond Coat Materials

Constituent	Current Bond Coat Metco 443	Metco 446	Metco 461	Metco 468
Ni	71.8	5.	74.	62.
Cr	18.4	7.	17.5	26.5
Al	5.8	55.5	5.5	7.
Fe	1.	25.		
Others	3.	7.5	3.	4.5

Single-layer property specimens were sprayed for each bond coat candidate using spray process parameters consistent with those used for the standard bond coat material. Test panels were machined for measurement of four point bend strength and modulus. Four point bend strength and elastic modulus of the bond coat specimens is shown in Figure 4.14.

- The Metco 446 (high aluminum content) material was found to be 25% weaker at room temperature and as much as 65% weaker at 538 C (1000 F) than the other two candidate materials.

- The elastic modulus for the Metco 446 material in comparison to the other bond coat materials was also lower.

- The coefficient of thermal expansion for the high nickel Metco 461 and 468 was similar to the standard bond coat.

- The coefficient of thermal expansion for the Metco 446 exceeded that of the fiber/aluminum material by approximately 17%; however, the character and slope of the curve would indicate that a similar coefficient of thermal expansion could be achieved by adjusting the aluminum content closer to the fiber/aluminum.

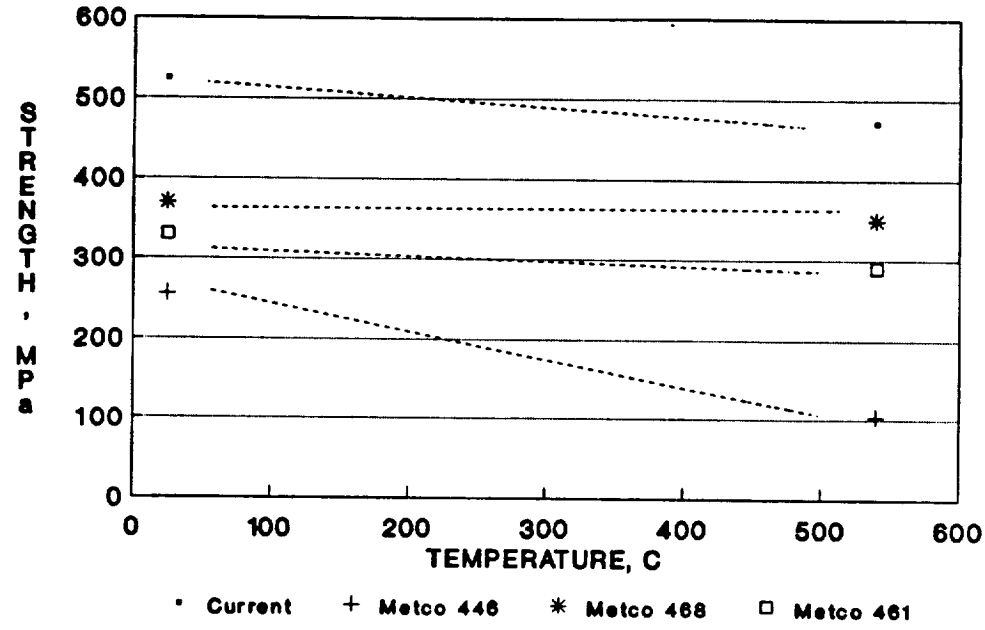

Four Point Flexure Strength

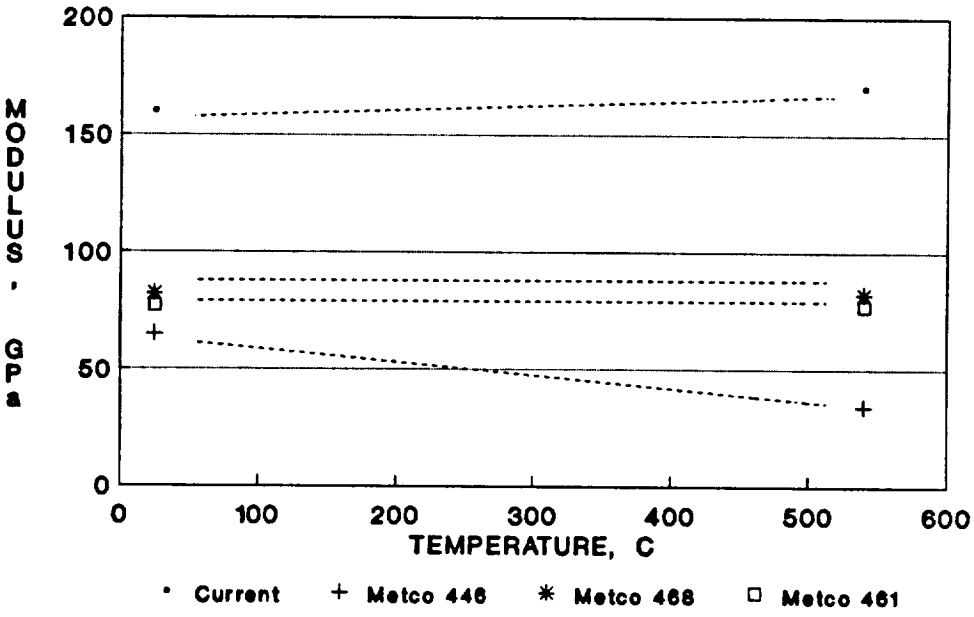

Figure 4.14: Properties of bond coat materials, strength and modulus of elasticity.

Even though material properties could be more closely matched, no change to the standard bond coat was made at this time given the successful test results of the baseline multi-layer coating on the V903 fiber reinforced aluminum piston crown. If it is desirable to substitute bond coats at a future date, an analytical assessment of the impact of the lower four point bend strength for these candidate materials would be required.

V903 Single Cylinder Head

Single-layer flat plate specimens were spray fabricated using the spray and robotic control parameters developed for applying the multi-layer coating system to the cylinder head inlay. Measured density and four point bend strength and modulus were determined to be equivalent to those of the piston crown materials. These data were shown previously in Table 4.4.

In addition, material properties were measured for alternate coating systems which were judged to provide potential improvements in cylinder head durability. The candidate material selected was an increased strength zirconia.

In order to affect an increase in strength for the top layer material, gun power was increased 20% over the baseline 35 KW setpoint. This decreased the porosity of the top layer from nominally 16% to 13%. The estimated improvement in strength was calculated to be as much as 50% over that of the baseline material.

L10 Piston Crown

An initial spray trial of the top layer zirconia material was made to verify the effective transfer of spray processing technology from the V903 to the L10 piston crowns. Measured density and four point bend strength and modulus values for the L10 top layer material were approximately 25% higher than those for the V903 material. These property changes were attributed to modifications in the robot motion control needed to traverse the steeper wall area of the L10 crown geometry. Even though there were noted differences in material properties, the strength-to-modulus ratio of the L10 material remained consistent with that of the V903. As a result, spray processing parameters were considered acceptable and used to produce first generation L10 piston crowns.

Based on V903 engine test results, it was viewed as necessary to further increase the strength of the zirconia top layer material. This was achieved by increasing the gun power by 20% over the baseline setpoint resulting in an 11% increase in strength. This change in top layer material property was incorporated in spray process modifications used to coat the L10 piston crowns.

Similarly, material properties and microstructures were evaluated for all other layers. A comparison of the ceramic/metallic intermediate layers for the L10 versus the V903 materials are summarized below.

- The microstructure of the 85/15 layer was consistent.
- The 40/60 material showed slight variation in metal content.
- Measured density and four point bend strength and modulus for the 85/15 material were consistent.

The variations in properties and microstructure in the intermediate layers were not judged to be significant enough to modify spray process parameters for these layers. A compilation of material properties for the intermediate layers as well as the baseline and increased power zirconia top layers are given in Table 4.5.

Table 4.5

Material Properties of Constituent Layers At 25 C

L10 Piston Crown

Property	85% Dense Zirconia	20% Incr. Power ZrO_2	85/15	40/60
Density, g/cm^3	5.10	5.10	5.34	5.85
% Porosity	13.8	13.8	---	---
Four Point Bend Strength, MPa (ksi)	25.1 (3.64)	28.9 (4.20)	31.9 (4.62)	113. (16.4)
Modulus of Elasticity, GPa ($X10^6$ psi)	15.8 (2.30)	18.3 (2.66)	19.8 (2.88)	39.3 (5.70)

4.3 Nondestructive Evaluation

Four methods of nondestructively evaluating thermal barrier coatings were evaluated; ultrasonics, fluorescent dye penetrant, and two methods of infrared imaging. Ultrasonic c-scan was unable to penetrate the porous thermal barrier coatings due to signal attenuation. Although initial low frequency tests appeared favorable for detecting delaminations, samples with known defects could not be resolved by ultrasonic inspection methods.

Fluorescent dye penetrate techniques were also evaluated. It was determined that a sensitive dye penetrant could be used to detect regions of inhomogeneities and delamination. Unfortunately, this technique is operator sensitive and the effects of remaining dye penetrant in the coating are unknown. Fluorescent dye penetrant could be a useful technique for initial development of plasma spray processing parameters, particularly for regions of complex geometry.

Mr. Doug Harris, APS Materials, and Mr. Mike Kelly, MRC-Mound DOE, investigated an infrared video thermography excited by a 8W CW laser beam. Defects in the coating resulted in perturbations in the thermal energy profiles. Although resolution was quite good for this technique, this scanning method was difficult to implement for complex geometry components.

The final technique evaluated was also a thermal wave imaging technique conducted by Dr. Robert Thomas and Dr. Tasdiq of Wayne State University. Their infrared imaging technique has proven extremely useful in the nondestructive evaluation of thermal barrier coatings. Drs. Thomas and Tasdiq have been able to resolve delaminations in thermal barrier coatings before and after engine evaluation. This technique has been proven useful in the decision making process for determining sections of the thermal barrier coatings which have delaminated. Figure 4.15 show an optical micrograph and a thermal image of the same locations. In this example, the delamination can be readily observed at the piston center section of the infrared image. Figures 4.16 and 4.17 show images of the thermal barrier coating that delamined during engine evaluation. The spalled region appears cooler in the infrared image while attached regions that have delaminated but remain intact are shown as bright regions in this image. As can be seen from these images, major changes in the thermal barrier coating were occurring after engine test and resolved by this technique. Regions of thermal barrier coating that have delaminated but are not connected to the surface have been resolved by the infrared imaging.

Infrared imaging has proven to be useful in determining the extent of damage in thermal barrier coatings. At this point in time, we have been limited to initial evaluation of the thermal imaging technique. Resolution limits, influence of deposits, and the full potential of this imaging system are unknown.

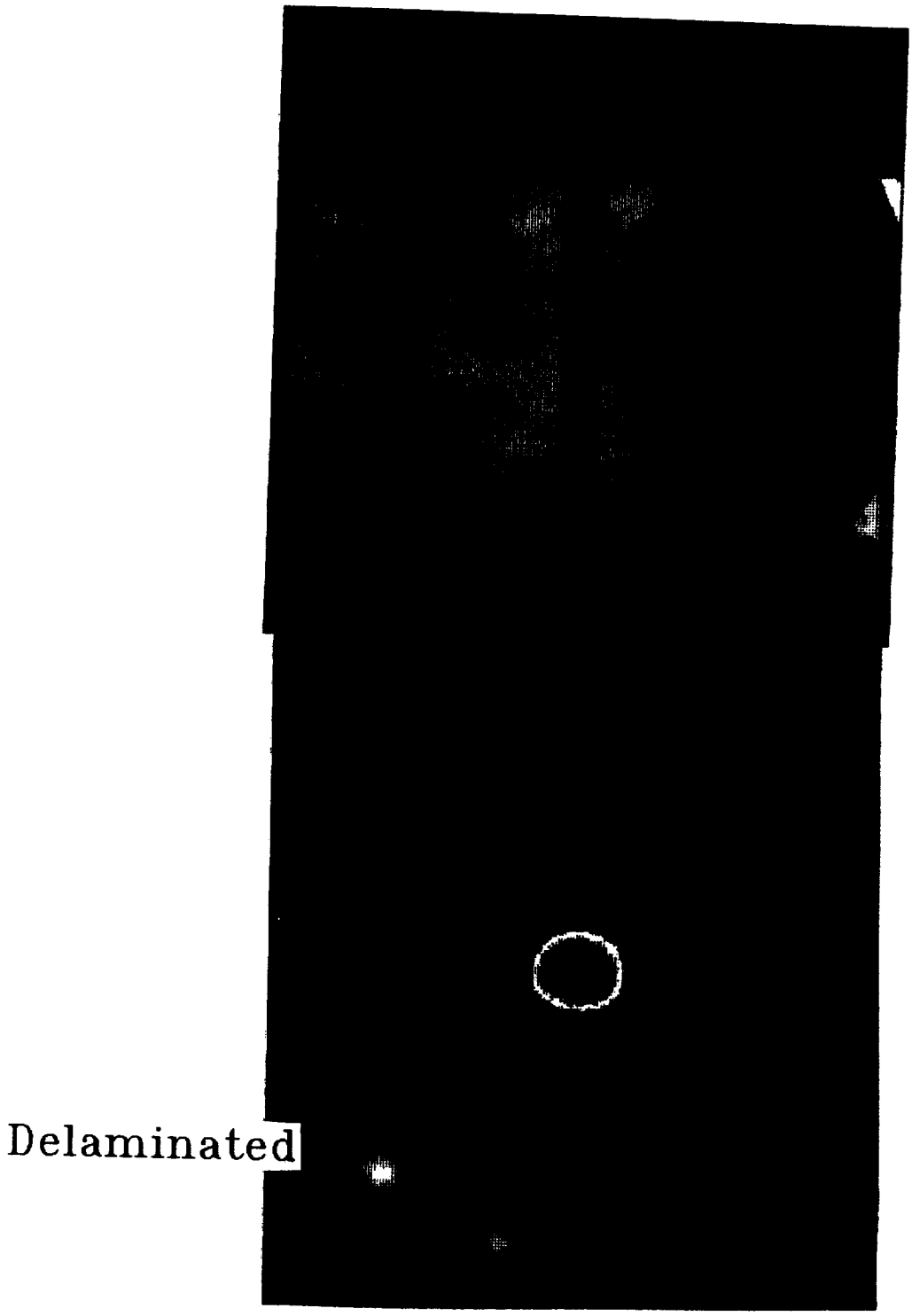

Figure 4.15: Comparison of rastered optical image and infrared image of the same piston showing delamination at the piston center.

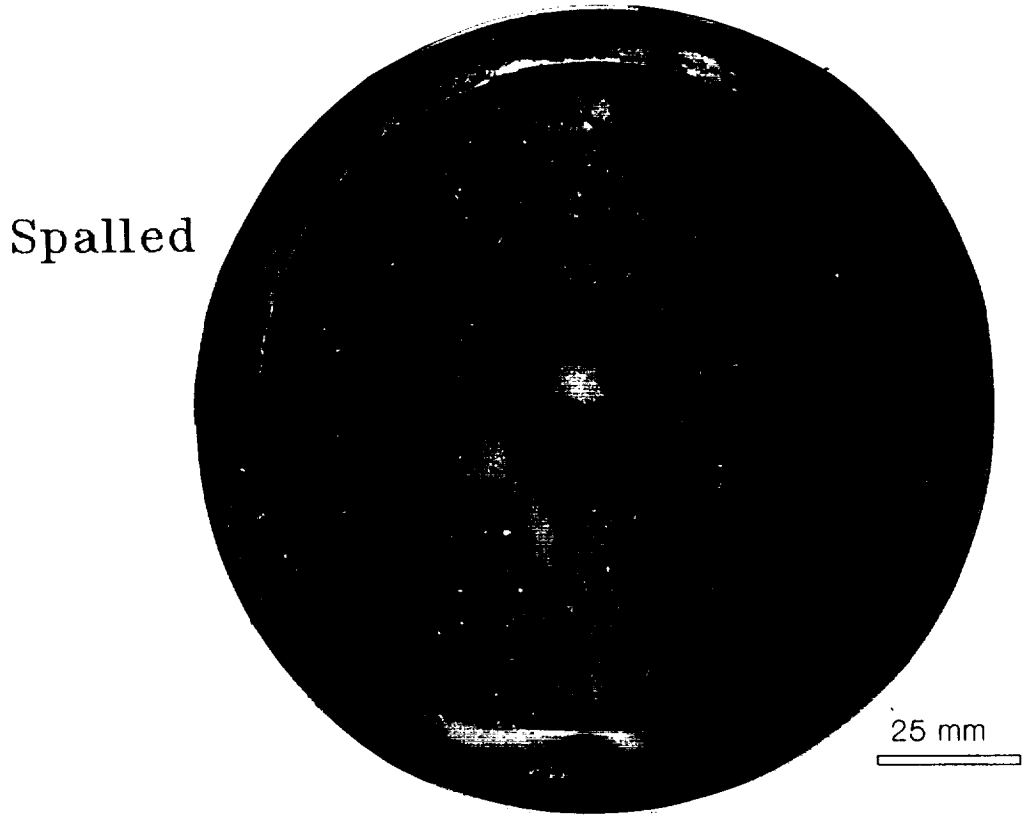

Figure 4.16: Optical photograph of piston rim spallation which occurred during turbocompound tests. Piston had previously survived 1.03 MPa (150 psi) BMEP for 50 hours.

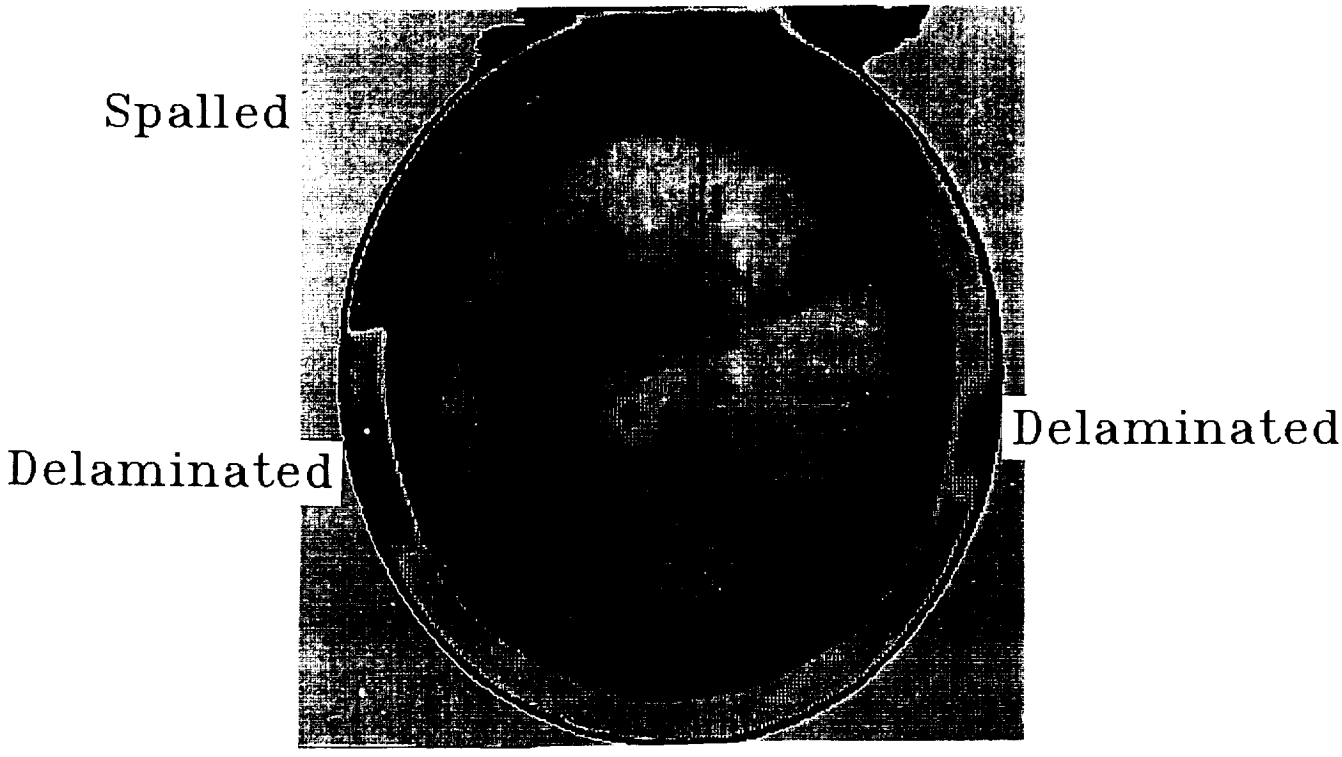

Figure 4.17: Infrared image of piston in Figure 4.16 showing areas where coating has been removed and areas that have delaminated but remain attached.

4.4 Thermal Shock and Environmental Screening

4.4.1 Prestress/Spray Process Methodology

A basic strength test was used to rank the candidate coating systems by measuring their resistance to thermal/mechanical strain. This test was initially defined based on UTC experience with evaluating turbine seal coatings. The burner rig test consisted of a snap acceleration to maximum operating temperature with the top surface of the coating increasing from an initial temperature of 65 ~ 95 C (150-200 F) to 760 ~ 815 C (1400-1500 F) in a fifteen second time frame. The greatest temperature gradient occurred at approximately 5 seconds and the maximum top surface temperature occurred at about fifteen seconds.

Initial screening of single-layer and multilayer candidate coating systems on ductile iron test panels for basic strength were spray fabricated and the coating machined to the target overall thickness of 2.54 mm (0.100 inch). The results obtained from the initial basic strength tests confirmed the analytical predictions that favored multilayered structures over single-layer coating systems.

In addition to providing a calibration of the analytical model, basic strength test results were used to verify coating properties particularly the stress free fabrication temperature. The stress free fabrication temperature is a measure of the coating residual strain state and is controllable through process setpoints. Strain discontinuities between layers can be minimized by control of the temperature during spray fabrication.

For this determination it was necessary to more closely simulate a diesel engine cycle, and, as a result, an evaluation of the basic strength rig test conditions was pursued. Based on preliminary one-dimensional transient analysis performed by Cummins for the baseline multilayer coating on ductile iron, the rig thermal cycle was retargetted to achieve a maximum surface temperature of approximately 675-730 C (1250-1350 F) with a maximum thermal gradient across the coating of approximately 480-540 C (900-1000 F) at a 7 second time point into the cycle.

The burner rig conditions were calibrated using the baseline multilayer coating system on a nickel-based superalloy test panel that had been instrumented with embedded thermocouples. A test cycle, C1, which most closely reflects the predicted diesel engine thermal environment, was created with a maximum thermal gradient across the coating of approximately 510 C (950 F) in seven seconds and a top surface temperature of 675 C (1250 F). Two additional test cycles, C2 and C3, representing maximum thermal gradients of 555 C (1030 F) and 705 C (1300 F) respectively were used to further screen thermal strain capability at higher temperatures. The three test cycles are shown in Figure 4.18.

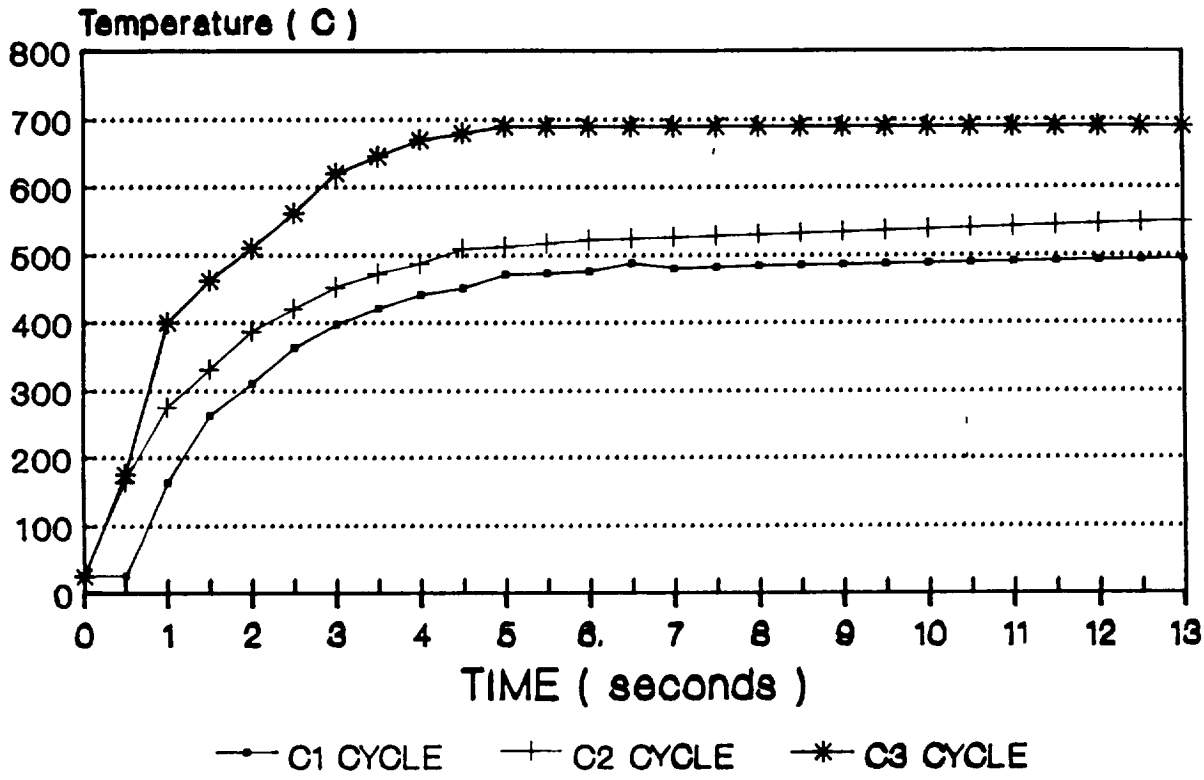

Figure 4.18: Test cycles used to thermal shock thermal barrier coatings.

Ductile iron test panels with the baseline multilayer coating system were fabricated at both a medium fabrication temperature and a medium (hybrid) fabrication temperature which incorporated a temperature spike through the bond coat region. These panels were then exposed to the same thermal cyclic test conditions. The panel fabricated at the medium fabrication temperature was initially tested and survived the C1 cycle. This panel was then run through five C1 cycles in succession with the panel being allowed to reach the initial soak temperature of 65 C (150 F) before being recycled to the maximum top surface temperature. Examination of the panel after the five cycles yielded no visible damage. The panel was then subjected to the more severe C2 and C3 test cycles. No damage was noted to occur after the C2 cycle; however, after the C3 cycle the coating showed moderate cracking of a secondary nature at the 40/60 to 85/15 interface.

The panel fabricated at the medium (hybrid) prestress temperature profile was exposed to the C3 rig cycle only and showed minimum cracking sensitivity. Given UTRC's experience, it was felt that this coating system would have survived the C2 rig cycle and have acceptable performance up to a 650 C (1200 F) maximum thermal gradient. These test results showed the superior strain capacity of the baseline multilayer coating system fabricated with the medium (hybrid) fabrication temperature control.

4.4.2 Contamination Screening

Evaluation of V903 engine tested pistons with thermal barrier coatings which had been subject to diesel fuel combustion were checked to determine if corrosion and erosion of the coating were taking place. Coatings evaluated by this method included the Plasma Technics and UTRC coatings. The Plasma Technics coatings were subjected to V903 multicylinder engine tests for 230 hours of engine operation on another program. UTRC thermal barrier coatings were evaluated after various hours of engine test in this program.

The coatings were evaluated using a Siemens 810 x-ray generator with a horizontal type diffractometer. This permitted the x-ray diffraction analysis of the coating with removal of the coating from the piston. Copper K-alpha radiation filtered through a nickel filter were used. Data was analyzed using a Siemens Diffrac 11 software coupled to the JCPDS computer file.

Plasma sprayed thermal barrier coatings were analyzed by x-ray diffraction before and after engine tests. In the case of the Plasma technics sample, the baseline material consisted of tetragonal and cubic zirconia.

Figure 4.19 shows the x-ray spectrum for the baseline unexposed sample with the peak location for tetragonal and cubic zirconia superimposed. The pattern closely matches the cubic phase and no peak splitting tetragonal phase were noted.

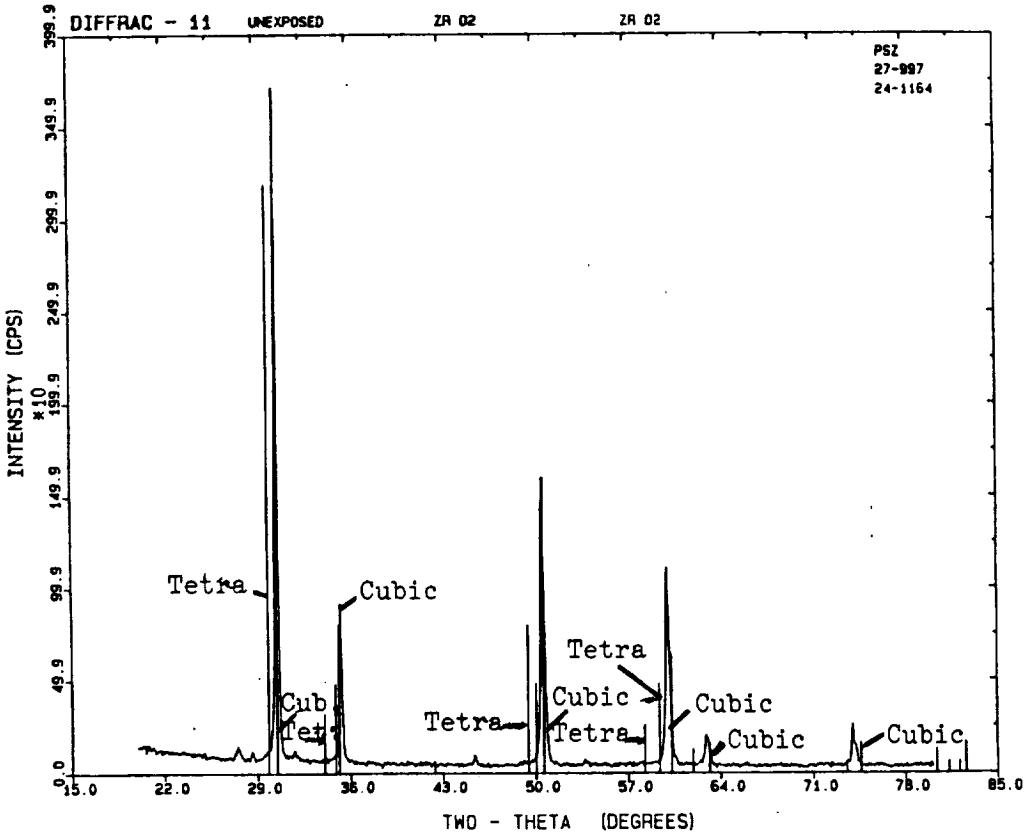

Figure 4.19: X-ray diffraction pattern of as-received thermal barrier coating.

Engine tested coatings were analyzed, both on the piston and after the coating was removed, by powder x-ray diffraction. The superposition of the baseline (unexposed) and exposed x-ray patterns are shown in Figure 4.20. These patterns were virtually identical although several small peaks were observed at low angles and attributed to minor amounts of phosphates. Detailed examination of the zirconia did not detect any evidence of the cubic zirconia being destabilized to monoclinic. From this evidence, it was concluded that the chemical and thermal environment was not severe enough to degrade the Plasma Technics plasma sprayed zirconia with 13 wt% yttria. Cracking and coating delamination observed on some pistons is believed to be due to the severe thermomechanical loading and the thermal expansion mismatch between the zirconia and the ductile iron piston.

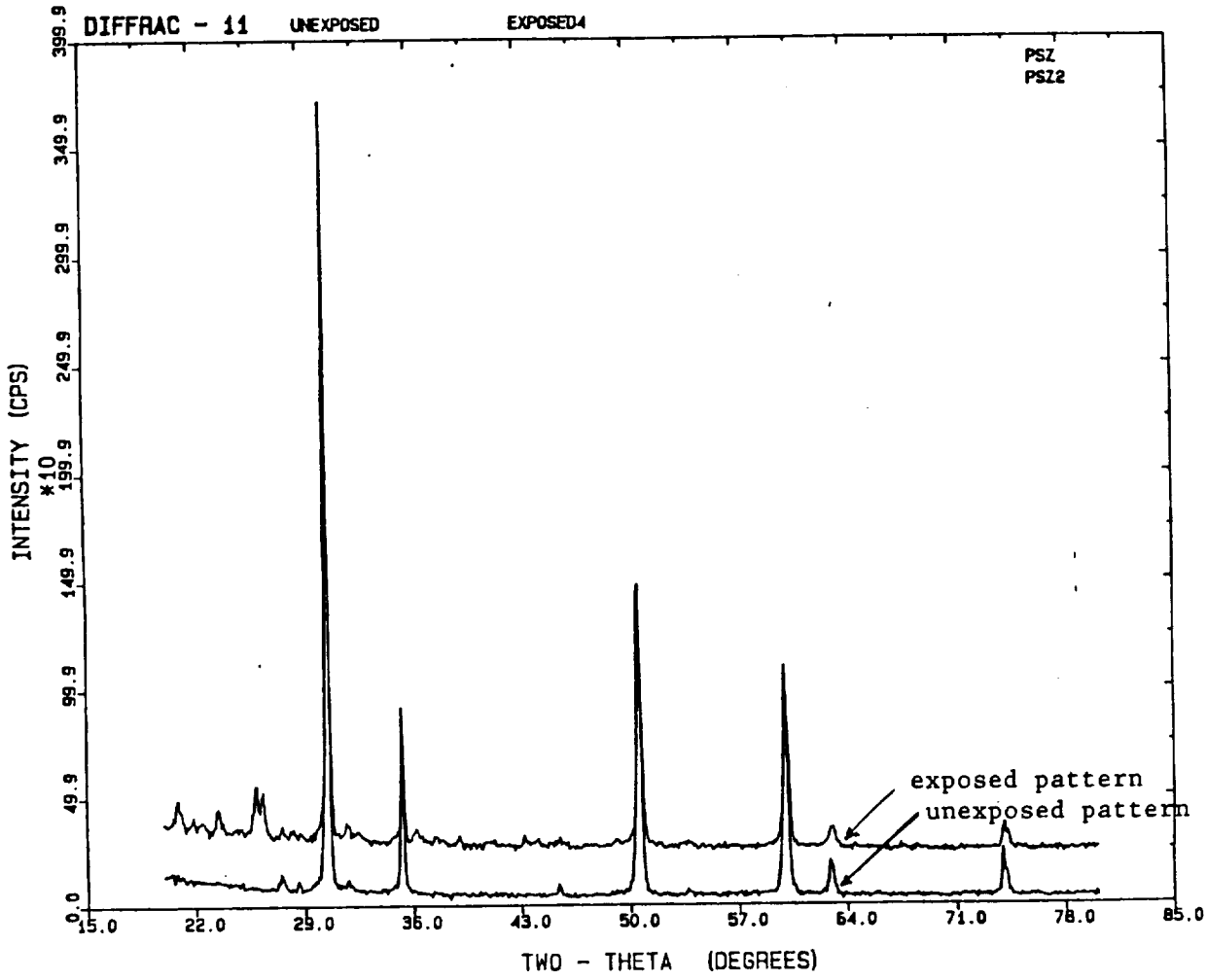

Figure 4.20: X-ray diffraction pattern of unexposed versus exposed plasma sprayed zirconia.

Evaluation of the UTRC coatings contained similar information. The UTRC coatings were found to be fully stabilized zirconia consisting of cubic zirconia. As shown in Figure 4.21 engine tested pistons remained cubic zirconia. In many cases, calcium sulfate build up was detected by x-ray diffraction analysis. In one case, one UTRC coating after engine test contained monoclinic zirconia. Occurrence of this phase was attributed to the original plasma spray processing. Appearance of monoclinic zirconia has not been observed in any other UTRC coatings.

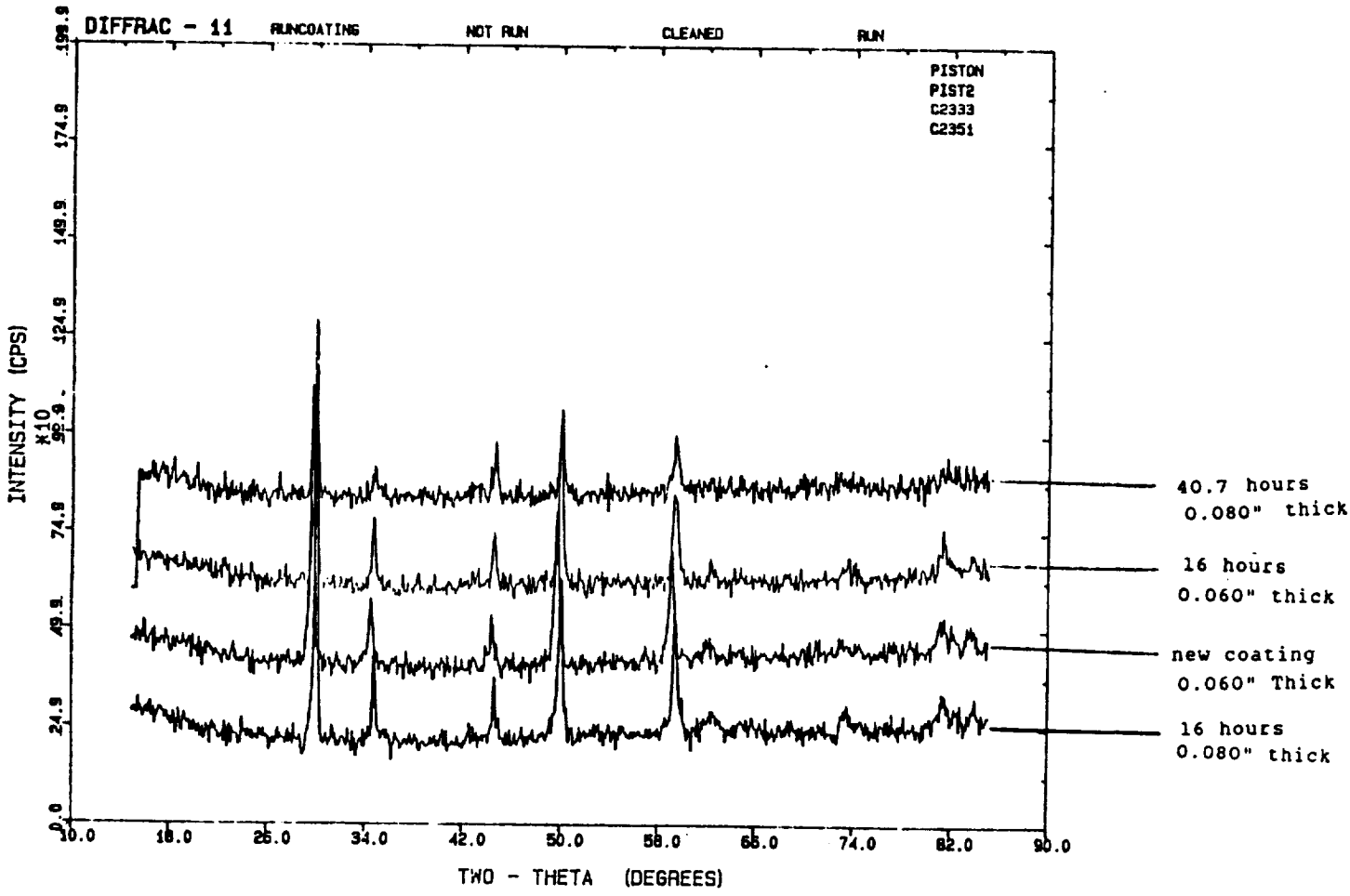

Figure 4.21: X-ray pattern of UTRC thermal barrier coatings.

UTRC reviewed the results of three of the pistons that have been engine tested at Cummins. The pistons include the Cummins engine tests #1, #3, and #5. Information on the engine test is provided in Table 5.3. Engine test #1 was a 0.08 inch thick coating. Visual inspection determined that there were typical mudflat cracks across the surface with some surface erosion. The coating was intact. This piston was tested at Cummins for approximately 50 hours.

The piston used in engine test #3 exhibited microcracking of the coating from the rim into the bowl. The coating was intact, no coating loss. UTRC and Cummins have determined that this piston has monoclinic phases through x-ray diffraction. We do not have any information that would indicate the reason for the presence of monoclinic zirconia containing monoclinic zirconia. It was believed that the presence of monoclinic zirconia was due to incorrect processing. However, evaluation of the records did not reveal any problems with this plasma spray run. The fabrication temperature profile was acceptable.

UTRC has determined that the percent yttria was correct in the piston, approximately 20%. SEM and energy dispersive x-ray analysis indicate the presence of Zr, Y, Fe, Ca, Zn, and S. Microprobe analysis at UTRC revealed Mg, Zn, P, Y, Ca, Cr, Co, Cu, Fe, and Zr. None of these materials would be expected to result in detrioration of the coating over the short time of the engine test. The piston was tested for a total 68 hours of mostly low load operating conditions.

The piston in engine test #5 had spalled in the center section of the piston as shown in the previous report. UTRC determined that the fabrication temperature was acceptable. They also confirmed Cummins x-ray diffraction results which revealed that there was not any monoclinic zirconia in the coating. SEM coupled with energy dispersive x-ray analysis revealed the presence of Pb, Co, Fe, Ca, Ni, Zn, Mg, Cr, Zr, and Y. Microprobe at UTRC detected Ar, Zn, Y, P, Mg, Ca, Cr, Co, Fe, and Ni. Cummins elemental analysis of the fuel used in this test in the attempt to resolve the potential of vanadium resulting in corrosive attack of the coating determined that the V was less than .1 ppm or at or below the limits of detectability. Note that UTRC also did not detect vanadium in any of their studies. Vanadium has been shown to destabilize the zirconia through preferential attack of yttrium.

In summary, x-ray diffraction has determined that the thermal barrier coating are not experiencing any significant phases changes in a diesel engine environment for relatively short test periods, less than 100 hours. Analysis of build up deposits on the surface of the coating has revealed that constituents in the fuel and lubricant can be vapor phase deposited on the surface of the coating. Calcium sulfate deposits have been identified on the coating. Phosphates, and carbonaceous materials have also been observed. At this point in time, the deposit build up does not appear to be damaging the thermal barrier coating.

5.0 TASK III - SINGLE CYLINDER ENGINE TESTS

The engine used for evaluation of the thermal barrier coatings was a Cummins V903 single cylinder research engine, Figure 5.1. The V903 engine uses a direct injection fuel system and has a 139.7 mm (5.5 inch) diameter bore and a 120.7 mm (4.75 inch) stroke. The engine test facilities, Figure 5.2, control the incoming air, water, and lubricant temperatures and pressures to the engine. By controlling the intake and exhaust flows, the engine can be operated in simulated turbocharged and turbocompound operations. Through the engine test cell control and data acquisition system, horsepower, brake specific fuel consumption, engine speed, heat rejection, temperature and pressures can be monitored and recorded. A description of the instrumentation and data collected is contained in Table 5.1.

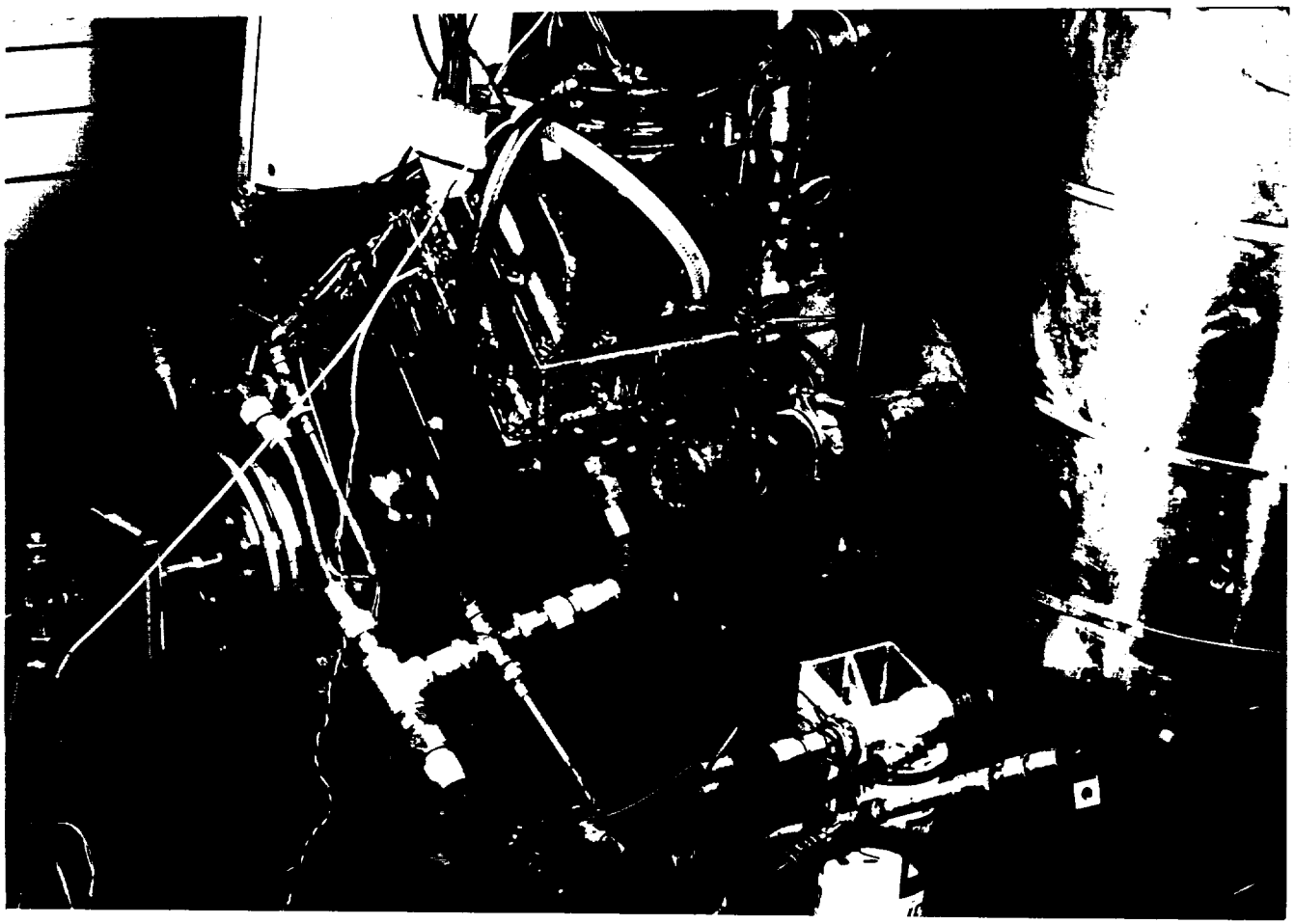

Figure 5.1: V903 Single Cylinder Research Engine

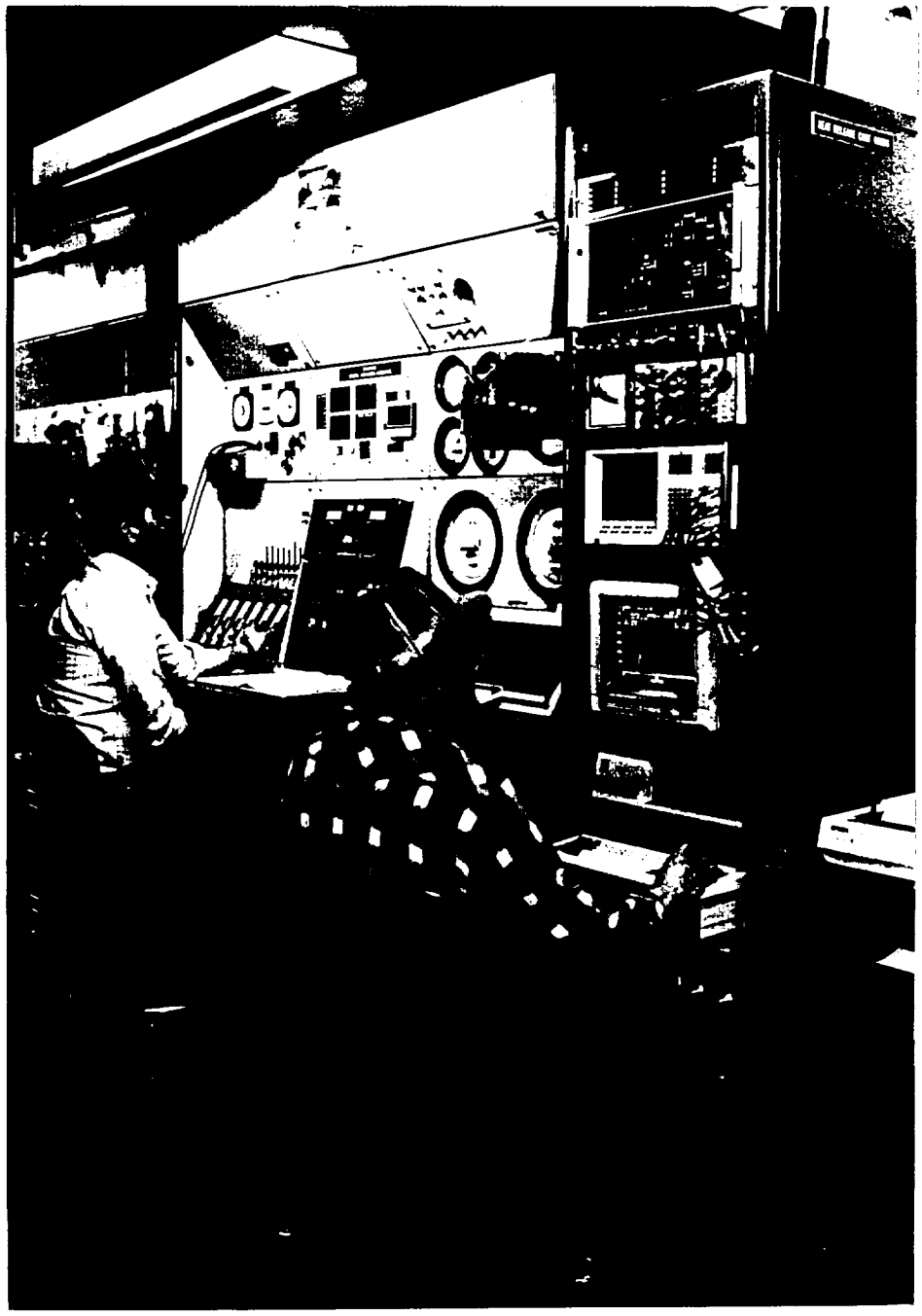

Figure 5.2: Engine test control console and heat release cart.

Table 5.1

Test Cell Data and Instrumentation

Data	Instrumentation
Engine Speed	Magnetic pick up
Engine Torque	Load cell
Fuel Consumption	Fuel scales
Oil, air and fuel temperatures	Heaters and coolers using electromechanical control
Exhaust blow-by	Flow orifice and manometer
Intake and exhaust temperatures and pressures	Thermocouples and manometer
Heat rejection	RTD combined with torque and fuel
Injection timing and quantity	Pressure transducer
	Accelerometer attached to injector

One major program goal for the thermal barrier coatings was 100 hours of operation at engine conditions that were representative of heavy duty diesel engine operation, 1.03 MPa (150 psi) BMEP or greater with peak cylinder pressures of approximately 13.8 MPa to 14.5 MPa (2000 to 2100 psi). In addition, the thermal barrier coating must be capable of surviving cyclic engine operations, hot shutdowns, and other severe operating conditions that are commonly encountered in commercial diesel engines. To determine the functional capabilities of the thermal barrier coatings, four types of engine tests were utilized. These engine tests were designed to provide a sequential increase in the thermal and mechanical stresses on the thermal barrier coating. The first test type consisted of steady state engine operations at a 30 to 1 air/fuel ratio. The steady state test is the least demanding of the tests, but provides actual engine operating conditions and reasonably high temperature and stresses. This test is used as the initial evaluation tool for the thermal barrier coatings. For example, the engine would be operated at 0.69 MPa (100 psi) BMEP for 8 hours followed by inspection. After inspection, the engine power was increased to 1.03 MPa (150 psi) for another 8 hour test followed by 1.38 MPa (200 psi), for an additional 8 hours with visual inspections after each step in power. Air fuel ratio was held constant at 30 to 1 for these tests.

If the coating survives the steady state tests, they are subjected to higher thermal stresses in transient or cyclic tests. These tests consist of cyclic testing between the full power condition 1.38 MPa (200 psi) BMEP and high idle. The cyclic test imposes severe thermal gradients and increased thermal transient stresses on the piston coating. Previous thermal barrier coatings would not survive the cyclic test sequence used in this program.

The third test type was an evaluation of the thermal barrier coating at the engine torque peak condition. Torque peak conditions impose high temperatures and mechanical stresses on the piston.

The fourth and final test is a an overload test that is the confirming test for the coating. Coatings that pass this test will probably survive the conditions required by future engines. The overload test was used to create higher temperatures on the piston surface which was achieved by decreasing the air/fuel ratio from 30 to 1 to 26 to 1.

5.1 Insulated Piston Screening Tests

5.1.1 Ductile Iron Pistons

The first insulated piston, piston #1, screening tests were conducted with an uncooled block and a water cooled head at 1.38 MPa (200 psi) BMEP level (450 HP rating at 2100 rpm). A ductile iron piston, piston #1, with a 2.03 mm (0.80 inch) thick multilayer coating was tested for 8 hours followed by visual inspection of the coating by removing the cylinder head. No coating damage was observed during this test. Additional testing included cyclic testing from rated condition to high idle. Cyclic testing was comprised of equilibrating the engine at rated conditions followed by decreasing the fuel to achieve the high idle condition, Table 5.2.

Table 5.2

Cyclic Test Conditions*

10 minutes rated power
4 cycles between rated and high idle
2 minutes rated
4 cycles between rated and high idle
2 minutes of rated
4 cycles between rated and high idle

*Repeat above cycle.
Total of 400 cycles between rated power and high idle.

The cyclic testing results in severe thermal cycles to the coated piston surface. Inspection of the piston indicated that no damage to the coating had occurred during the cyclic test.

However, because of difficulties encountered in operating the research engine at rated power at 2100 rpm and engine dynamometer coupling failures at torque peak, subsequent engine tests for piston #1 and other pistons were conducted at a 2600 rpm rating at 1.03 MPa (150 psi) BMEP, and 1.38 MPa (200 psi) BMEP, at the 30 to 1 air/fuel ratio. After 8 hours of engine operation at the lower load, and 10 hours at the higher load, inspection revealed that the coating on piston #1 was still in excellent condition. The piston coating was then subjected to an additional 6 hours of overload testing at a 26 to 1 air/fuel ratio. This overload condition results in additional thermal stresses to the coating. Visual inspection

once again revealed that the fully stabilized coating was in excellent condition, and that there was no material loss condition. X-ray diffraction analysis revealed that the coating surface was fully stabilized zirconia without any monoclinic phases. In some regions of the piston, calcium sulfate was observed which is due to deposition from the sulfur in the fuel and calcium in the lubricant.

A summary of the piston screening test results for the five pistons evaluated are contained in Table 5.3.

Table 5.3
Summary of Coated Piston Screening Tests
Ductile Iron Pistons

- Piston #1 - 2mm (0.08 inch) thick coating survived total of 42 hours which included 10 hours at 600 HP equivalent, 8 hours of cyclic tests, 6 hours of overload test at 26 to 1 air fuel ratio and two hot shut downs. Coating condition was excellent. Additional tests to determine temperature of coating has resulted in segmented microcracks after 600 HP operation.
- Piston #2 - 1.5mm (0.06 inch) thick coating survived 4 hours at 300 HP and 12 hours at 450 HP equivalent. Inspection revealed that the coating was eroding at the piston rim and the coating was "soft". Test stopped.
- Piston #3 - 2mm (0.08 inch) thick coating survived 68 hours of total test with 8 hours at 450 HP and 8 at 600 HP equivalent. Inspection revealed microcracks after the 600 HP test. X-ray inspection revealed monoclinic zirconia. Chemcial analysis revealed that the yttria content was correct.
- Piston #4 - 1.5mm (0.06 inch) thick coating survived 19.7 hours of test. Coating extensively damaged due to hot plate failure.
- Piston #5 - 2.54mm (0.100 inch) thick coating spalled after 46 hours at 600 HP equivalent. Coating was inspected after 2 hours of 600 HP test and found to be in excellent condition.

Piston #5, was the only piston that had spalled during piston screening tests. The ductile iron piston evaluated had a 2.54 mm (0.100 inch) thick coating. The objective of this test was to develop additional confidence on the coating at the 1.38 MPa (200 psi) BMEP level under steady state conditions. Therefore, the coating was evaluated at the 0.35 MPa (50 psi), and 1.03 MPa (150 psi) conditions for two hours at each condition to confirm basic engine performance followed by engine evaluation at the 1.38 MPa (200 psi) BMEP. The piston coating was visually examined after 2 hours at the highest load condition, and determined to be in excellent condition without any evidence of coating deterioration. Engine testing continued at the high load condition. After 46 hours of engine operation, the engine brake specific fuel consumption did not repeat previous values and fuel consumption had increased. Engine brake specific fuel consumption did not repeat previous points since compression ration, air motion, and possibly engine sealing was affected by the coating loss. After checking the data, the engine test was stopped to allow inspection of the piston. The coating had delaminated in the central portion of the piston, Figure 5.3. Inspection of engine hardware confirmed that engine instrumentation was in place and that impact damage was ruled out as a primary cause of coating spallation.

C-2.

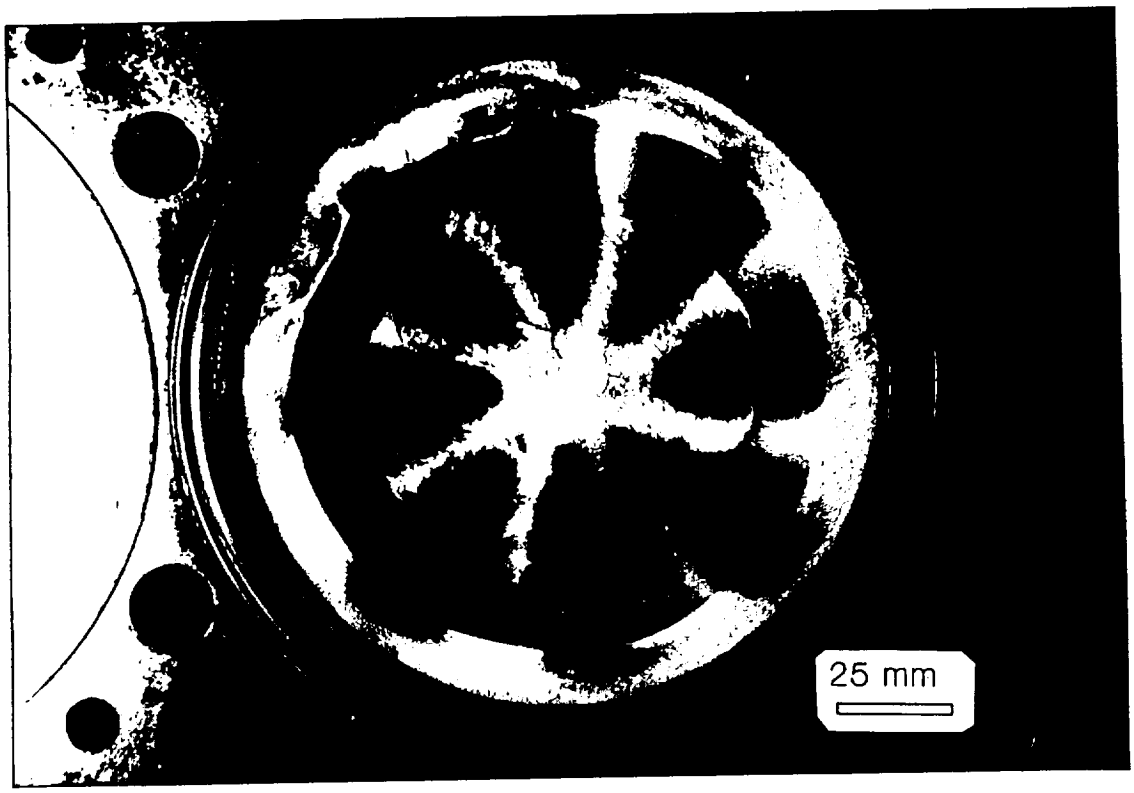

Figure 5.3: 2.54 mm (0.100") coating that spalled during engine evaluation, piston #5.

X-ray diffraction of the coating confirmed that the zirconia was still cubic with no evidence of monoclinic zirconia. Microprobe analysis of the coating did not detect any evidence of fuel penetration nor was there any evidence of chemical attack of the coating. The main cause of coating spallation in this test was that the coating strength had been exceeded during the engine test.

5.1.2 Fiber Reinforced Aluminum Pistons

In view of the test results on the 2.54 mm (0.100 inch) thick coating on the ductile iron piston, the test conditions selected for evaluation of a fiber reinforced aluminum piston with the same version of the multilayer 2.54 mm (0.100 inch) thick coating were more conservative. The piston was evaluated in a stepwise fashion at 0.34 MPa (50 psi), 0.52 MPa (75 psi), 0.69 MPa (100 psi), 0.86 MPa (125 psi), and 1.03 MPa (150 psi) BMEP (maximum 335 KW (450 HP). Previous modeling indicates that the higher thermal expansion fiber reinforced aluminum piston results in higher stresses in the thermal barrier coating. Engine tests of this piston were successful at the 335 KW (450 HP) condition, therefore test time was increased to achieve the program goals. Engine testing of this piston has been conducted for 100 hours, Figure 5.4, without any obvious signs of coating deterioration on the fiber reinforced aluminum piston.

THIS PAGE LEFT INTENTIONALLY BLANK

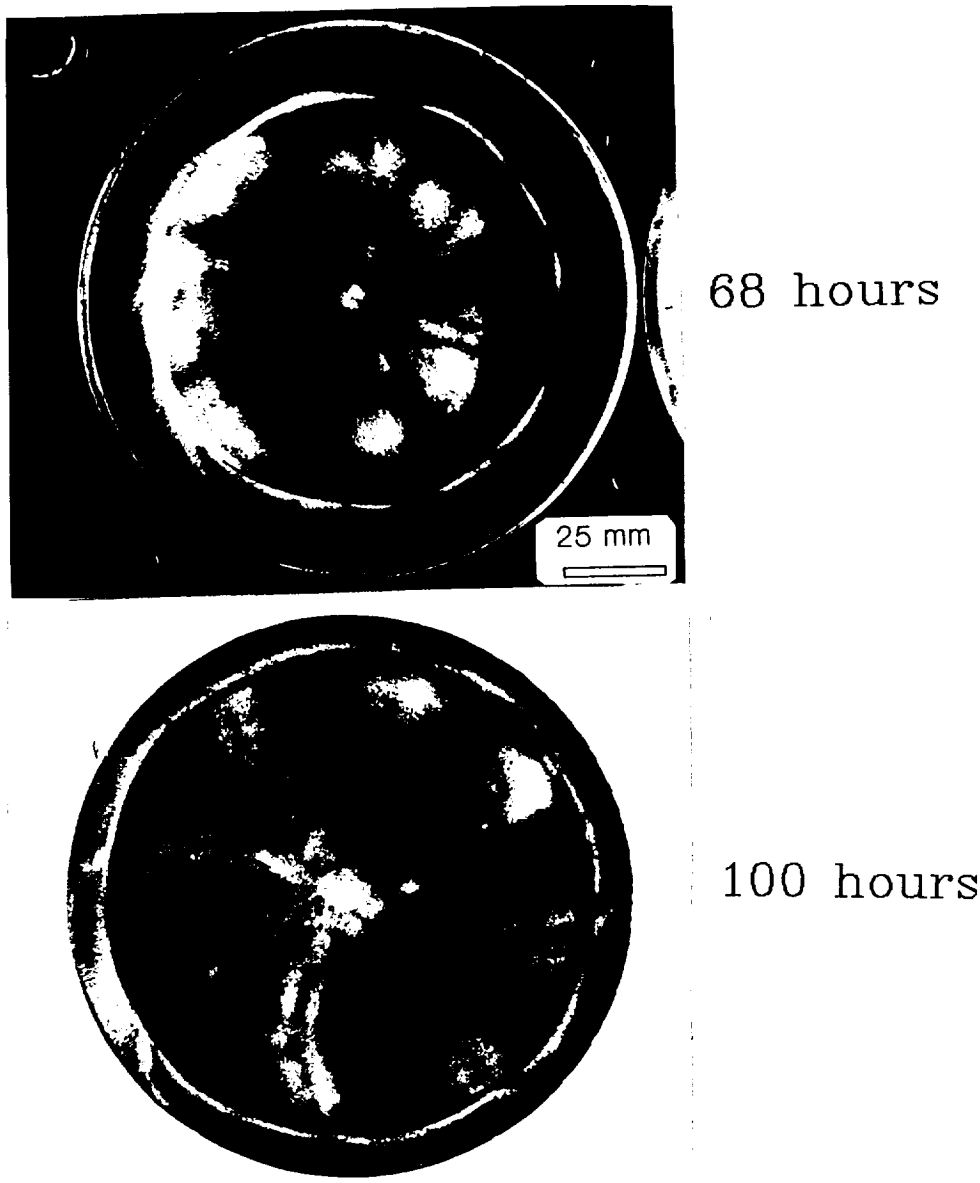

Figure 5.4: Thermal barrier coating on a fiber reinforced aluminum piston at 68 hours and 100 hours (test conclusion).

5.1.3 Post-Test Coating Evaluations

Several V903 from single cylinder engine tests and L10 coated piston crowns from multicylinder engine tests were evaluated to characterize coating material behavior as a result of both cyclic and steady state temperature exposure. Both V903 and L10 crowns representing baseline coating properties and L10 piston crowns with an increased strength top layer zirconia were evaluated. The primary focus was to establish the coating response to time at temperature and, therefore, develop a better understanding of material properties required to achieve longer term durability. Selected sections of the tested piston crowns were prepared for through thickness coating metallographic analysis.

THIS PAGE LEFT INTENTIONALLY BLANK

A V903 ductile iron piston crown, piston #5, Table 5.3 with a baseline multilayer coating was analyzed after approximately 46 hours at 1.38 MPa (200 psi) BMEP test condition. This piston crown exhibited local top layer coating deterioration in a rose petal configuration across the center area of the dome. Metallographic evaluation and micro-probe analysis provided an initial assessment of factors affecting coating performance. The results showed that none of these factors contributed significantly to coating material deterioration. Most noteworthy results are as follows.

- Even though radial cracks were noted in areas correlating to the fuel injection impingement, none turned laminar. Therefore, material loss cannot be attributed to this mechanism.

- Trace amounts of calcium, magnesium and other fuel residues were found on the coating surface only. The material loss cannot be attributed to fuel penetration into the coating structure.

It was, therefore, concluded that the primary cause of material loss was exceeding the basic out-of-plane strength of the top layer and, thereby, producing laminar cracks. This deterioration was further aggravated by subsequent impact damage of the coating trapped between the piston crown and head.

Additional evaluations were conducted on L10 piston crowns tested successfully for 400 hours at 1.83 MPa (265 psi) BMEP steady state and high idle to maximum power cyclic operating conditions in a 6 cylinder engine. These L10 piston crowns typically exhibited local rim coating cracking and deterioration predominantly at layer interfaces. Metallographic and micro-probe analyses helped identify those factors influencing coating performance. Major findings of the evaluations are as follows.

- Coating structure exhibited radial cracking on the rim in areas associated with direct fuel or flame impingement, but did not indicate evidence of radial cracks turning laminar to effect material loss.

- The zirconia top layer microstructure exhibited no change indicating that the ceramic material did not undergo significant thermal aging/sintering to affect material loss.

- The CoCrAlY particles in the cermet layers did not show aluminum depletion zones nor formation of alumina scale indicating that these layers were not subject to additional strain through oxidation growth.

- Chemical interaction of the contaminant deposited on the crown edge and top surface with the coating material was minimal with no apparent degradation on material properties indicating no contribution to material loss.

In this case it was concluded that the primary cause of material loss was due to a thermal strain mismatch between layers locally at the edge probably aggravated by strong in-plane thermal gradients. Also, the contaminant deposited during test on the crown edge was judged

to accelerate the cracking due to a mechanical interaction of the contaminant with the cylinder wall.

5.2 Insulated Cylinder Head Screening

Two cylinder heads were prepared for engine evaluation at Cummins by UTRC. The cylinder heads had a coating of 2.0 mm (0.08 inch) and 2.54 mm (0.100 inch) on the combustion surface. The coating consisted of a the standard 40/60, and 85/15 zirconia CoCrAlY layers with a fully stabilized zirconia top coat. In the processing of each cylinder head process interruptions occurred that were related to electrical power surges that occurred during plasma spraying. Numerous robot shut downs that occurred during the processing of the coating on each of these two cylinder heads. In addition, there was a shut down of approximately 1/2 hour during spraying of the 2mm (0.08 inch) thick coating. Even though the cylinder head coating processing was not as desired, it was decided to fully machine and evaluate the cylinder heads by V903 single cylinder engine test.

The 2mm (0.080 inch) thick coating was prepared for engine evaluation. The cylinder head was tested in a watercooled cylinder head configuration at .34 MPa (50 psi), .69 MPa (100 psi) and 1.03 MPa (150 psi) BMEP for approximately 2 hours at each test condition. Inspection of the cylinder head after test revealed that the coating had delaminated with the major damage associated with the pressure transducer location, Figure 5.5.

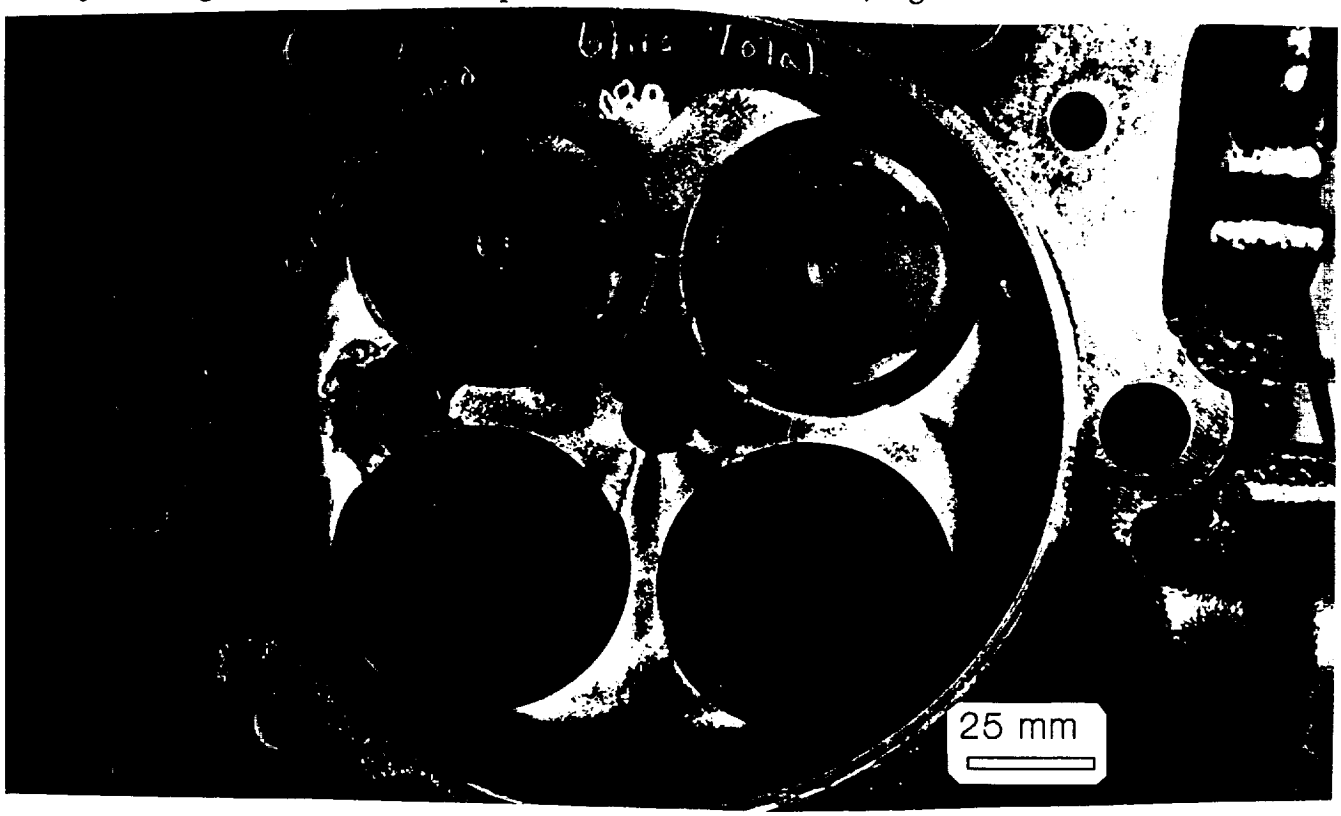

Figure 5.5: Photograph of coating spallation on cylinder head associated with pressure transducer interference.

Interference between the metal pressure transducer sleeve and the coating may have resulted in damage at the location. The second cylinder head with the 2.54mm (0.100 inch) thick coating was prepared for engine evaluation. In this cylinder head, the cylinder head pressure transducer sleeve was modified to avoid the potential interference between the sleeve and the coating. The cylinder head was subjected to the same test conditions as the first cylinder head, 2 hours at each load point. Removal of the cylinder head after this test revealed that the head was in excellent condition with no visible cracking or spalling.

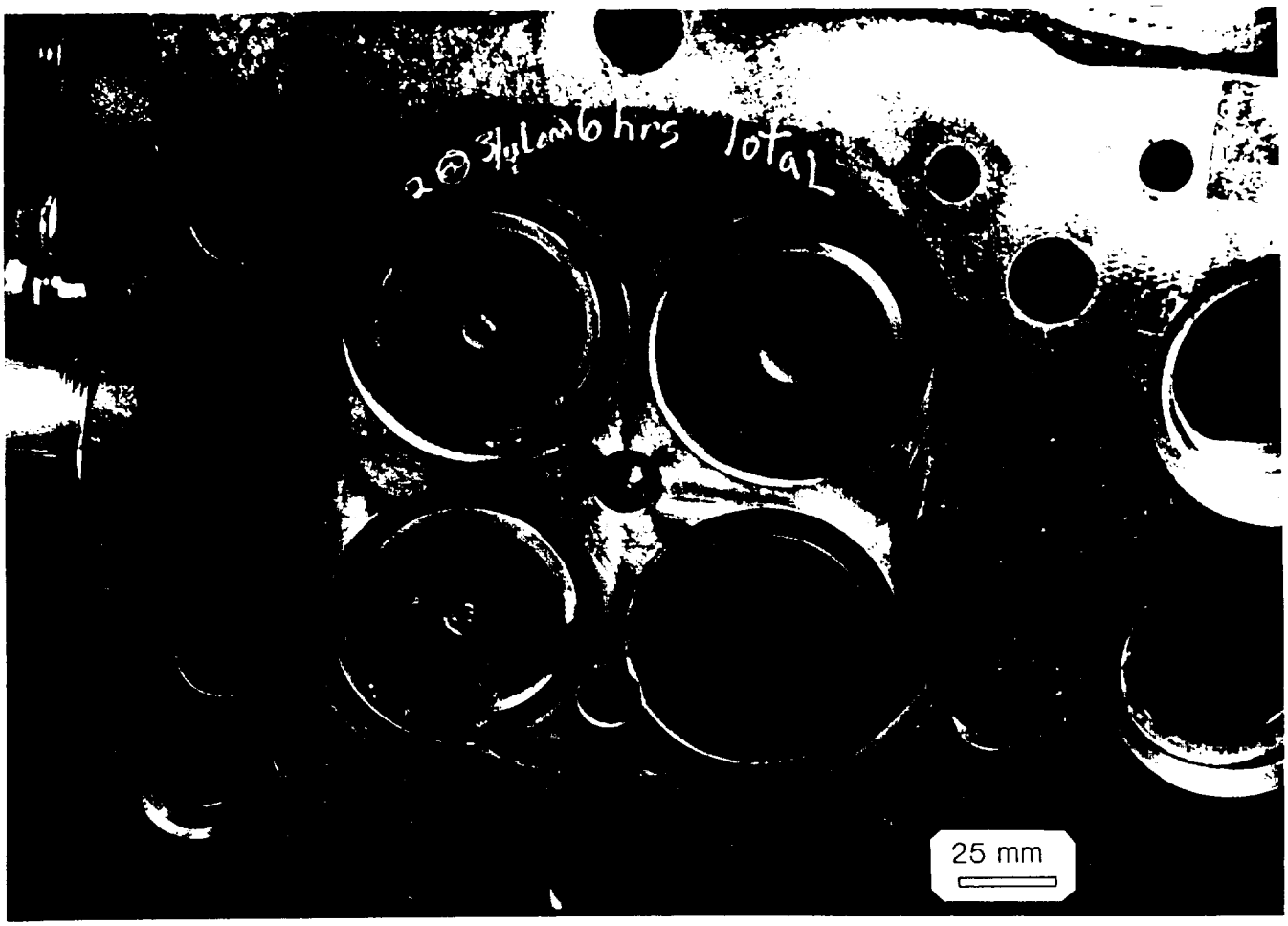

Figure 5.6: Cylinder head after 6 hours of engine evaluation.

After inspection, the cylinder head was re-installed along with an insulated piston that had been contour ground. This engine assembly was tested up to 1.10 MPa (160 psi) BMEP through a stepwise increase in load. At the conclusion of this test, the cylinder head coating had cracked at the valve bridges, Figure 5.7. Two locations at the valve bridge had also spalled. After this test series, additional modeling and bench testing of cylinder head simulations was conducted as previously discussed in prior sections.

THIS PAGE LEFT INTENTIONALLY BLANK

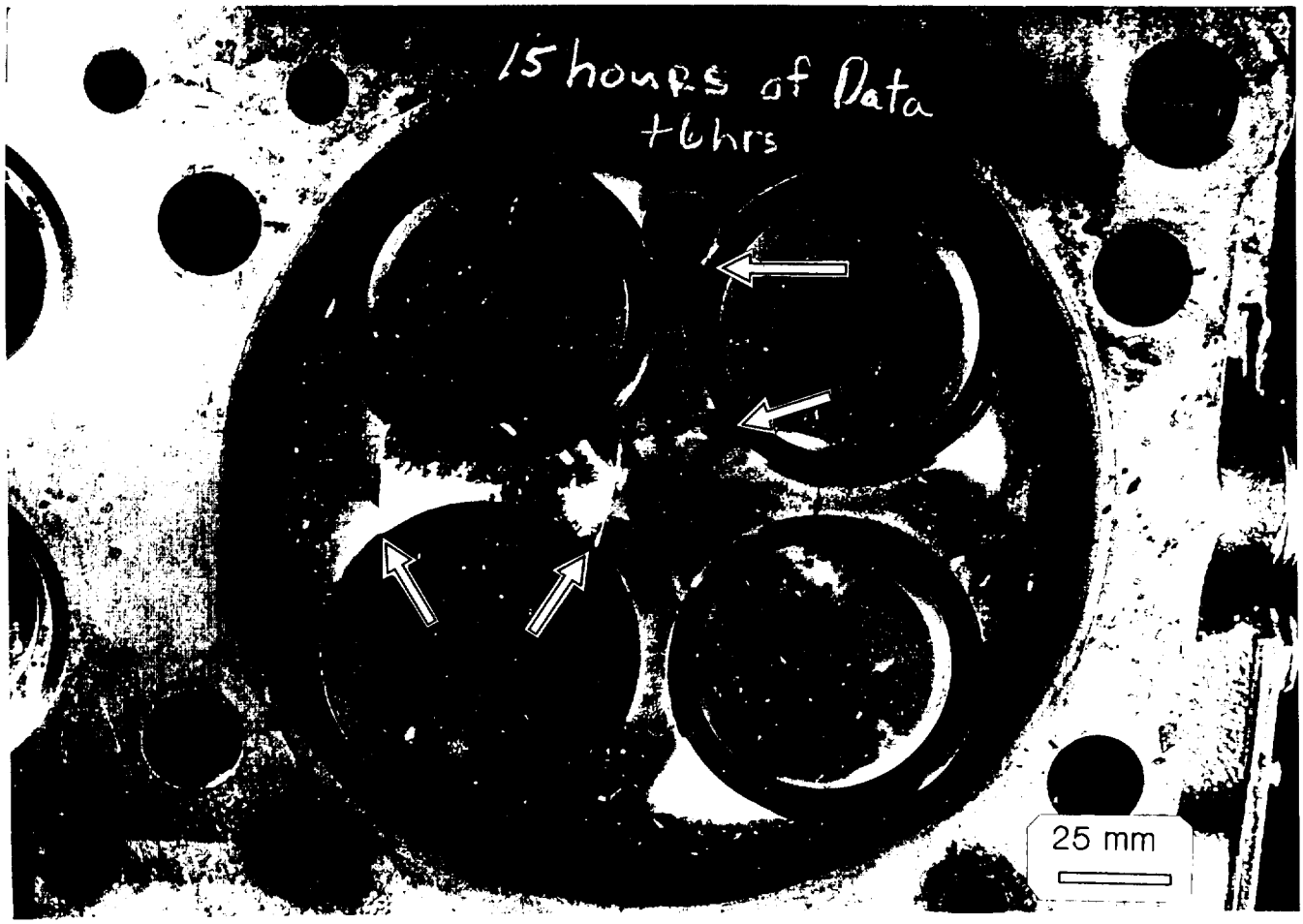

Figure 5.7: Cylinder head showing spalling of valve bridges after 21 hours of operation.

After review of the stresses in the cylinder head, bench and engine evaluation of the cylinder head coating at Cummins, two additional cylinder heads were prepared for engine test. A cylinder head with a 2.54mm (0.100 inch) thick coating consisting of a stronger intermediate layer, 70/30 substituted for 85/15, and an improved zirconia top coat referred to as "New Zirconia" which had higher strength and lower elastic modulus.

THIS PAGE LEFT INTENTIONALLY BLANK

The third engine test was conducted with the new zirconia in an oil cooled cylinder head configuration up to 160 psi BMEP with a metal piston. The cylinder head was tested under a wide variety of engine loads and speeds for approximately 20 hours. Inspection of the cylinder heads after this test revealed that the cylinder head was in excellent condition, Figure 5.8.

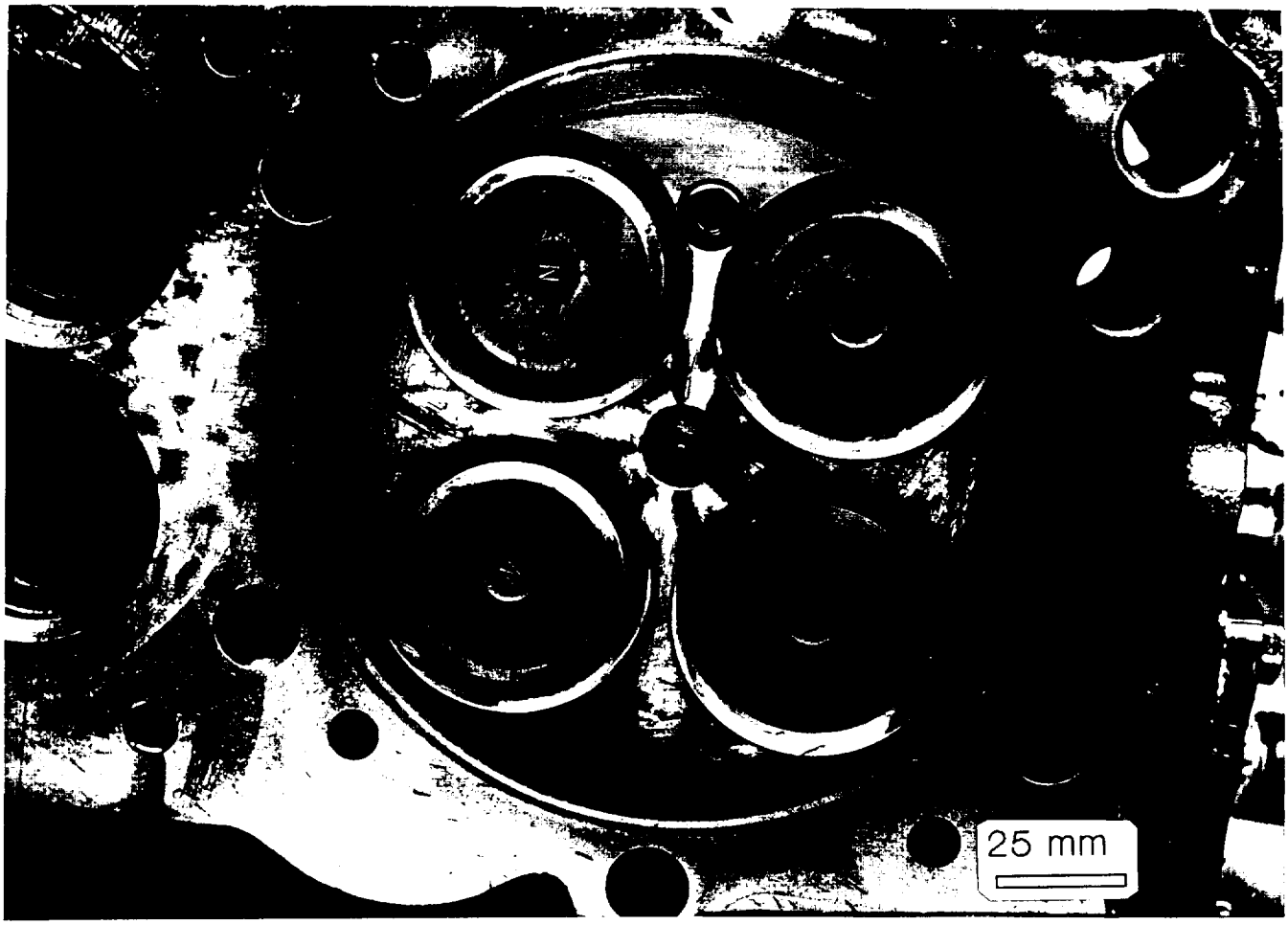

Figure 5.8: "New" zirconia cylinder head after 20 hours with coating intact.

5.3 Insulated Engine Tests

Engine Performance

The thermal barrier pistons for this test were plasma sprayed to an oversize thickness and then were contour ground at Coors Ceramics to final dimensions. After measuring the coated piston bowl geometry, a metal piston was machined to match the ceramic coated pistons. Engine fuel economy was determined for the metal engine and the engine containing the insulated piston in the turbocharged and turbocompound configurations. Cooling for these

THIS PAGE LEFT INTENTIONALLY BLANK

tests consisted of a water cooled block and cylinder head as well as a water cooled cylinder head configuration. Engine conditions that were held constant for fuel economy comparisons were as follows: water temperature, 80 C (176 F); air temperature, 60 C (140 F); oil temperature, 110 C (230 F); fuel temperature, 32 C (90 F); air fuel ratio held constant at 30 to 1, engine speed 2600 rpm. A fuel reading required approximately 2.5 minutes during which time the engine torque was averaged. Approximately 10 fuel readings were obtained per engine condition evaluated. Readings were obtained from several individual engine builds and over a data collection period of six months. Figure 5.9 shows the average fuel economy and 95% confidence intervals for the turbocharged engine configuration. Individual data points for the insulated pistons for two different engine builds evaluated in the turbocharged engine condition are shown in Figure 5.10. This data is also contained in average fuel economy data in Figure 5.9. Figure 5.11 shows the data obtained for the turbocompound engine simulation. From these tests, it was concluded that the insulated piston in a set of controlled tests for a the V903 single cylinder research engine results in a fuel economy that was at least equal to or better than the baseline engine. Other factors, such as minor changes in lubricant viscosity, temperatures and pressures, complicate the data analysis. However, the trends for this engine indicate a fuel economy benefit. Other recent engine tests under another program on a multicylinder engine with six insulated pistons confirm the above conclusions.

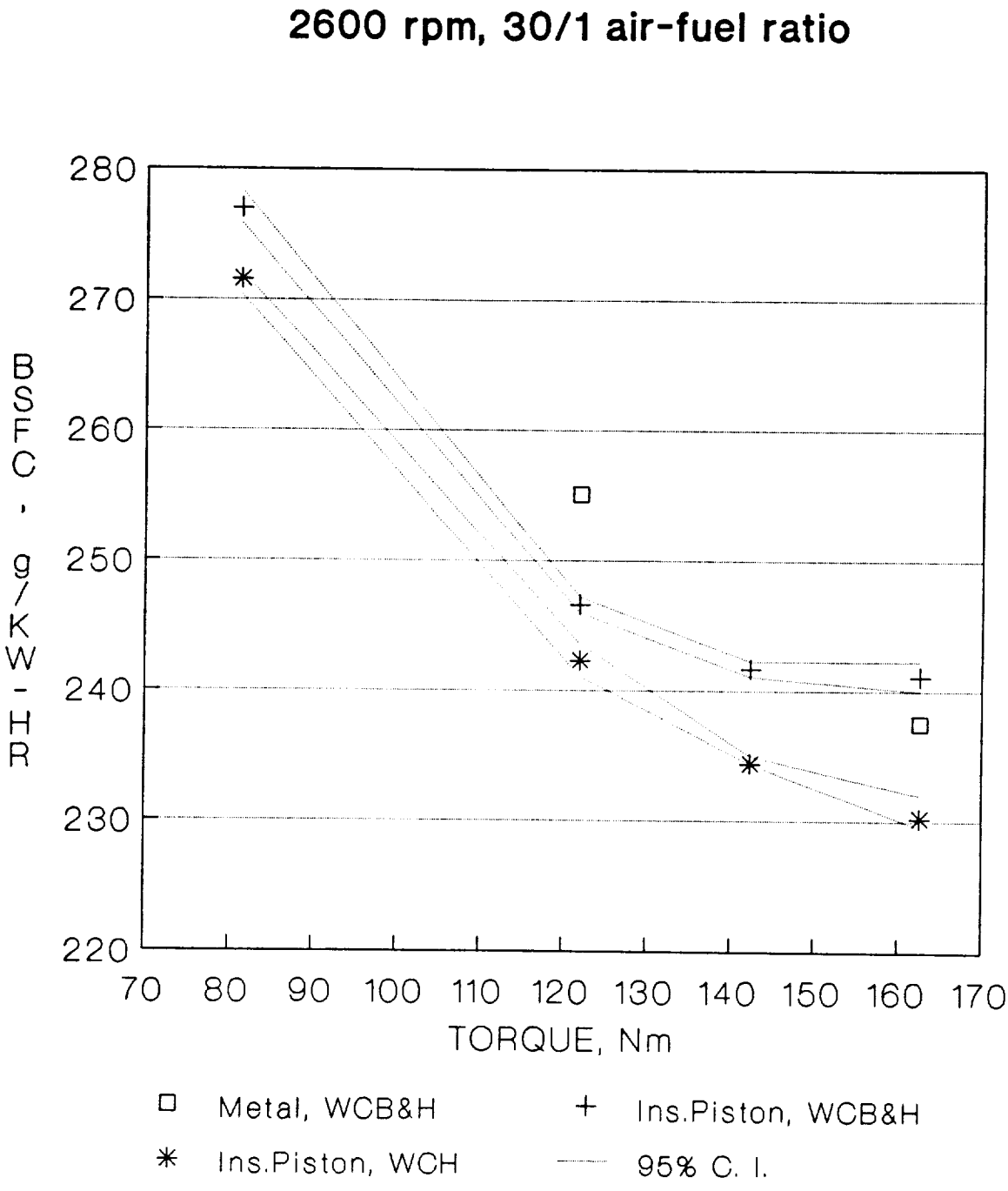

Figure 5.9: Average fuel economy and 95% confidence intervals for water cooled engines with and without insulated pistons.

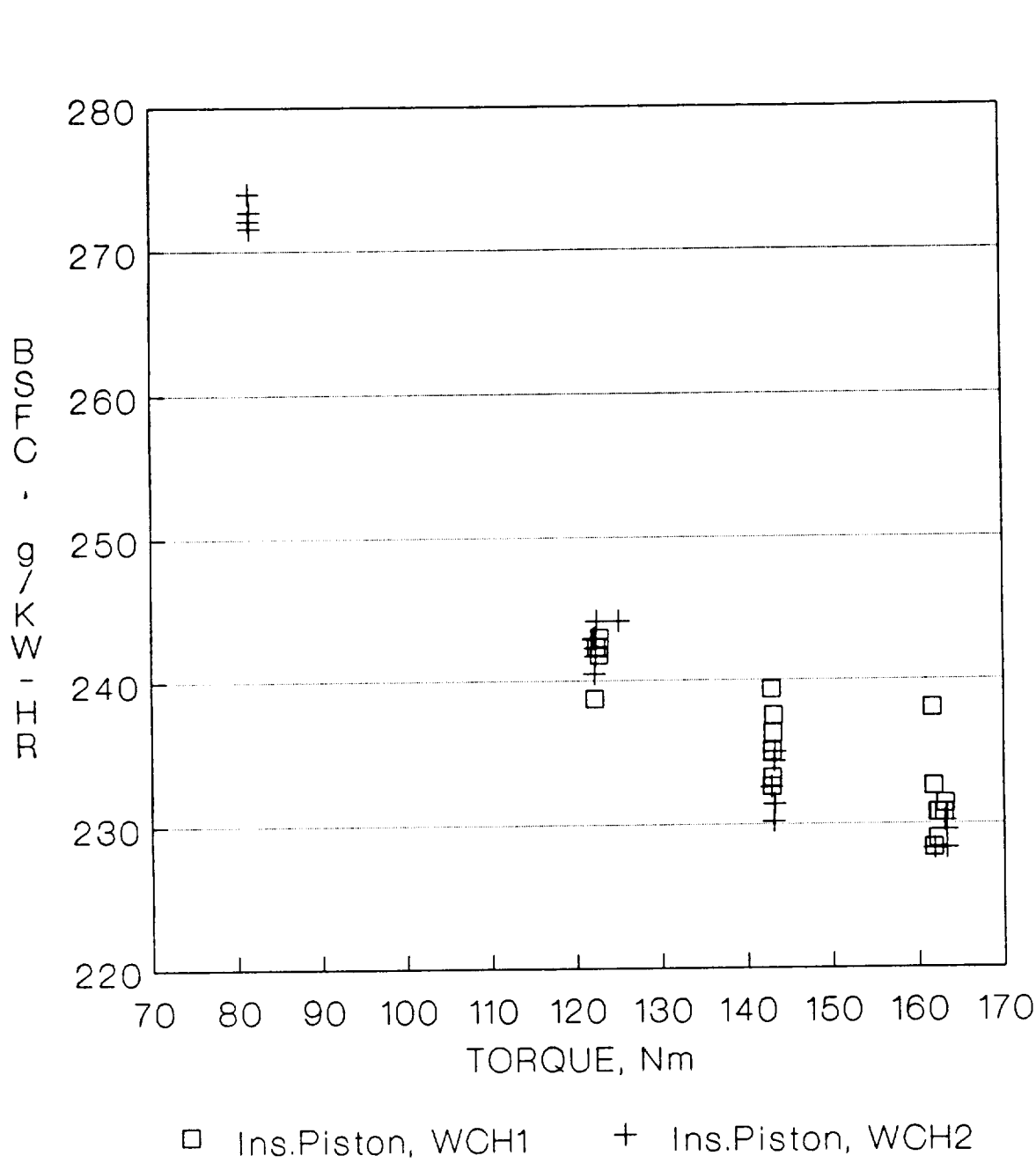

Figure 5.10: Individual fuel economy data showing typical variation from engine build to engine build.

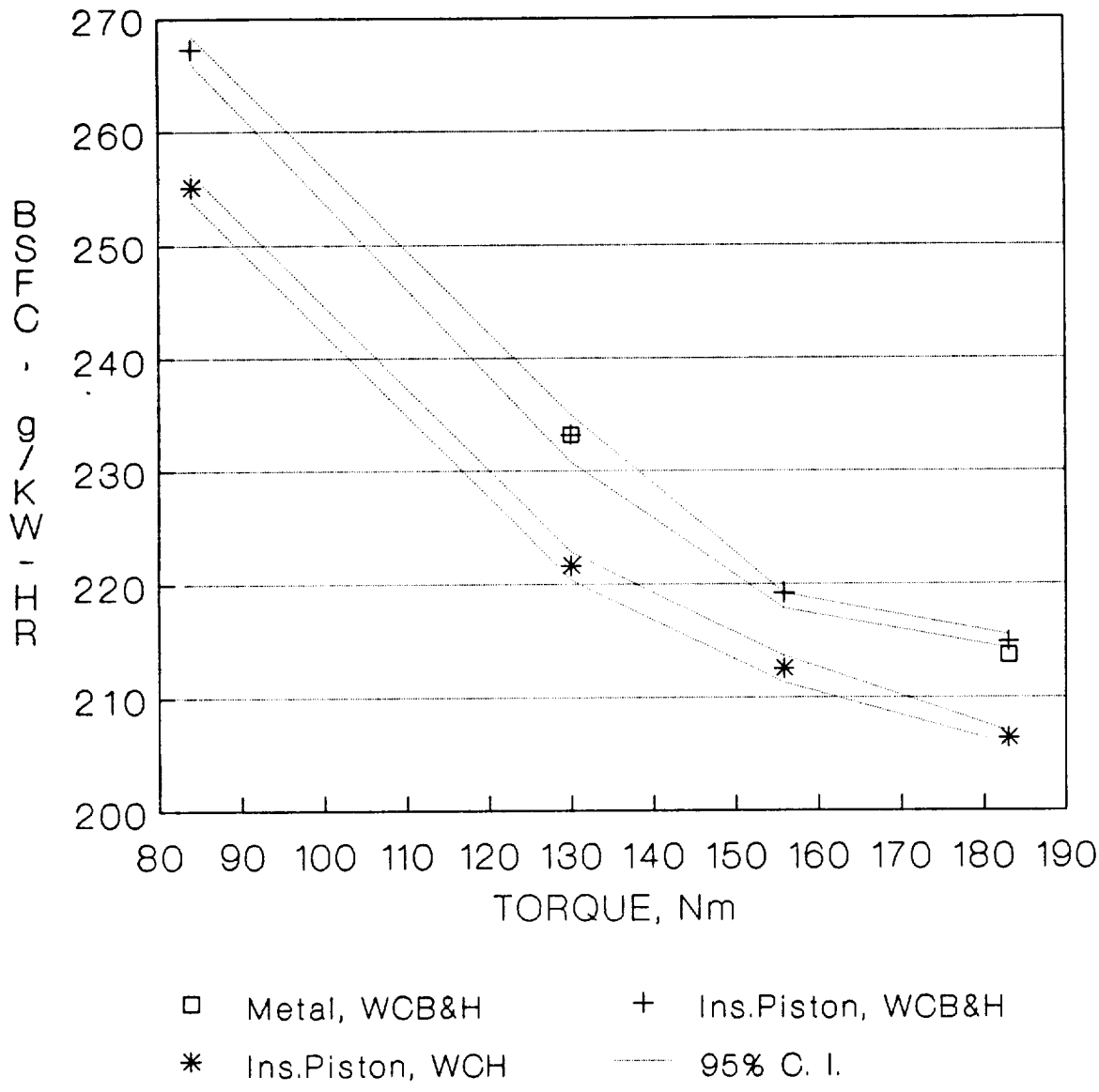

WCB&H = Water cooled block and head
WCH = Water cooled head

Figure 5.11: Predicted engine fuel economy for a simulated turbocompound test case. Fuel economy predicted based on actual engine fuel economy and predicted turbocompound work.

5.4 Engine Heat Rejection

The heat rejection for the V903 single cylinder engine was obtained for three engine configurations. Heat rejection was calculated for the water cooled baseline metal engine, a metal engine with an oil cooled cylinder head, and the fully insulated engine with the oil cooled cylinder head. The thermal barrier coatings used in the fully insulated engine met the program thermal conductance goals. The specific hardware for the insulated engine consisted of a contour ground multilayer coating on the piston and a ground multilayer coating on the cylinder head. The piston coating layers were 40/60 ZrO_2/CoCrAlY, 85/15 ZrO_2/CoCrAlY, with the 85% dense ZrO_2 top coat. The cylinder head coating was comprised of 40/60 ZrO_2/CoCrAlY, 70/30 ZrO_2/CoCrAlY, with a higher strength ZrO_2 top coat obtained by plasma spraying the baseline zirconia at a higher plasma gun power.

The engine heat rejection was calculated using the energy balance approach. Fluid temperatures and flow rates were obtained for air, fuel, coolant, and lubricant coming into the engine and leaving the engine. Fuel energy input was established by measuring the fuel mass flow rate and multiplying to by the lower heat value of the fuel, 18500 BTU/lbm.

The summation of the energy coming into the engine was balanced with the energy leaving the engine. Equating in flows with out flows yields:

$$\dot{H}int + \dot{E}fuel = \dot{H}exh + \dot{Q}cyl + \dot{Q}un + \dot{W}eng$$

where,

$\dot{H}int$ = Total enthalpy flux of air coming into the engine.

$\dot{E}fuel$ = Total fuel energy coming into the engine.

$\dot{H}exh$ = Total enthalpy flux of combustion products leaving the engi

$\dot{Q}un$ = Unaccounted heat transfer including heat transfer for endinç

$\dot{W}eng$ = Work output of the engine.

Enthalpy calculations were determined by existing computer programs at Cummins which account for the sensitivity to temperature and equivalence ratio. These programs are based on functional curve fits to JANAF data.

Figures 5.12, 5.13, and 5.14 summarize the information obtained for the various engine configurations percentage of available fuel energy. Figures 5.15 and 5.16 compare the results of the metal baseline engine to the oil cooled metal engine and the insulated engine. As can be seen in Figures 5.15 and 5.16, the heat rejected to the coolant was lowest for the oil cooled engines. As a percent of fuel energy the heat rejected to the coolant in the water cooled baseline was approximately 22% at 120 ft-lb while in the case oil cooled engines, both insulated and metal, typically had 13% rejected to the oil coolant. This signifies a 40% reduction in heat rejection to the coolant. Also, note that the unaccounted portion increased for the oil cooled engines. This result has been primarily attributed to the higher surface temperatures of the oil cooled engines.

Although major differences were observed between the baseline water cooled engine and the oil cooled engine, no significant changes in heat rejection were observed between the metal engine with an oil cooled cylinder head and the insulated engine with an oil cooled cylinder head. Previous predictions, Figure 3.1, suggest that an oil cooled metal engine configuration reduces heat rejection by approximately 15 to 20%. In the current data, oil cooling reduced heat rejection by approximately 40%. This level of heat rejection reduction was indistinguishable from the insulated engine.

Because minor variations in fuel rate, cylinder heat oil flow rates, and total flow rate could mask any change in heat rejection between the insulated and metal engines with oil cooled cylinder heads, matched pair sampling was used to attempt to distinguish the differences for a set engine condition. Engine test data from the 60 ft-lb torque, 2600 rpm data was scanned to determine the data points which had similar fuel rates, cylinder head oil flow rates and total oil flow rates since these factors were considered to be the major variables for the test. The heat rejection data for eight pairs of matched samples is contained in the following table.

Heat Rejection to Oil For Oil Cooled Cylinder Heads (BTU/hr)

Metal Engine	Insulated Engine
35776	35556
36147	35736
36259	38514
41250	40711
37617	38389
38941	38656
37143	38883
36017	35707

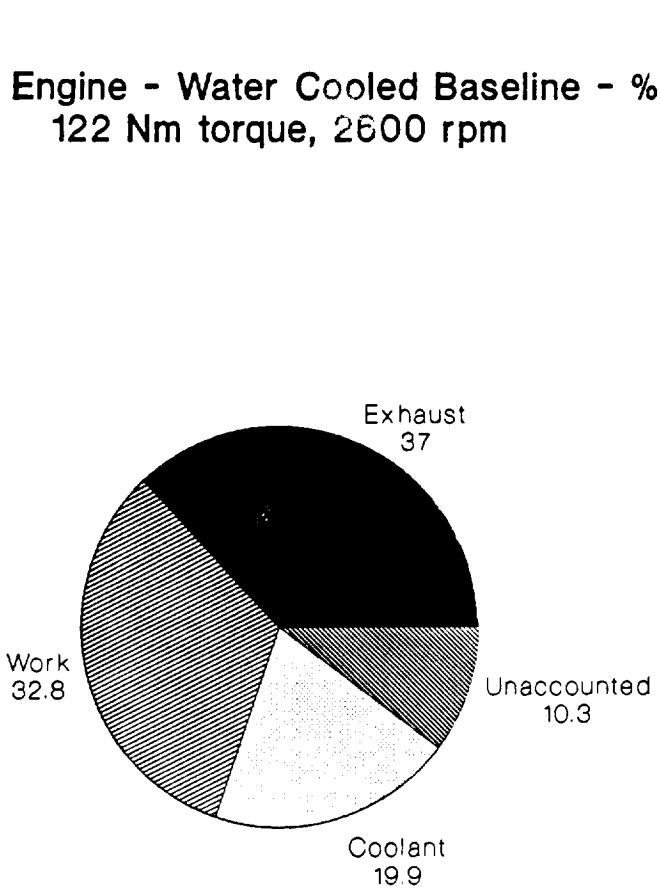

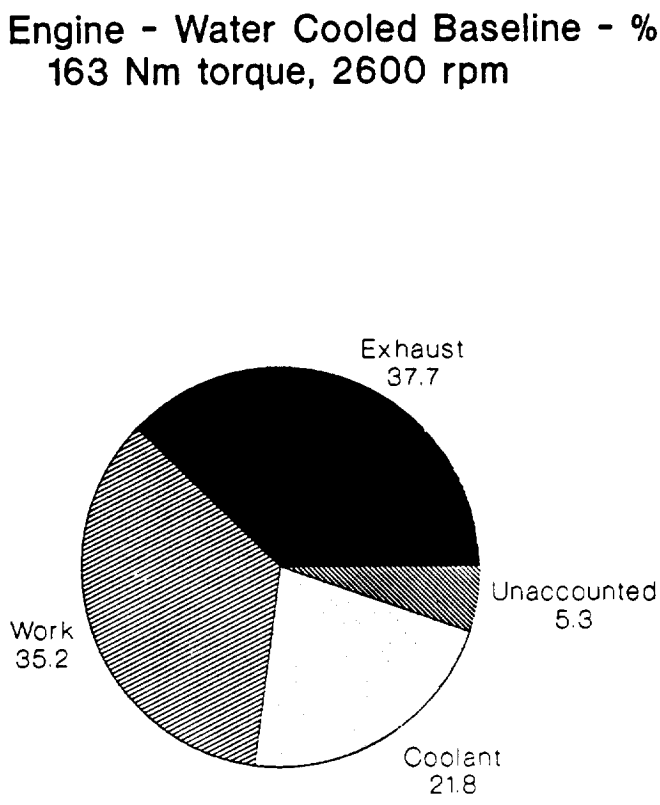

Figure 5.12: Heat rejection as a percent of fuel energy - water cooled baseline.

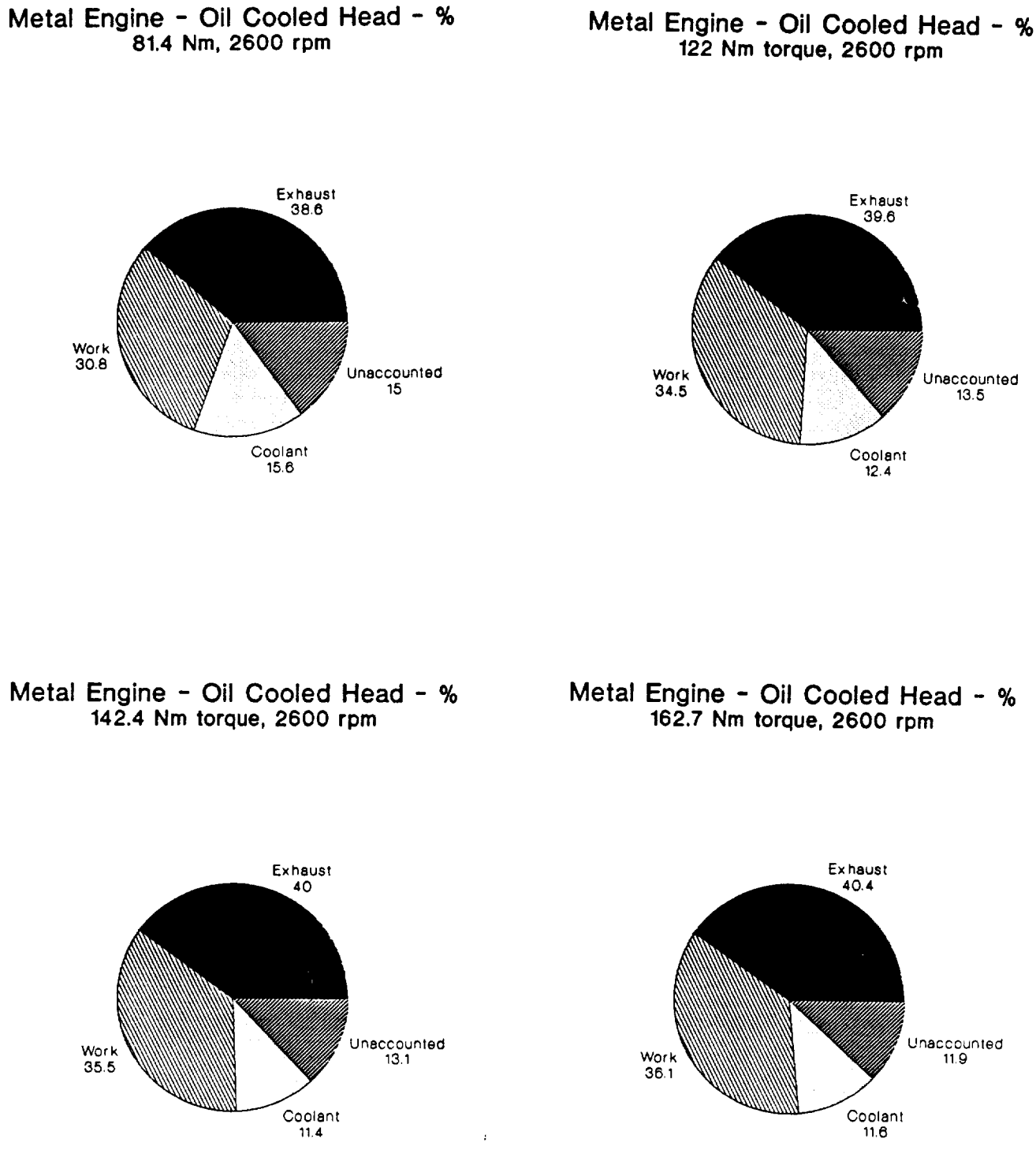

Figure 5.13: Heat rejection as a percent of fuel energy - metal engine - oil cooled head.

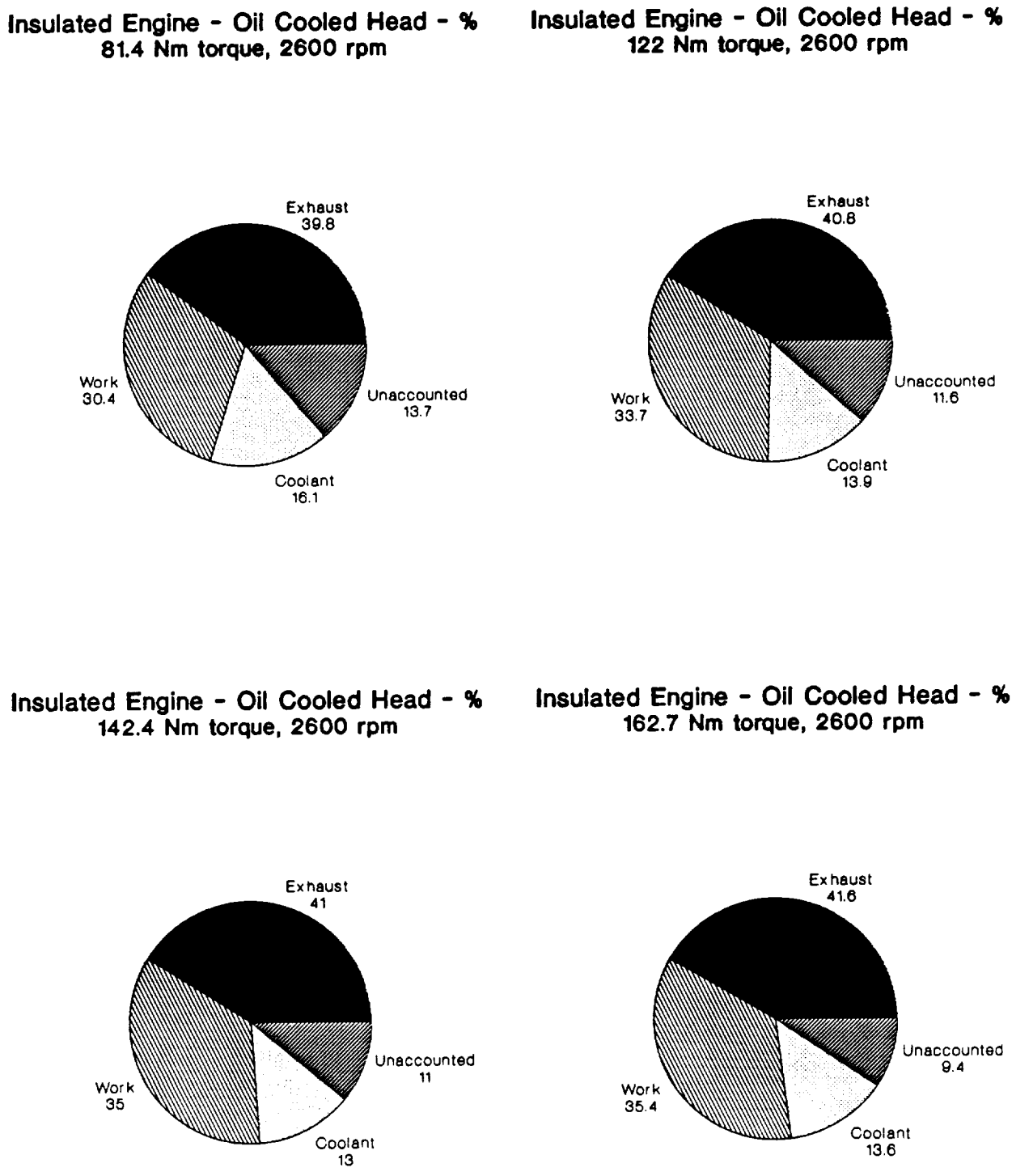

Figure 5.14: Heat rejection as a percent of fuel energy - insulated engine.

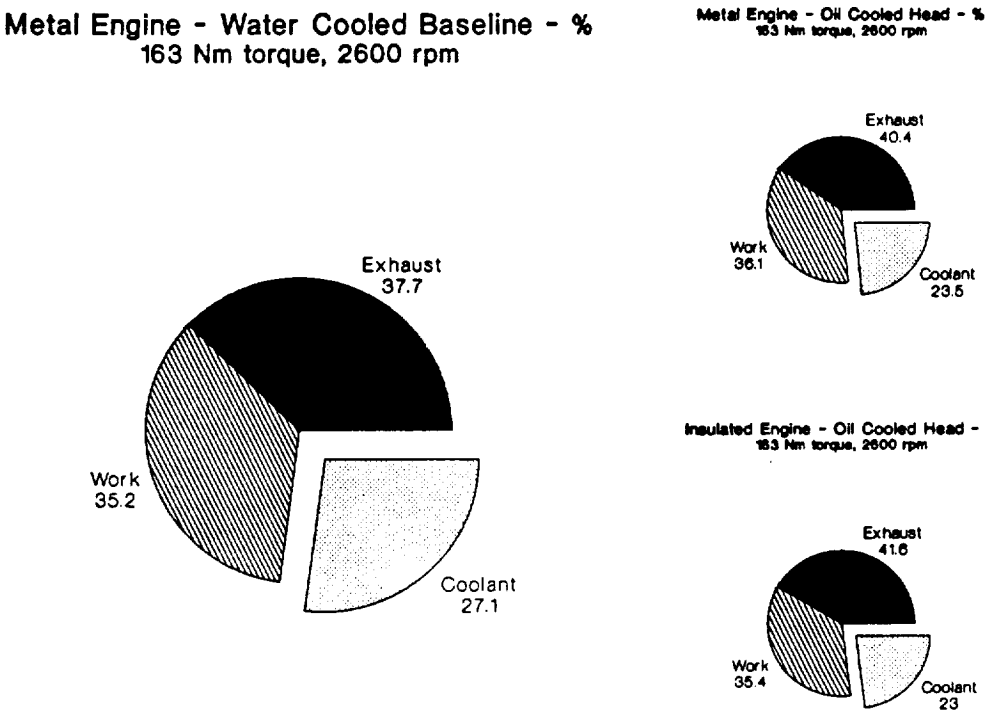

Figure 5.15: Comparison of heat rejection with unaccounted and coolant combined.

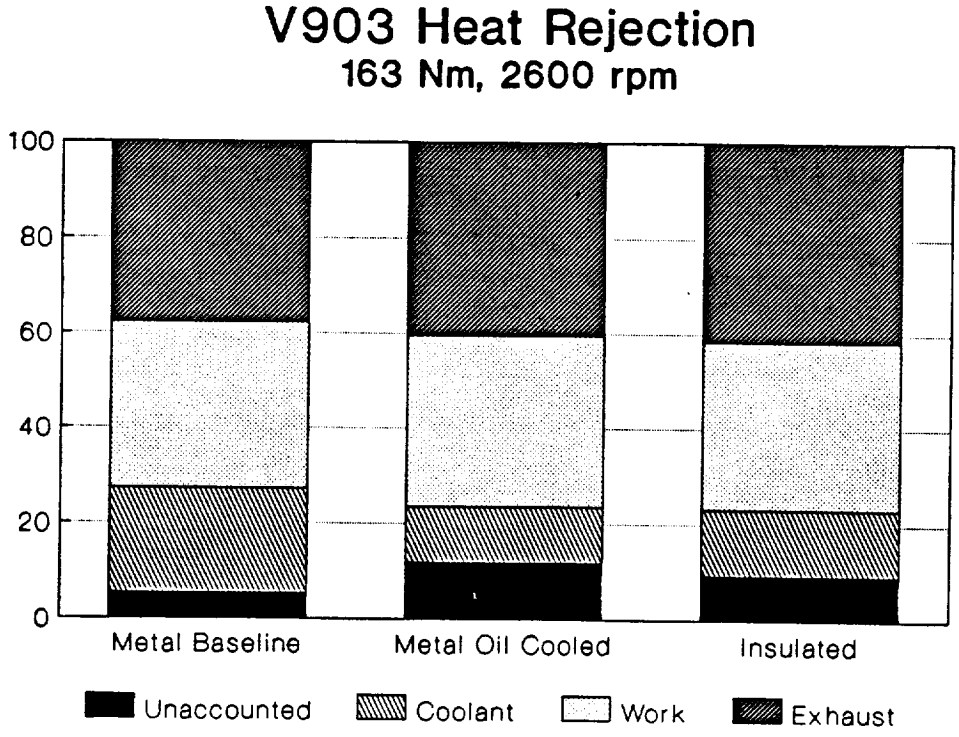

Figure 5.16: Comparison of heat rejection.

For this test, matched pair hypothesis testing was used to determine if the heat rejection for the metal engine was equal to the insulated engine. From statistical tables, the T-statistic at a 95% confidence level was 2.365. The calculated T-statistic for the matched pairs sampling was 0.976. Since 0.976 lies between 2.365, the hypothesis that the heat rejections were equal was accepted.

In summary, converting from a water cooled baseline engine to an oil cooled engine decreased coolant heat rejection by approximately 40%. Investigation of the oil cooled metal engine and the oil cooled insulated engine heat rejection data revealed that the effect of insulation on heat rejection was insignificant compared to the change from water cooling to oil cooling. For this engine system, modification to an oil cooled cylinder head decreased coolant heat rejection significantly more than predicted from the models. Predicted change in heat rejection was approximately 20%, but the observed values were closer to 40% for this engine.

Evaluation of cylinder head and exhaust temperatures suggest that the thermal barrier coating is effective, although it could not be detected via the heat rejection calculations. Exhaust temperatures were 40 F higher for the insulated engine at the same fuel rate whereas metal cylinder head temperatures were 20 F lower.

Additional information obtained from these tests indicate the thermal barrier coating has more of an effect on the engine than can be obtained from the heat rejection calculations. Figure 5.17 shows the diesel engine exhaust temperature for the oil cooled metal engine versus the oil cooled insulated engine. Individual exhaust temperature measurements were plotted versus fuel rate in Figure 5.17. As can be seen, for identical fuel rates and equivalence ratios the insulated engine exhaust temperature was higher than the oil cooled metal engine by approximately 40 F.

It was also observed that the % unaccounted heat rejection increased for the oil cooled engine configurations, this observation was related to the higher metal temperature experienced for the oil cooled engines due to higher coolant temperatures.

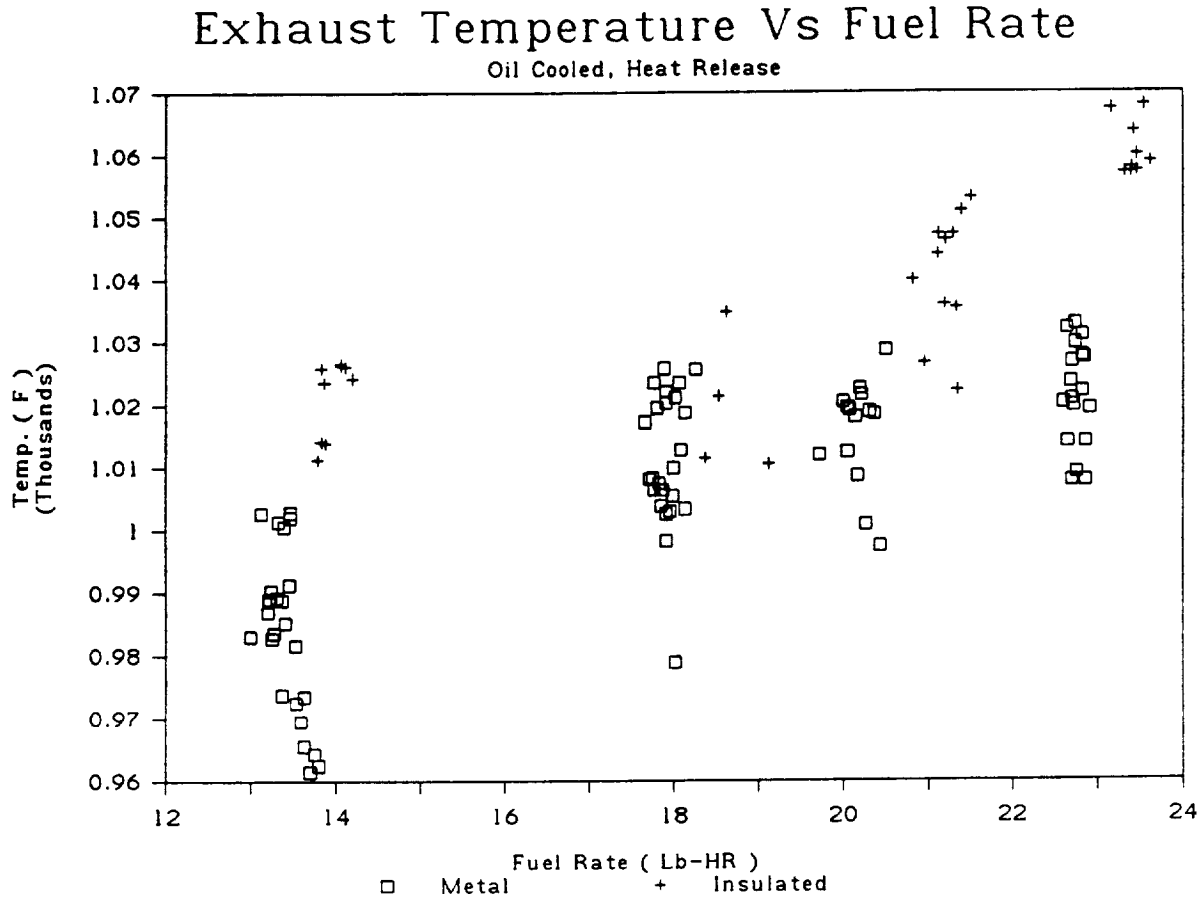

Figure 5.17: Exhaust temperature versus fuel rate.

This result could also be seen in percentage of exhaust energy in Figure 5.14. Cylinder head temperature was another indication that the combustion face insulation was decreasing the cylinder head temperatures. Figure 5.18 presents the cylinder head temperatures versus fuel rate. The cylinder head temperatures were approximately 20 F cooler for the insulated engine.

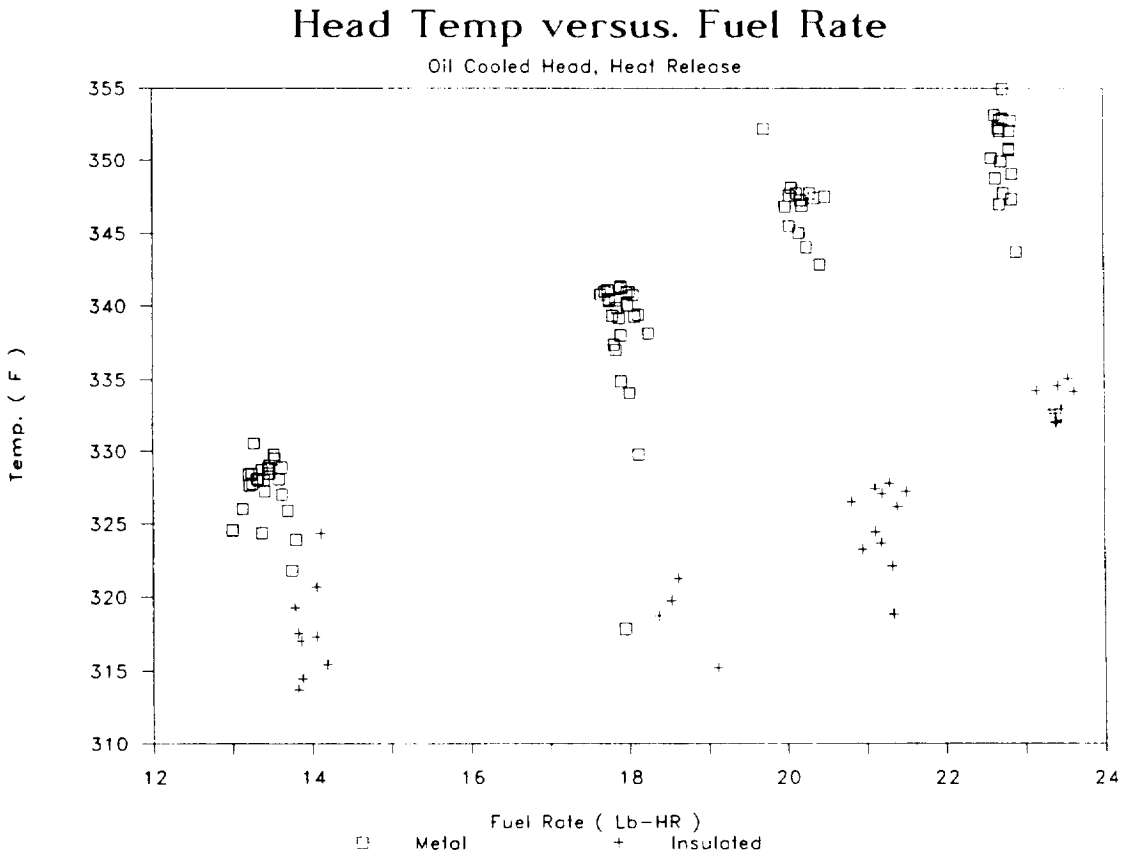

Figure 5.18: Cylinder head temperature versus fuel rate, oil cooled insulated versus metal.

5.5 Apparent Heat Release

Engine data were obtained for the metal engine and an insulated version of the V903 engine. The insulated engine contained an insulated cylinder head surface and an insulated piston. The thermal barrier coatings consisted of designed multilayer coating systems which met the program thermal conductance goals. Total coating thickness was 2.54mm (0.100 inch) and was comprised of 0.051mm (0.020 inch) of 40/60 ZrO_2/CoCrAlY, 0.051mm (0.020 inch) of 85/15 ZrO_2/CoCrAlY, and 1.52mm (0.060 inch) top layer of fully stabilized zirconia. This coating successfully met program durability goals of 100 hours of engine operation. Coating surfaces were ground to print dimensions. In the case of the metal piston bowl, the metal piston bowl was machined to match the contour ground thermal barrier coating on the insulated piston.

The final engine configuration chosen for evaluation of the back to back tests was an oil cooled cylinder head with an uncooled block. Information on the brake specific fuel consumption was obtained at a 30 to 1 air fuel ratio, 2600 rpm engine speed, intake manifold temperature of 60C and inlet oil temperature of 110C. In addition to the normal data acquisition system, this series of tests incorporated an optical encoder to accurately determine crankshaft position and a cylinder head pressure transducer, Figure 5.19. This instrumentation permitted averaging of individual firing cycles in order to calculate the apparent heat release for each engine configuration.

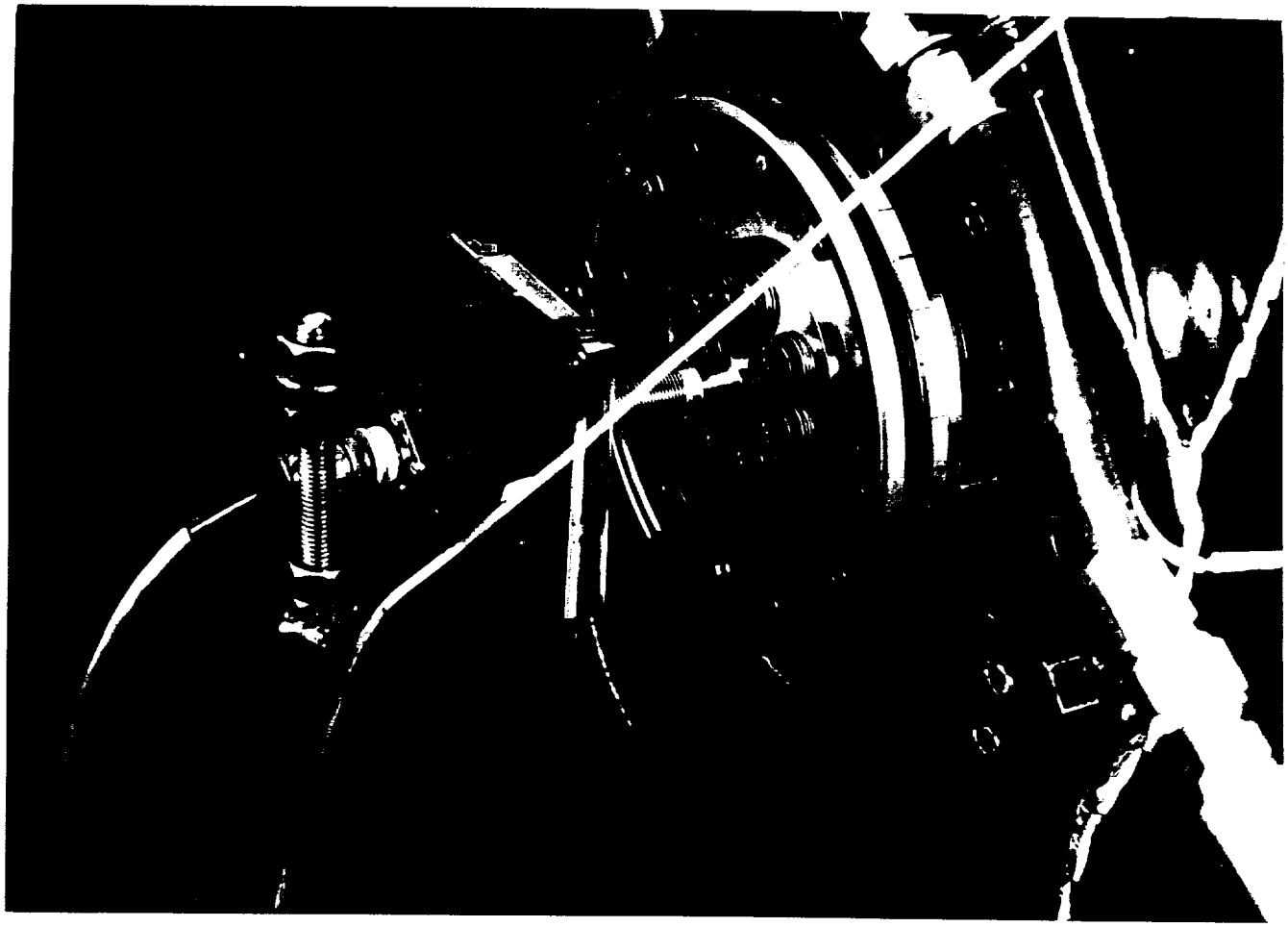

Figure 5.19: Optical encoder used in heat release studies.

Engine Performance

In these studies, it was determined that under the operating conditions selected for the engine that the insulated engine fuel economy had degraded. Data obtained from the test series are presented in Figure 5.20. The insulated engine fuel consumption was on average two percent higher than the metal engine in the turbocharged configuration. Hypothesis testing revealed that the fuel economies were statistically different at the 95% confidence level.

In order to explain the fuel consumption differences between the metal and the ceramic coated engines, heat release analysis was performed. The apparent rate of heat release was obtained by running the in-cylinder pressure data in Cummins in-house computer program TRANSENG. This program solves the energy equation to obtain the apparent heat release.

To facilitate data collection a shaft encoder was directly coupled to the engine crankshaft to give correctly phased data at half crank angle intervals. Eighty cycles of pressure data were collected and averaged to provide a more representative record of the combustion process. This method is superior to taking one random cycle of in-cylinder pressure data.

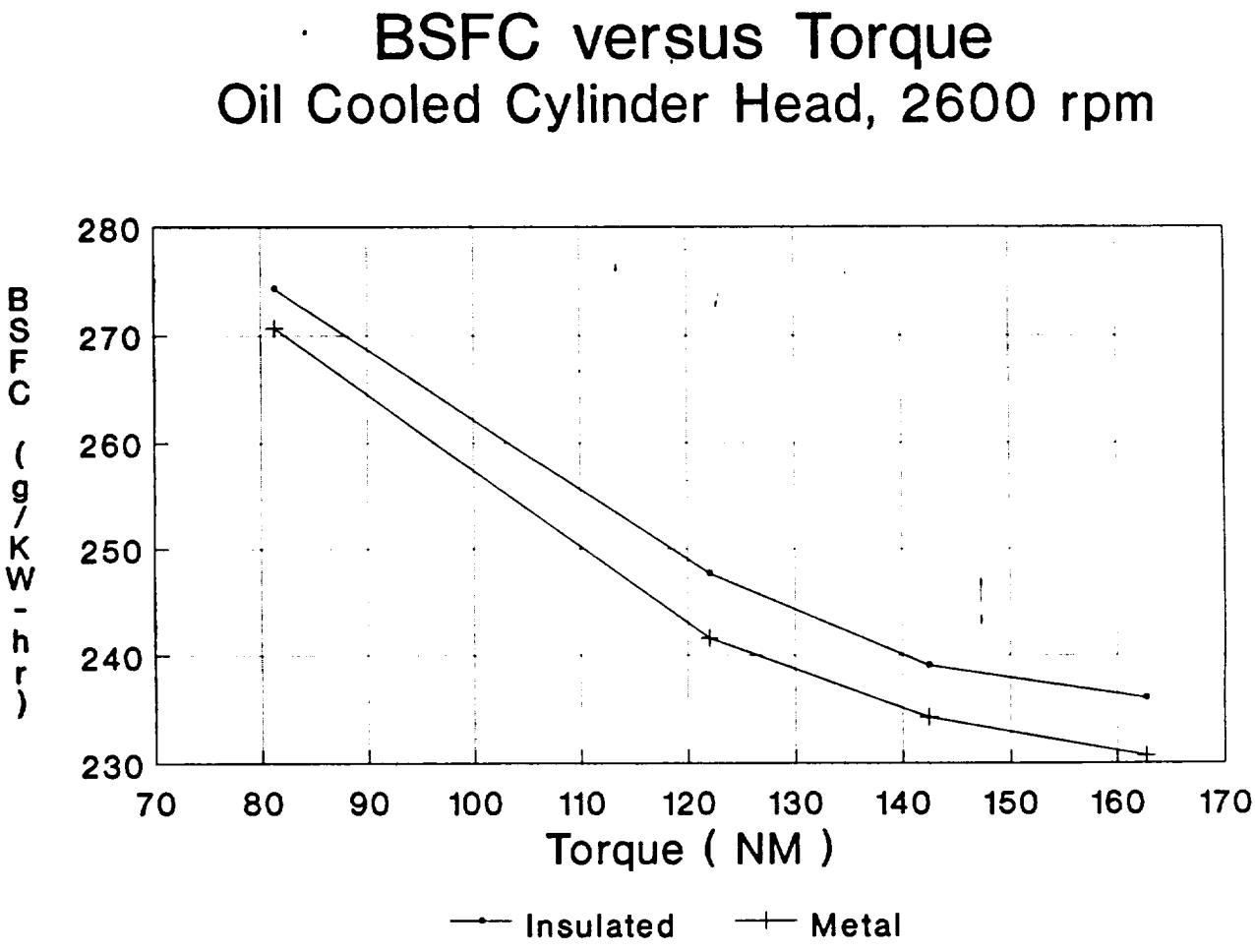

Figure 5.20: BSFC versus torque for insulated and metal engines at turbocharged configuration.

However, any interpretation of apparent heat release curves must consider the limits of the methodology. The energy equation is solved and any unaccounted energy is considered a loss due to heat transfer. The ubiquitous long tail end of combustion is always present due to this heat transfer and other errors in pressure and blow-by measurements. Thus, in analyzing apparent heat release curves, a ninety percent burn point is picked for comparison instead of the end of combustion. Nevertheless, apparent heat release curves reveal the amount of premixed and diffusion burning fractions, the durations, the peaks and any abnormalities in combustion.

Data for heat release analysis were all taken at 2600 RPM and three different brake mean effective pressure levels of .55 MPa(80 psi), .97 MPa(140 psi) and 1.10 MPa(160 psi) under both turbocharged and turbocompound conditions. All the apparent heat release curves showed that the ceramic engine had shorter ignition delays than the metal engine. This difference increased from one degree crank angle at high load to three degree crank angle at low load. In general, the ceramic engine seemed to have less pre-mixed burning fractions and less vigorous diffusion burning than the metal engine. Total combustion duration as compared at the ninety percent burn point showed a definite longer duration for the ceramic engine. Figures 5.21 and 5.22 show the different apparent heat release curves for both the turbocharged and turbocompound conditions at the same 1.10 MPa (160 psi) level.

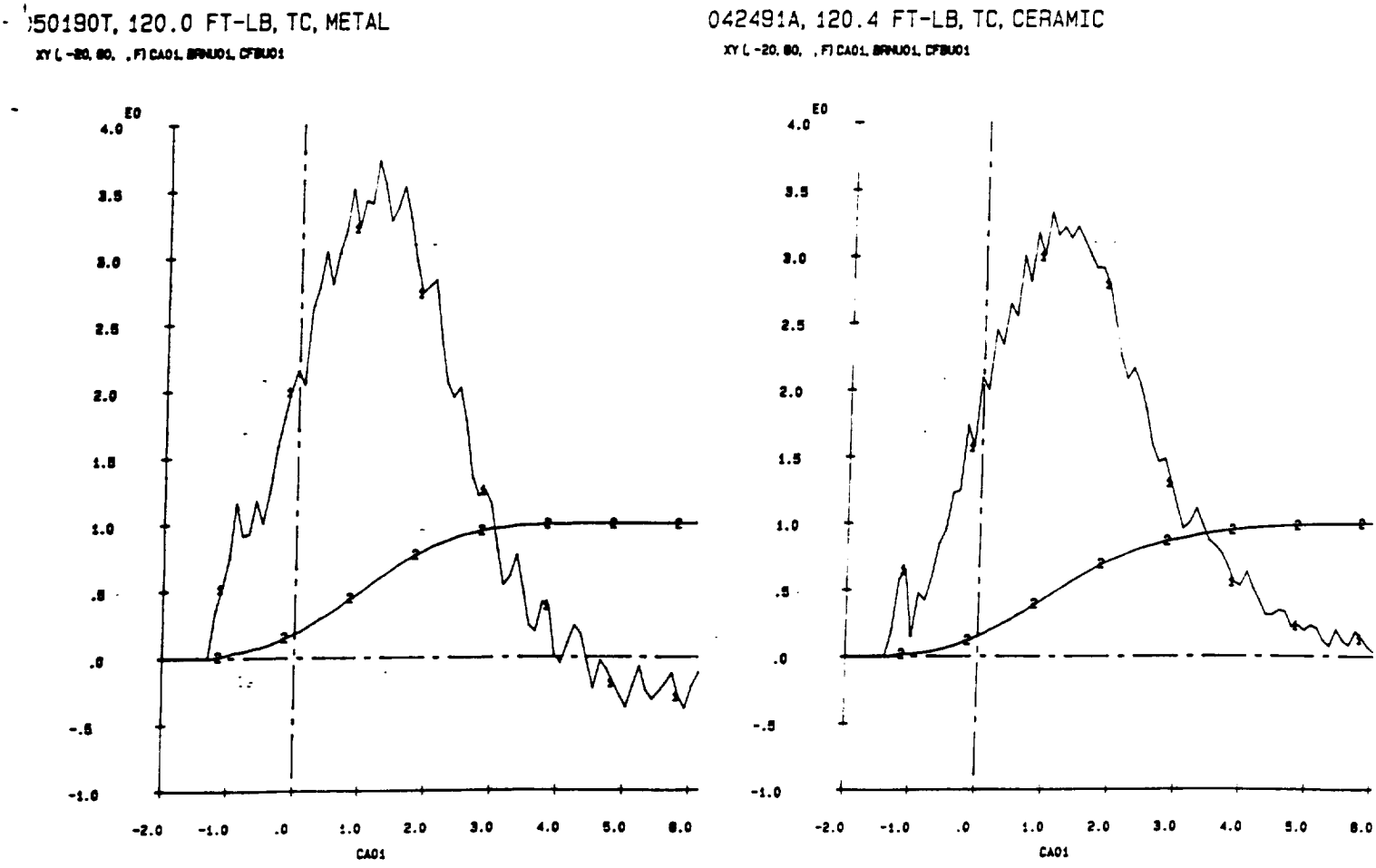

Figure 5.21: Apparent heat release for turbocharged engine with and without insulation.

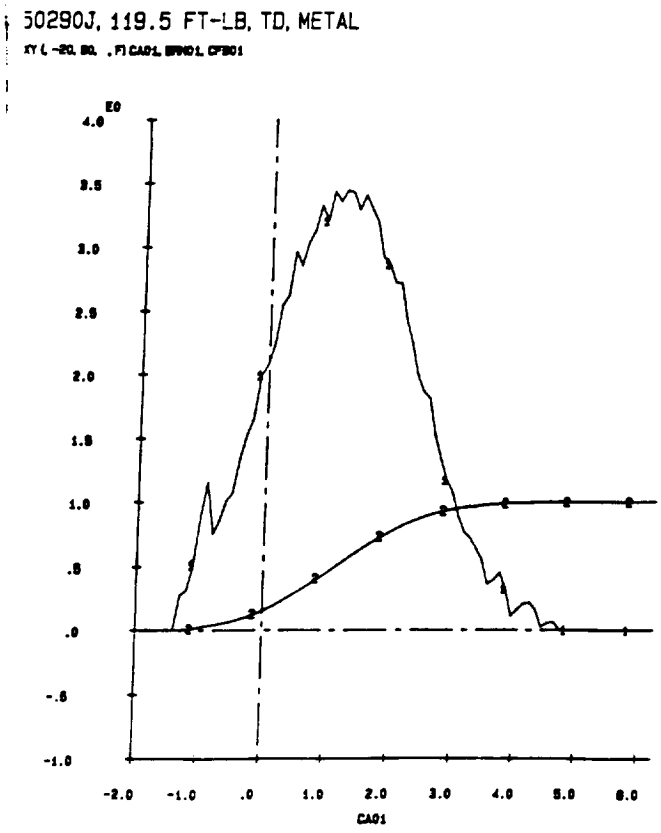

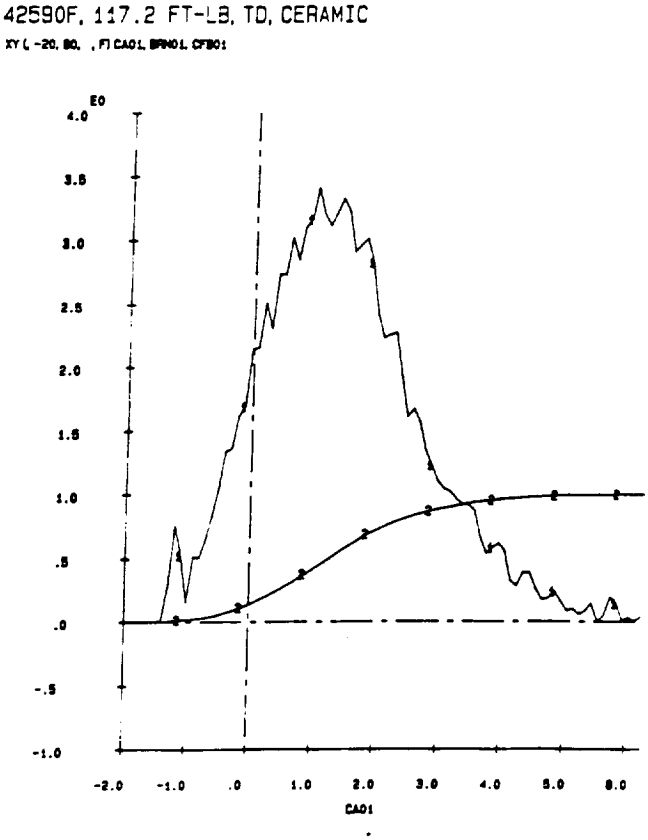

Figure 5.22: Apparent heat release for turbocompound engine with and without insulation.

A maximum difference of 28 percent in combustion duration was observed for the high load, turbocharged condition. The shorter ignition delay in the ceramic engine compared to the metal engine is probably due to the higher in-cylinder gas temperature at the start of fuel injection that accelerates fuel vaporization and also increases the pre-ignition reaction rates. Some experimental studies reported in the open literature have shown an exponential decrease of ignition delay with increased temperature. This shorter ignition delay period permits less fuel mixing with air during the delay period and thus less pre-mixed burning in the ceramic engine.

The combustion duration increase prevalent in all test points could be due to changes in the fuel injection process and/or the combustion process. For instance, there may be fuel leakage, a decreased injection pressure and a longer injection duration with the higher component temperatures. Combustion degradation due to poor air-fuel mixing resulting from a decrease in injection pressure and air turbulence diffusivity could all contribute to a longer combustion duration.

Figure 5.23 and 5.24 show the V903 piston and cylinder head at the conclusion of the multiple test series. The piston was evaluated for 200+ hours and the cylinder head for 100+ hours over a wide range of engine operating conditions. The majority of the test was conducted at 2600 rpm at a 30 to 1 air fuel ratio with a significant test portion, approximately 50% at rated engine power. The piston had a few radial cracks along the rim and a few minor edge chips. These chips were caused by impact damage from previous cylinder head coating delamination. The cylinder head exhibited radial cracks at the injector bore and additional segmentation cracks in the coating. Both coatings were essentially intact at the test conclusion which was a major improvement in coating performance. Previous to this program coatings evaluated would fail in a few hours of engine operation. Many coatings would delaminate at 1/4 or 1/2 load conditions.

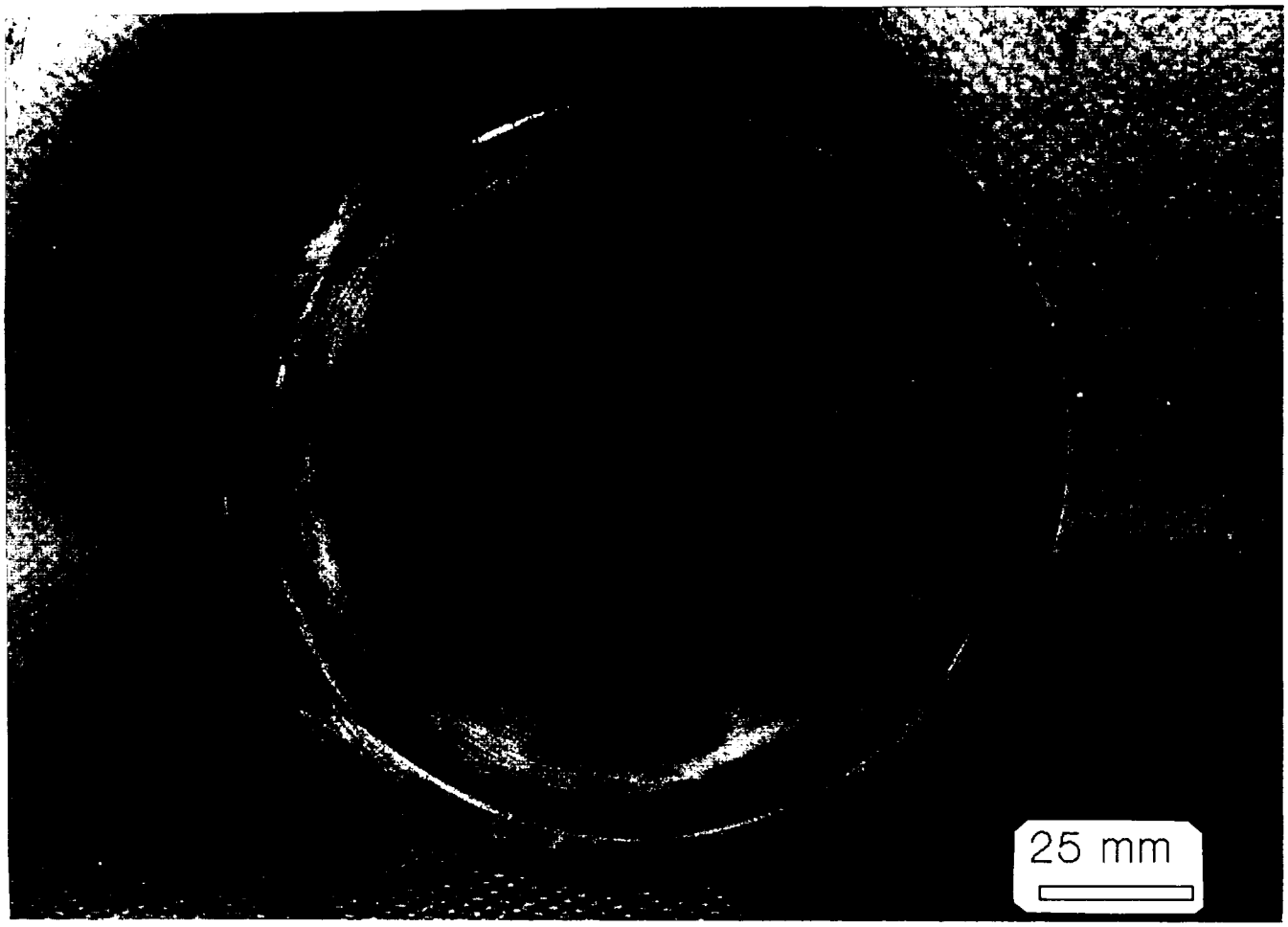

Figure 5.23: Piston at test conclusion.

THIS PAGE LEFT INTENTIONALLY BLANK

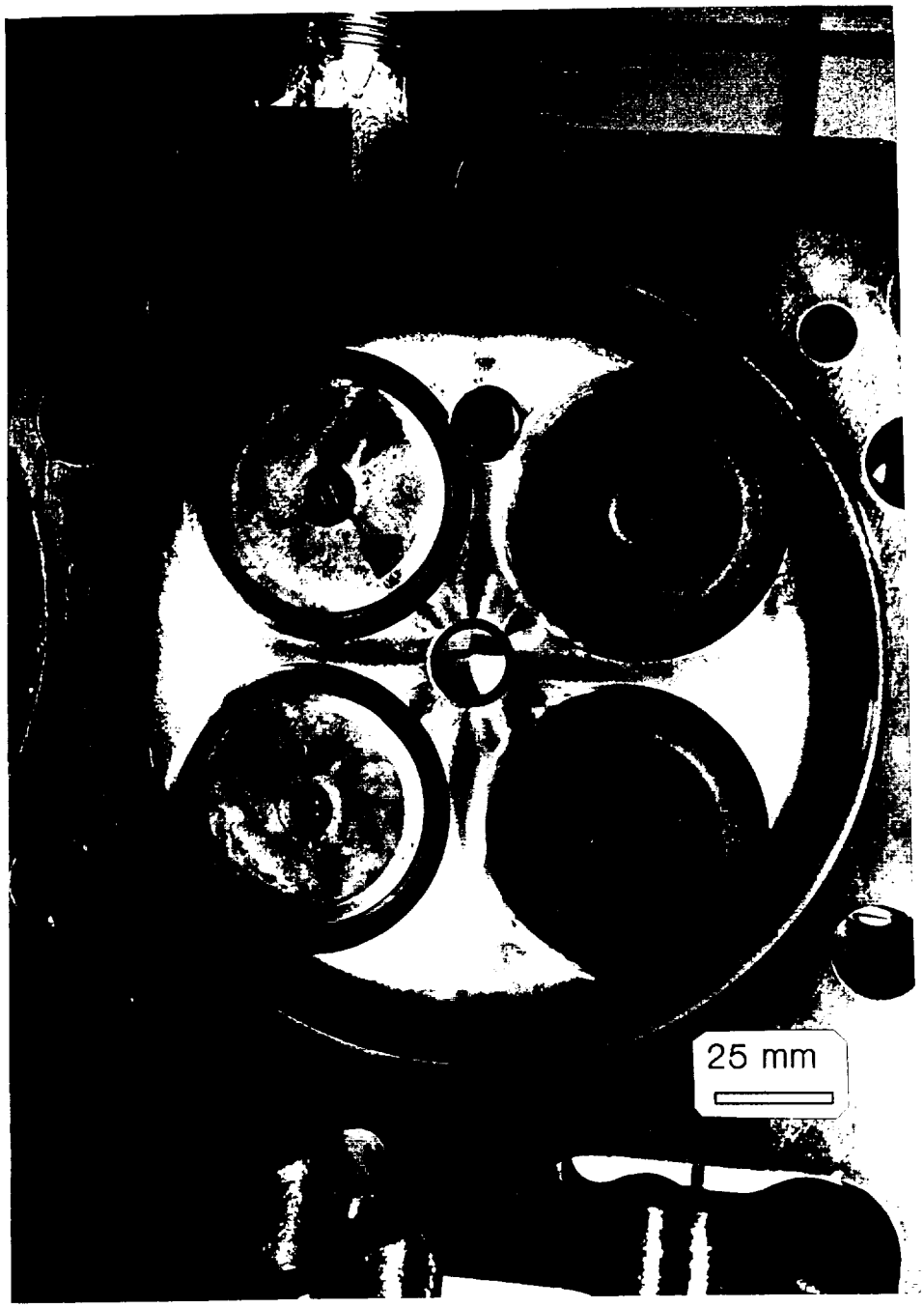

Figure 5.24: Cylinder head at test conclusion.

THIS PAGE LEFT INTENTIONALLY BLANK

6.0 CONCLUSIONS

Thick thermal barrier coatings, 2.5 mm (0.1 inch thick), on piston and cylinder heads which had a thermal conductance less than 410 W/m^2K exceeded the 100 hour engine durability goals set forth in this program. However, engine fuel economy data obtained using insulating hardware did not provide any significant motivating force for pursuing the current fuel economy approach, i.e., the direct substitution of insulating coatings for current metal hardware designs, in order to obtain diesel fuel economy benefits.

Critical review of all engine data generated in this program suggests that at best the insulated engine fuel economy was equal to the existing metal hardware designs. Engine build to build variability, changes in friction, and instrumentation variability were complicating factors. Limited apparent heat release data revealed that the oil cooled insulated engine had a shorter ignition delay and a longer combustion duration than the oil cooled metal engine. The longer combustion duration coincides with the observation that the insulated engine fuel economy was two percent worse on average than the metal engine for this series of back to back engine tests. It was also clear that the slight increase in exhaust energy was insufficient to make up for the increase in fuel consumption. Through out the data collection it was apparent that the volumetric efficiency of the oil cooled insulated engine was lower than the equivalent metal engine.

The test results generated on this engine suggested that a number of factors can influence fuel economy and may have led to erroneous conclusions in earlier programs:

1) coating loss during a test
2) incorrect bowl geometry and/or coating surface roughness

All these factors have an effect on engine fuel economy primarily yielding results that were degraded compared to an intact, insulated piston with a ground bowl geometry with equivalent surface roughness to a metal piston used in this program. Engine test data reported in this program was obtained using contour ground ceramic surfaces. However, some fuel economics were obtained using as-sprayed coatings which had poorer fuel economies, but were not reported because coating geometry and surfaces were not to print.

The test results generated on the program confirm a number of observations reported in the literature:

1) Volumetric efficiency of the oil cooled insulated engine was less than the water cooled and oil cooled metal engines under identical operating conditions.

2) Shorter ignition delays were observed with insulated engines.

3) Combustion duration was extended for an insulated engine.

4) Exhaust temperatures were slightly higher for insulated engines at comparable fuel rates and air/fuel ratios.

5) Engine fuel economy ranged from equivalent to some test data for metal engines to two percent worse than the oil cooled metal engine used in the final back-to-back engine tests.

It was also apparent that the thermal barrier coatings modified the combustion process as based on apparent heat release data. It was observed that the insulated piston surfaces did not have as much carbon build up, and local surface temperatures or peak temperatures exceeded the cycle average gas temperatures used as boundary conditions. It was clear that our understanding of the thermal barrier coatings for diesel engine applications and approaches to maximize their usefulness is in its infancy. Diesel engines are complex, highly fuel efficient systems. Direct substitution of the insulating coatings for metal hardware did not lead to a methodology for significantly improving fuel economy. However, the information generated indicates that the insulating coatings have modified the combustion processes. An exploratory approach may be required to determine if insulated coatings can improve diesel engine systems from the standpoint of fuel consumption or emissions reductions.

7.0 RECOMMENDATIONS

1) Determine if insulating coatings can improve the thermal fatigue life of cylinder heads and pistons for highly rated commercial and military engines.

2) Basic investigations should be conducted to determine if thermal barrier coatings can improve combustion or modify NOx/particulate trade offs in diesel engines. This effort should be exploratory in nature and should be conducted as a function of coating thickness and modifications to coating structure.

Commercial multicylinder diesel engines in conjunction with single cylinder research engines should be used on these investigations. These engines provide the proper test environment, are emissions certified, and permit lower overall test costs.

8.0 ACKNOWLEDGEMENTS

The author wishes to thank a number of contributors that greatly assisted in the preparation of the coating materials, data, testing and other information contained in this report.

The assistance of United Technologies Research Center is gratefully acknowledged for their assistance in development of the materials properties, guidance for coating development and actual coating development for this program. The assistance of Roberta P. Huston in one dimensional modeling and the materials properties is acknowledged, the assistance of Al J. Scharman in the preparation of coated cylinder heads and pistons for evaluations. The assistance of Richard Novak and Al Matarese in the development and carrying out of the overall program is gratefully acknowledged.

Assistance of Tony Rotilleco of Metco in allowing the use of METCO facilities for plasma spraying prototype parts is acknowledged.

Dr. Robert Thomas and Dr. Tasdiq Ahmed, Wayne State University, developed and greatly assisted in non destructive evaluation of thermal barrier coatings by infrared imaging.

The assistance of APS Materials, Inc. and Plasma Technics, Inc. for experimental plasma spray trials in the initial portions of this program is acknowledged.

Within Cummins, numerous people contributed to the report. The author wishes to thank Sharon Frisch for thermal modeling, Kevin Hoag for performance modeling, Don Roehling for two dimensional modeling of piston coatings, Angie Manon for three dimensional modeling of cylinder head coatings, Joe Willock for engine testing, Henry Ng for heat release calculations, Paul Wiczynski for assisting in performance measurement, and Barb Rees for manuscript preparation. Also, the overall guidance of Dr. Jim Patten throughout the program is gratefully acknowledged.

The technical and financial assistance of the DOE/NASA Heavy Duty Transport Program in supporting this effort through Contract DEN3-331 is acknowledged. Also, the help of Mr. Murray Bailey and Mr. James Wood for their assistance, support throughout the program, and review of the report is acknowledged.

Numerous people assisted throughout the program and the effort was truly a team effort.

9.0 REFERENCES

1. Turbine Engine Hot Section Technology 1986, Proceedings of a NASA Conference, Oct. 21-22, 1986, NASA Conference Publication 2444.

2. Coatings for Heat Engines, Proceedings of the First NATO Advanced Workshop on Coatings for Heat Engines held at Acquafredda di Maratea, Italy, April 1-6, 1984, edited by R. L. Clarke, J. W. Fairbanks, and Dr. I. Kvernes.

3. R. L. Holtman and co-authors, "An Investigation of Enhanced Capability Thermal Barrier Coating for Diesel Engine Components", DOE/NASA/0326-1, Aug. 1984.

4. R. J. Bratton, S. K. Lou, and S. Y. Lee, "Evaluation of Present Day Thermal Barrier Coatings for Industrial/Utility Applications, "Thin Solid Films, [73], 429-437, (1980).

5. K. L. Hoag, M. C. Brands, and W. Bryzik, "Cummins/TACOM Adiabatic Engine Program, "SAE 850356, (1985).

6. H. Eaton and R. C. Novak, "Development of Low Modulus Material for Use in Ceramic Gas Path Seal Systems, "NASA CR165469, Oct. 1981.

7. R. A. Miller, "Current Status of Thermal Barrier Coatings - An Overview", Surface and Coating Tech. 30, 1987.

8. W. F. Calosso, and A. R. Nicoll, "Process Requirements for Plasma Sprayed Coatings for Internal Combustion Engine Components", ASME 87-ICE-15, (1987).

9. I. Kvernes, "In-Service Performance of Ceramic and Metallic Coatings in Diesel Engines", SAE 860888, (1986).

10. A. P. Batakis and J. W. Vogan, "Rocket Thrust Chamber Thermal Barrier Coatings", NASA CR-175022, (1985).

11. R. A. Miller, "An Oxidation Based Model for Thermal Barrier Coating Life, "J. Am. Ceram. Soc. [67] 517-521 (1984).

12. S. Stecura, "Optimization of the NiCrA1Y/$Zr0_2$ - Y_20_3 Thermal Barrier System, "NASA Tech. Memo 86905.

13. R. J. Keller, "Research and Development for Improved Thermal Barrier Coatings", AFWAL-TR-84-4008, (1984).

14. T. E. Strangman, J. Neumann, and A. Liu, Thermal Barrier Coating Life-Prediction Model Development, NASA CR-179648, 1987.

9.0 REFERENCES (Cont'd)

15. K. L. Hoag, S. R. Frisch, and T. M. Yonushonis, "Thermal Analysis of the Effect of Thick Thermal Barrier Coatings on Diesel Engine Performance", Proceedings of the 24th Automotive Technology Development and Contractor's Coordination Meeting SAE P-197, 1986.

16. T. Morel, E. F. Fort, P. Blumberg, "Effect of Insulation Strategy on Diesel Engine Heat Rejection and Performance, "SAE 850506, 1985.

17. N. Watson, M. Marzouuk, "A Nonlinear Digital Simulation of Turbocharged Diesel Engines", SAE 770123, 1977.

18. N. Watson, N.P. Kyrtatos, and K. Holmes, "The Performance Potential of Limited Cooled Diesel Engines", Proc. Instn. Mech. Engrs., Vol 197A, 1983.

19. G. Woschni, "A Universally Applicable Equation for the Instantaneous Heat Transfer Coefficient in the Internal Combustion Engines, "SAE 670931, 1967.

20. W. J. Seale and D. H. C. Taylor, "Spatial Variation of Heat Transfer to Pistons and Liners of Medium Speed Diesel Engines, "Proc. Instn. Mech. Engrs., Vol 185, 1970.

21. Cummins Engine., C. H. Moore, personal communication.

NASA
National Aeronautics and Space Administration

Report Documentation Page

1. Report No.	2. Government Accession No.	3. Recipient's Catalog No.
NASA CR-187111	--	--

4. Title and Subtitle
Thick Thermal Barrier Coatings
For Diesel Components

5. Report Date

6. Performing Organization Code
--

7. Author(s)
T.M. Yonushonis

8. Performing Organization Report No.

10. Work Unit No.
--

9. Performing Organization Name and Address
Cummins Engine Co., Inc.
MC 50183, Box 3005
Columbus, IN 47202-3005

11. Contract or Grant No.
DEN3-331

13. Type of Report and Period Covered
Contractor Report

12. Sponsoring Agency Name and Address
U.S. Department of Energy
Office of Propulsion Systems
Washington, DC 20585

14. Sponsoring Agency Code
DOE/NASA/0331-1

15. Supplementary Notes
Final Report. Prepared under Interagency Agreement DE-AI01-86CE50162.
Project Manager, M. Bailey, Propulsion Systems Division, NASA
Lewis Research Center, Cleveland, OH 44135

16. Abstract

An engineered thick thermal barrier coating consisting of multiple layers of zirconia and CoCrAlY with a zirconia top layer and having a system thermal conductance less than 410 w/m^2K exceeded the 100 hour engine durability goals set forth in this program. The thermal barrier coatings were intact at the test conclusion.

Back to back single cylinder research engine tests were conducted with water-cooled, metal hardware and oil-cooled, thermal barrier coating insulated hardware to determine apparent heat release and fuel economy. Apparent heat release data revealed that the insulated engine had a shorter ignition delay and a longer combustion duration than the metal engine. The insulated engine fuel economy was approximately two percent worse on average for this series of tests. There was no attempt to optimize engine efficiency of the insulated engine by modifying the engine timing, coating, or other techniques.

17. Key Words (Suggested by Author(s))	18. Distribution Statement
Thermal barrier coating, diesel engine.	Unclassified - unlimited STAR Category 85 DOE Category UC-96

19. Security Classif. (of this report)	20. Security Classif. (of this page)	21. No of pages	22. Price*
Unclassified	Unclassified		

NASA FORM 1626 OCT 86

*For sale by the National Technical Information Service, Springfield, Virginia 22161